LBL-4316

APPLICATION OF GENERALIZED CLASSICAL TRAJECTORIES IN NUCLEAR PHYSICS

Herbert Massmann Leser
(Ph. D. thesis)

September 1975

Prepared for the U. S. Energy Research and Development Administration under Contract W-7405-ENG-48

LBL-4316

DISCLAIMER

TABLE OF CONTENTS

ACKNOWLEDGMENTS

I wish to express my sincere gratitude for the encouragement and guidance of Prof. John O. Rasmussen, under whose direction this work was made possible.

Special thanks are due to Drs. Mike Guidry and Peter Ring, whose collaboration with certain parts of this work is deeply appreciated.

I am also very indebted to Profs. William Miller and Jorrit de Boer for stimulating discussions and valuable suggestions.

Thanks are also in order to Raul Donangelo for many discussions we had on the subject.

My stay here in Berkeley was made possible thanks to a fellowship from the Convenio U. de Chile-U. of California.

This work was performed under the auspices of the U.S. Energy and Research Development Administration.

Application of Generalized Classical Trajectories in Nuclear Physics

by

Herbert Massmann Leser

ABSTRACT

A new semi-classical method, the so-called uniform semiclassical approximation, is described briefly and then applied to two nuclear physics problems. The basic features of this method are that the dynamics of the problem is treated completely classically (that is, one solves classical equations of motion), but the quantum mechanical superposition principle is retained by evaluating a phase along the classical trajectory and adding probability amplitudes for indistinguishable processes rather than probabilities themselves.

The first problem considered is the backscattering from a deformed nucleus and the excitation of rotational states in the target at energies up to the Coulomb barrier. The multiple Coulomb excitation calculations are in quantitative agreement with a very different method (the de Boer-Winther code). A nuclear optical potential is also considered and the nuclear-Coulomb interference for heavy ions is studied.

The second problem considered is the tunneling through a two-dimensional barrier. This problem (which is supposed to simulate the penetration through a two-dimensional fission barrier) is investigated by a fully quantum-mechanical coupled-channel calculation and by the uniform semiclassical approximation. A quantitative agreement is found.

I. Introduction

The main focus of this thesis will be on the application of the so-called uniform semiclassical approximation (USCA) to some heavy-ion nuclear physics problems. The USCA is a semi-classical method which was developed in recent years by molecular theorists and has been applied to molecular scattering and reaction problems.[1-5]

The appeal of semiclassical methods is that they usually lead to simple models and intuitive physical pictures and also usually simplify considerably the sometimes cumbersome quantum mechanical calculations. In nuclear physics, however, semi-classical methods have not been widely used to describe collisions between nuclei. The reason is that until recently only light nuclei were available as projectiles, and direct reactions with light projectiles could fairly accurately be described by the distorted-wave Born approximation (DWBA) or its generalization, the coupled-channel Born approximation (CCBA) where the coupling between some channels is included. In recent years, increasingly heavier ions at nuclear research energies became available as projectiles, and soon the old methods of describing the collision were pushed to their limits. Even for one of the simplest problems, the Coulomb excitation of rotational states in the scattering of a spherical nucleus on a deformed nucleus, the most sophisticated coupled-channel code available[6] could only handle cases for which the Sommerfeld parameter η is less than 30. Today, with the heavy-ion beams available, Coulomb excitation experiments are being performed for which the Sommerfeld parameter is of the order of 400; cases for which an exact coupled channel calculation is at this

moment completely hopeless. For this reason the application of classical mechanics and semiclassical methods to nuclear heavy-ion reactions have become popular.

Pure classical mechanics, with such classical concepts as friction, are being used to describe the fusion cross section and the energy loss of the projectile in heavy-ion collisions.[7,8] In these calculations the projectile moves in a potential according to the classical equations of motion (including friction). The hope in this type of calculations is that they will reproduce the rough features of the problem considered. However, as shown by Glendenning[9], classical trajectories can also be used to predict the qualitative features of cross sections. In order to get a quantitative agreement one has to evaluate along the classical trajectories a phase, which essentially measures the number of De Broglie wavelengths along the trajectory. Only if this phase information is retained, and the contribution from the various trajectories which lead to a given exit channel are added coherently, can quantitative agreement be expected. The semiclassical methods differ from the classical methods in that the phase information along the trajectories is retained.

In the semiclassical calculations so far used for nuclear reactions, the restriction to real trajectories was made. Even in the case when the interaction potential used was a complex optical potential, the potential was split into a real part giving the trajectories and an imaginary part to give the attenuation along the trajectory,[10, 11]. The problem with such classical real trajectories is that not all regions of space can be reached by classical trajectories, that is, there are classically inaccessible shadow regions, whereas the quantal waves do reach into the

"shadow" region. In other words, when using only real classical trajectories one finds such discontinuities like the caustics (which separate illuminated regions from shadow regions) which in turn produce singularities in the cross-sections; while, when using quantum mechanics, the transition between the illuminated and shadow regions is smooth, producing no singularity in the cross sections.

Almost simultaneously, semiclassical treatments using generalized classical trajectories (allowing the classical trajectories to be complex) have been applied to several problems. The classical scattering with heavy ions was considered by Malfliet[12] and Koeling and Malfliet[13] using the USCA (which was mainly developed by Miller[1-3]) and by Knoll and Schäffer[14] who use a somewhat different approach. The agreement between these semiclassical calculations and the exact DWBA results is impressive.

In this thesis we will in chapter II first consider some of the theoretical aspects of the USCA and then apply this method to two very different problems.

In chapter III we will apply it to the backscattering of heavy ions from deformed nuclei at energies below and up to the Coulomb barrier. At energies very much below the Coulomb barrier, only the electromagnetic interaction, which can Coulomb excite rotational states of the target, is of importance. At some higher bombarding energies, the complex nuclear cal interaction potential between the projectile and the target cannot be neglected and will also be included. The restriction to backscattering allows us to reduce the problem to a two-dimensional one, which is much easier to solve but still experimentally interesting and of importance. For backscattering energies well below the Coulomb barrier, that is, for

cases where the nuclear force can be neglected, we will compare our calculations with results using the de Boer-Winther code for multiple Coulomb excitation,[15] which is based on a very different semi-classical approximation. A short outline of this method is given in Appendix A.

In chapter IV we will apply the USCA to a simple two-dimensional fission barrier penetration model. It has been customary to estimate the lifetimes of fissioning nuclei by using the one-dimensional WKB approximation to evaluate the probability for the system to penetrate the fission barrier. Since a complete dynamical calculation of a two-dimensional barrier penetration has not been performed until now and the USCA method allows us to do it, it is of interest to perform such a calculation to find out the effects of the additional approximations usually made in solving the multidimensional barrier penetration problem. Also, an exact coupled channel code was developed which solves the same two dimensional barrier penetration problem, and this code allows us to compare the USCA solution to exact results.

In chapter V the main conclusions regarding the application of the USCA method to these nuclear physics problems will be summarized.

II. USCA Theory

1) The Schrödinger Equation.

In this chapter the basic equations of the uniform semi-classical approximation (USCA) will be derived. These equations were first derived by W. H. Miller[1,2] and an excellent review is given in reference (3). The derivation that will be presented here, however, is based on the derivation given by R. A. Marcus,[4] and by J. N. Connor and R. A. Marcus.[16]

The general problem that will be considered is that of a collision-like system with N degrees of freedom for which there exists a classical analog to the quantum mechanical Hamiltonian. Of the N degrees of freedom one will be the relative translational coordinate R of the collision partners, the remaining N-1 coordinates being "internal" degrees of freedom which are quantized in the asymptotic regions, that is for $R \longrightarrow \infty$. The quantization is most easily achieved if one describes the "internal" degrees of freedom in terms of action-angle variables.[17] Let q_i be the angle variable for the i^{th} internal degree of freedom (i = 1, ..., N-1) and J_i its canonically-conjugate momentum, the so-called action variable. Let P be the canonically conjugate variable of the coordinate R. If the classical hamiltonian for the system is $H(J_i, q_i; P, R)$, then the quantum-mechanical hamiltonian operator in the coordinate representation is found by making the following replacements in the classical hamiltonian

$$J_i \longrightarrow i\hbar \frac{\partial}{\partial q_i} + 2\pi\hbar\xi_i \qquad (1a)$$

$$P \longrightarrow -i\hbar \frac{\partial}{\partial R} \tag{1 b}$$

The Schrödinger equation we wish to solve is therefore

$$H\left(-i\hbar \frac{\partial}{\partial q_i} + 2\pi\xi_i, q_i, -i\hbar \frac{\partial}{\partial R}, R\right)\Psi = E\Psi \tag{2}$$

The quantum mechanical action variable operator $-i\hbar \frac{\partial}{\partial q_i}$ differs from the classical action variable J_i by the quantity $2\pi\hbar\xi_i$, where ξ_i is a constant. In a WKB approximation the constant ξ_i is 0 or 1/2 depending on the type of the i^{th} internal degree of freedom one is considering.

In the asymptotic region $(R \longrightarrow \infty)$ we assume that all the degrees of freedom are uncoupled, and the system is in some internal state described by the quantum numbers $\underset{\sim}{n}$ $(\equiv (n_1, \ldots, n_{N-1}))$. Also, the hamiltonian does not depend (in the asymptotic region) on the coordinate q_i when action variables are used, so the Schrödinger equation is:

$$H_o\left(-i\hbar \frac{\partial}{\partial q_i} + 2\pi\hbar\xi_i, -i\hbar \frac{\partial}{\partial R}, R\right)\varphi^{(o)}_{\underset{\sim}{n}E} = E\varphi^{(o)}_{\underset{\sim}{n}E} \qquad (R \longrightarrow \infty) \tag{3}$$

The wave function $\varphi^{(o)}_{\underset{\sim}{n}E}$ is periodic in the angle variables $\underset{\sim}{q}$ with unit period, and one therefore has the solution:

$$\varphi^{(o)\pm}_{\underset{\sim}{n}E}(\underset{\sim}{q}, R) = f(R)\, e^{i\left(\pm k_{\underset{\sim}{n}} R + 2\pi \sum_{j=1}^{N-1} q_j n_j\right)} \tag{4}$$

where $\underset{\sim}{q}$ represents $(q_1, \ldots, q_{N-1})$, $f(R) \cdot e^{\pm i k_{\underset{\sim}{n}} R}$ is the radial

wavefunction and the wave number $K_{\underset{\sim}{n}} = |P_{\underset{\sim}{n}}|/\hbar$ is determined from energy conservation. If $\mathcal{E}_{n_j}$ is the internal energy of the j^{th} internal degree of freedom (n_j being a quantum number in the asymptotic region for that degree of freedom), then one has:

$$E = \frac{\hbar^2 K_n^2}{2m} + \sum_j \mathcal{E}_{n_j} \tag{5}$$

where m is the reduced mass of the system. The $\pm$ in equation (4) refers to an "outgoing" and "incoming" wave respectively. In equation (4) n_j is an integer, the quantum number for the j^{th} internal degree of freedom.

The classical action variable J_j is related to the quantum number n_j through the relation

$$J_j = 2\pi\hbar(n_j + \xi_j) \tag{6}$$

The value of ξ_j is known from WKB solutions for various standard problems. If n represents the angular momentum of a planar rotor, then $\xi = 0$. If n corresponds to the quantum number of an harmonic oscillator or an angular momentum of an orbital motion in three dimensions, then $\xi = \frac{1}{2}$ (for the z component of the latter $\xi = 0$), etc..[8].

2) The WKB Ansatz

As in the one-dimensional case, we will make the ansatz

$$\Psi = A e^{\frac{i}{\hbar}\Phi} \tag{7}$$

and substitute this wavefunction into the Schrodinger equation (2) keeping only the terms of the lowest order in $\hbar$. Following Dirac,[18] the lowest order in $\hbar$ leads to

$$H\left(\frac{\partial \Phi}{\partial q_i} + 2\pi\hbar\xi_i, q_i; \frac{\partial \Phi}{\partial R}, R\right) = E \tag{8}$$

Introducing the function W defined by

$$W \equiv \Phi + \sum_j 2\pi\hbar q_j \xi_j \tag{9}$$

equation (8) becomes:

$$H\left(\frac{\partial W}{\partial q_i}, q_i; \frac{\partial W}{\partial R}, R\right) = E \tag{10}$$

Keeping the next higher-order term in $\hbar$ one finds an equation involving the amplitude A

$$\frac{\partial}{\partial \underset{\sim}{q}}\left(A^2 \dot{\underset{\sim}{q}}\right) + \frac{\partial}{\partial R}\left(A^2 \dot{R}\right) = 0 \tag{11}$$

where

$$\dot{R} = \frac{\partial H}{\partial P} \tag{12a}$$

$$\dot{\underset{\sim}{q}} = \frac{\partial H}{\partial \underset{\sim}{J}} \tag{12b}$$

Equation (11) is a conservation equation. The equation for W (equation (10)) is identical to the Hamilton-Jacobi partial differential equation for Hamilton's characteristic function W in classical mechanics.[17] The total time derivative of Hamilton's characteristic function is[17]

$$\frac{dW}{dt} = P\dot{R} + \sum_{j=1}^{N-1} J_j \dot{q}_j \tag{13}$$

from which we find:

$$W = C + \int_{t_o}^{t} P\dot{R}\,dt' + \sum_{j=1}^{N-1} \int_{t_o}^{t} J_j \dot{q}_j\,dt' \tag{14}$$

where the constant C is chosen so that for $t < t_o$ (t_o is a time before any interaction takes place) the phase of the wave function is the same as in the uncoupled case (see eq. (4)).

One finds

$$\frac{W}{\hbar} = \int_{t_o}^{t} \kappa(t')\dot{R}(t')\,dt' - \underset{\sim}{K}_{n(\mu)} R^{(o)} + 2\pi \sum_{j=1}^{N-1} \left[\int_{t_o}^{t} \left(n_j(t') + \xi_j\right) \cdot \dot{q}_j(t')\,dt' + \left(n_j^{(\mu)} + \xi_j\right) q_j^{(o)} \right] \tag{15}$$

where $q_j^{(0)} = q_j(t=t_o)$, $R^{(0)} = R(t=t_i)$, and $n_j(t)$ is a continuous variable related to the classical action variable through eq.(6). The superscript μ on n_j indicates that it is the initial value (integer) of $n_j(t)$ in the asymptotic region (that is for $t \longrightarrow -\infty$). There is another condition that the phase Φ has to satisfy[19] and it is that when P changes sign from negative to positive (i.e. if the radial coordinate goes through a turning point), then the phase $\Phi/\hbar$ decreases by $\pi/2$.

The integrals in eq. (15) are line integrals, the integration being performed along the classical trajectories which the system traces.

The amplitude A is determined by integrating the conservation equation (11) over a tube spanned by classical paths starting at a distance R, going toward the interaction region and out to the distance R again. Flux will enter and leave this tube only at the extremes of the tube and one has

$$\left[A^2 \dot{R} \prod_j dq_{f_j} \right]_{(\mu)} + A^2 \dot{R} \prod_j dq_{f_j} = 0 \tag{16}$$

The first term is the flux entering the tube (the index μ refers to the initial situation; $\dot{R}_\mu < 0$), the second term represents the flux leaving at the other end. $\left(\prod_j dq_{f_j}\right)_\mu$ and $\prod_j dq_{f_j}$ are related by a Jacobian:

$$\prod_j dq_{f_j} = \frac{\partial(q_{f_1}, \ldots, q_{f_{N-1}})}{\partial(q_{f_1}^{(\mu)}, \ldots, q_{f_{N-1}}^{(\mu)})} \left(\prod_j dq_{f_j} \right)_\mu \tag{17}$$

Substituting (17) into (16) one finds the amplitude at the distance R after the scattering in terms of the amplitude at R before the projectile moves into the interaction region

$$A(R) = A^{(\mu)}(R) \sqrt{\frac{v^{(\mu)}}{v}} \left(\frac{\partial(q_{f_1}, \ldots, q_{f_{N-1}})}{\partial(q_{f_1}^{(\mu)}, \ldots, q_{f_{N-1}}^{(\mu)})} \right)^{-\frac{1}{2}} \tag{18}$$

with $v \equiv |\dot{R}|$

Since the incoming part of the wave function (7) has to go over into the unperturbed incoming wave function (eq. (4)) for $t < t_o$, one finds

(using eqs. (7), (15) and (4)) that $A^{(\mu)}(R) = f(R)$. For the wave function Ψ in the asymptotic region, one finally finds

$$\Psi \underset{R\to\infty}{\sim} \varphi^{(0)-}_{\underset{\sim}{n}^{(\mu)}E} - \sqrt{\frac{v^{(\mu)}}{v}}\left(\frac{\partial(q_1,\dots,q_{N-1})}{\partial(q_1^{(\mu)},\dots,q_{N-1}^{(\mu)})}\right)^{-1/2} f(R)\, e^{\frac{i}{\hbar}\phi} \tag{19}$$

with

$$\frac{\phi}{\hbar} = \int_{t_0}^{t} K(t')\dot{R}(t')dt' - K_{\underset{\sim}{n}^{(\mu)}} R^{(0)} + 2\pi\sum_{j=1}^{N-1}\left[\left(n_j^{(\mu)} + \xi_j\right)q_j^{(0)} + \right.$$

$$\left. + \xi_j q_j + \int_{t_0}^{t}\left(n_j(t') + \xi_j\right)\dot{q}_j(t')dt'\right] + \frac{\pi}{2} \tag{20}$$

3) The integral expression of the S-matrix

The S-matrix can be found from the asymptotic form of the wave function (eq. (19)). The elements of the S-matrix are defined by:

$$\Psi \underset{R\to\infty}{\sim} \varphi^{(0)-}_{\underset{\sim}{n}^{(\mu)}E} - \sum_{\underset{\sim}{n}^{(\nu)}} S_{\nu\mu}\sqrt{\frac{v^{(\mu)}}{v^{(\nu)}}}\,\varphi^{(0)+}_{\underset{\sim}{n}^{(\nu)}E} \tag{21}$$

where $\varphi^{\mp}$ are the incoming and outgoing waves defined in eq. (4). Once the S-matrix is known, the transition probabilities for the system from an initial state $\underset{\sim}{n}^{(\mu)}$ to a final state $\underset{\sim}{n}^{(\nu)}$ is given on the usual way by

$$P_{\nu\leftarrow\mu} = |S_{\nu\mu}|^2 \tag{22}$$

From eqs. (19) and (21) one finds (since the two asymptotic expressions for the wave function must be equivalent)

Multiplying both sides by $\exp\left(-2\pi i \sum_j n_j^{(\nu)} q_j\right)$ and integrating over all the internal degrees of freedom, using the fact that

$$\int_0^1 \cdots \int_0^1 \exp\left(-2\pi i \sum_j n_j^{(\nu)} q_j\right) \exp\left(2\pi i \sum_j n_j^{(\nu')} q_j\right) \prod_j dq_j = \delta_{\nu\nu'} \tag{24}$$

one finds for the S-matrix

$$S_{\nu\mu} = \lim_{R\to\infty} \int_0^1 \cdots \int_0^1 \sqrt{\frac{v^{(\nu)}}{v}} \left(\frac{\partial(q_1, \ldots, q_{N-1})}{\partial(q_1^{(\mu)}, \ldots, q_{N-1}^{(\mu)})} \right)^{-\frac{1}{2}} e^{\frac{i}{\hbar}\Delta} \prod_{j=1}^{N-1} dq_j \tag{25}$$

with

$$\Delta = \left(\int_{t_0}^{t} K(t') \dot{R}(t') dt' - K_{\underset{\sim}{n}^{(\mu)}} R^{(0)} - K_{\underset{\sim}{n}^{(\nu)}} R \right) + \frac{\pi}{2} +$$

$$+ 2\pi \sum_{j=1}^{N-1} \left(\int_{t_0}^{t} \dot{q}_j(t') n_j(t') dt' + n_j^{(\mu)} q_j^{(0)} - n_j^{(\nu)} q_j \right) \tag{26}$$

Equation (25), which expresses the S-matrix elements in terms of a multi-dimensional integral, is not useful for practical calculations, and it is only when the integrals in (25) are evaluated by asymptotic methods that one obtains a useful expression for the S-matrix.

4) The USCA S-matrix

In this thesis we are studying semiclassical systems, that is systems that can be described when keeping only the lowest terms in an expansion of the Schrödinger equation in terms of $\hbar$. That is, we are interested in the case where $\hbar$ is small compared with the action that is characteristic to the problem.

If we let $\hbar$ go to zero, the term $\exp(i\Delta/\hbar)$, and therefore the integrand of the integral in eq. (25), will become highly oscillatory. Therefore, there will be contributions to the integral only for values of $\underset{\sim}{q}$ for which the phase Δ becomes stationary, i.e. at saddle points. At the saddle points one has

$$\frac{\partial \Delta}{\partial \underset{\sim}{q}} = 0 \tag{27}$$

In order to find the saddle points, one has to find the roots of eq. (27). The integration of eq. (25) by the saddle point method in the general multidimensional case, for which there are many roots to eq. (27) (several of them could be lying "close" together or be multiple roots), is a very complicated problem, some aspects of which, however, have been well studied.[16,20-22] The one-dimensional case is the simplest and since this is the only case we shall need later, all our effort will be concentrated on understanding this case in detail. In other words, the general integral we want to evaluate asymptotically is:

$$I = \int_0^1 g(x) e^{\frac{i}{\hbar} f(x)} dx \tag{28}$$

where f is a function which, we shall suppose, has two saddle points (x_1 and x_2) in the region of interest. Even this very much simplified problem has many aspects, which we shall now consider one by one beginning with the simplest.

a) f real, primitive approximation, classically accessible case. When the "phase" function f(x) is real, there may occur two situations: either the two solutions of eq. (27) (i.e. $f' = \frac{df(x)}{dx} = 0$, are real, or they are complex, one being the complex conjugate of the other. The first situation is called, for reasons to be seen later, the classically accessible or allowed case; the second situation is referred to as the classically inaccessible or forbidden case. For the classically accessible case one has that x_1 and x_2 (the two solutions of $f'(x)=0$ in the interval $[0,1]$) are real. Fig. II1 shows a sketch of how the phase f(x) might look. At the stationary phase points x_1, x_2, the second derivative of the phase function will necessarily have opposite signs (we assume that f(x) is a continuous function), and without loss of generality we will assume that x_1 is the point for which $f''(x_1)>0$ and x_2 is the point for which $f''(x_2)<0$. The so-called primitive approximation is obtained when f is expanded as a quadratic around the points x_1 and x_2:

$$f(x) \underset{\substack{x \text{ close} \\ \text{to } x_1}}{\simeq} f_1 + \frac{1}{2}\left|f_1''\right|(x-x_1)^2 \tag{29a}$$

$$f(x) \underset{\substack{x \text{ close} \\ \text{to } x_2}}{\simeq} f_2 - \frac{1}{2}\left|f_2''\right|(x-x_2)^2 \tag{29b}$$

Where the notation $f_1 \equiv f(x_1)$, $f_1'' \equiv \left(d^2f(x)/dx^2\right)_{x_2}$, etc. has been used. Remembering that in the limit $\hbar \to 0$ the only contribution to the integral I (eq. (28)) comes from points near the stationary phase points x_1 and x_2 we find (substituting the expansions eq. (29) into eq. (28)):

$$I \simeq \int_{-\infty}^{+\infty} g(x) e^{\frac{i}{\hbar}\left(f_1 + \frac{|f_1''|}{2}(x-x_1)^2\right)} dx + \int_{-\infty}^{+\infty} g(x) e^{\frac{i}{\hbar}\left(f_2 - \frac{|f_2''|}{2}(x-x_2)^2\right)} dx \quad (30)$$

The limits of integration should only include points close to x_1 in the first integral (close to x_2 for the second), but since points x far away from x_2 do not contribute to the integral, one can replace the limits of integration by $-\infty$, $+\infty$. From eq. (30) we find:

$$I \simeq g(x_1) e^{\frac{i}{\hbar} f_1} \int_{-\infty}^{+\infty} e^{\frac{i}{\hbar}\frac{|f_1''|}{2} v^2} dv + g(x_2) e^{\frac{i}{\hbar} f_2} \int_{-\infty}^{+\infty} e^{-\frac{i}{\hbar}\frac{|f_2''|}{2} v^2} dv$$

$$\simeq g_1 e^{\frac{i}{\hbar} f_1} \sqrt{\frac{2\pi i\hbar}{|f_1''|}} + g_2 e^{\frac{i}{\hbar} f_2} \sqrt{\frac{2\pi i\hbar}{-|f_2''|}}$$

$$\simeq g_1 \sqrt{\frac{2\pi\hbar}{|f_1''|}} e^{i\left(\frac{f_1}{\hbar} + \frac{\pi}{4}\right)} + g_2 \sqrt{\frac{2\pi\hbar}{|f_2''|}} e^{i\left(\frac{f_2}{\hbar} - \frac{\pi}{4}\right)}$$

(31)

This is the so-called primitive approximation to the integral I. The physical meaning of the different terms in eq. (31) will become clear in later chapters, when application of eq. (31) to specific examples is made. To further understand the structure of the saddle points let us analytically continue the function f into the complex plane. The expansion of $f(z)$ around the saddle point $z_1 = x_1$ becomes(eq. (29a)):

$$f(z) = f_1 + \frac{1}{2}|f_1''|\left\{\left[(x-x_1)^2 - y^2\right] + 2i(x-x_1)y\right\} \quad (32)$$

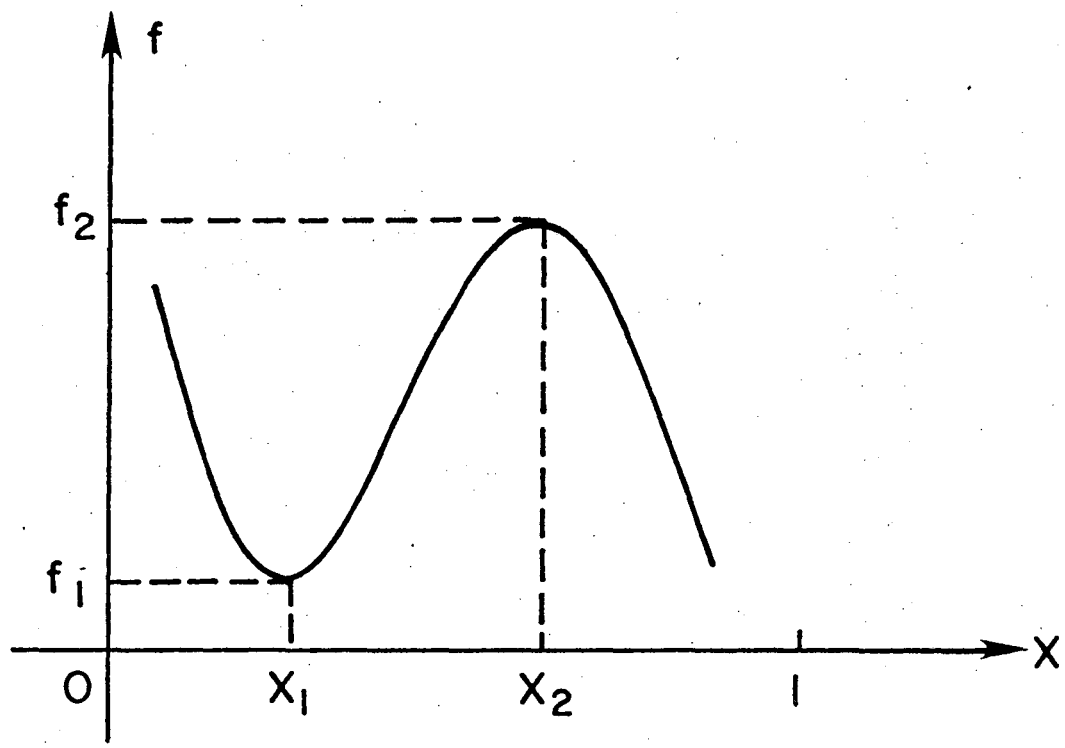

Fig. II-1 Sketch of the phase function f (x) XBL759-4068

where $z = x + iy$. The equipotential contours of the real and imaginary part of $\frac{i}{\hbar} f(z)$ are shown in Fig. II2. When looking in the complex plane for the path of steepest descent over the saddle point x_1, one has to look at the equipotential contours of $\text{Real}\left(\frac{i}{\hbar} f(z)\right)$ (Fig. II2a). The path of steepest descent is drawn with a heavy line. When looking for the path in the complex plane for which the phase of the integral does not change (the stationary phase path) when one goes over the saddle, then one has to look at the equipotential contours of $\text{Imag}\left(\frac{i}{\hbar} f(z)\right)$ (Fig. II2b). There are two stationary phase paths one could choose. One of the paths coincides with the path of steepest descent, and is, of course, the path one has to choose. Fig. II3 shows a diagram of the equipotentials of $\text{Real}\left(\frac{i}{\hbar} f\right)$ when the two saddles are considered. The path in the complex plane one has to follow in integrating the integral in eq. (28) is also shown. Both saddle points contribute to the integral.

b) f real, primitive approximation, classically inaccessible case. As already mentioned, the classically inaccessible case (sometimes also called the classically forbidden case) occurs when there are no real roots to the equation $f'(x) = 0$, but only complex solutions. If z_1 is a solution, then $z_2 = z_1^*$ is also a solution. Since in this case also, the second derivative has opposite signs for the two saddle points, and in addition one is the complex conjugate of the other, one deduces that they must be purely imaginary. The equations equivalent to eqs. (29) or (32) in this case are:

$$f(z) \underset{\text{close to } z_1}{\simeq} f_1 + \frac{i}{2}|f_1''|\left\{\left[(x-x_0)^2-(y-y_0)^2\right]+2i(x-x_0)(y-y_0)\right\} \quad (33a)$$

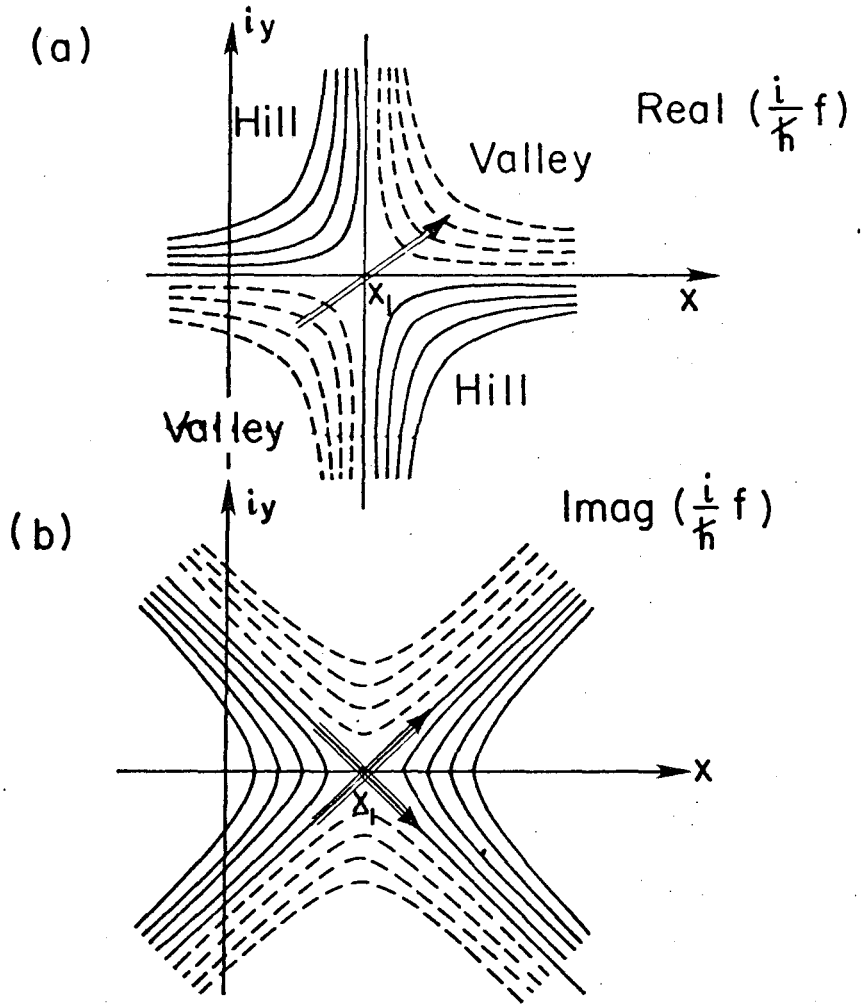

XBL759-4065

Fig. II-2 Equipotential contours of $if(z)/\hbar$ in the vicinity of a saddle point for which $\partial^2 f/\partial x^2 > 0$: a) shows the real part of $\frac{i}{\hbar} f(z)$ with the path of steepest descent shown by the arrow; b) shows the imaginary part of $if(z)\hbar$ with the stationary phase path shown by arrows.

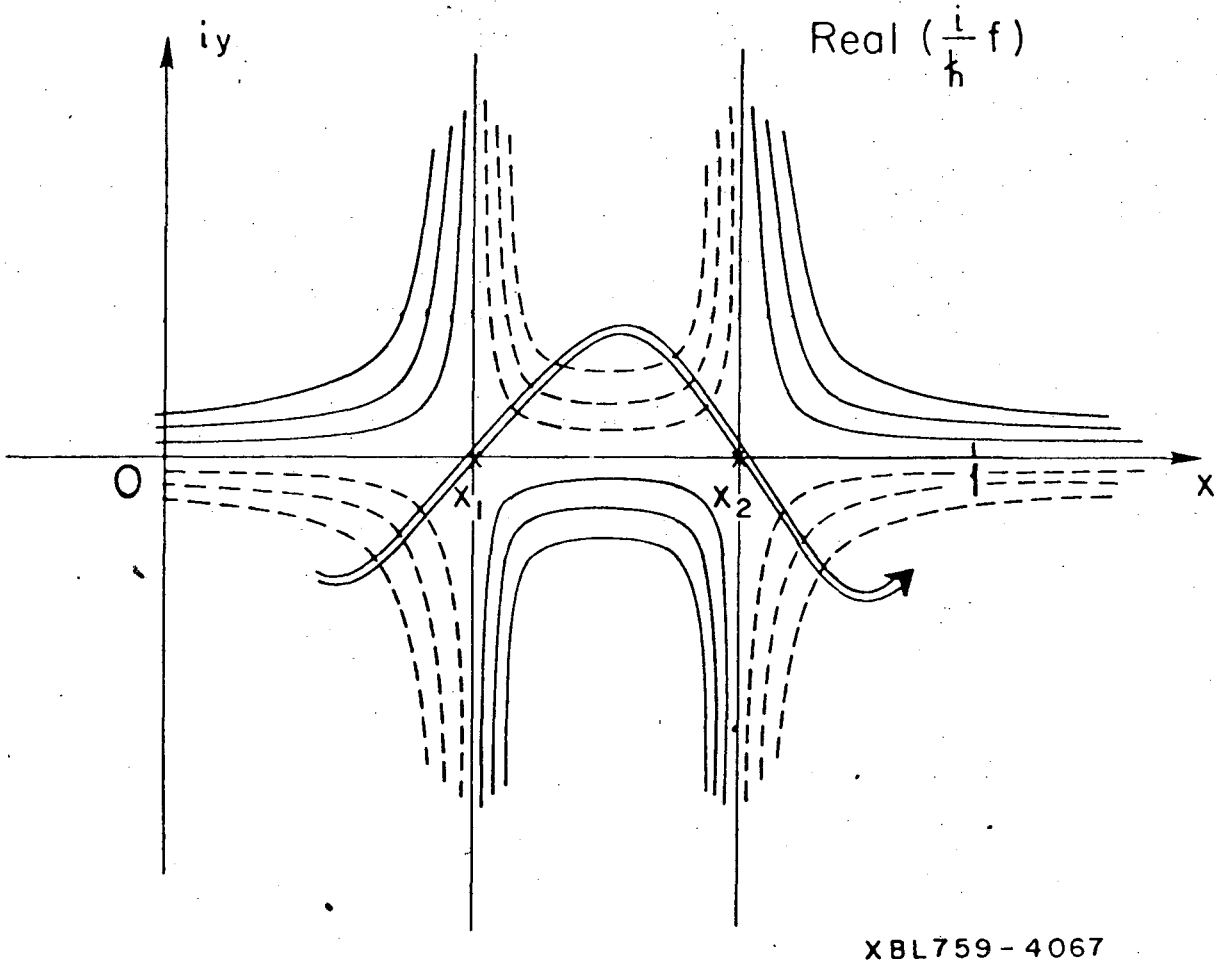

Fig. II-3 Equipotential contours of Real $\frac{i}{\hbar} f(z)$ in the presence of the two saddle points for the classically accessible case. The integration path which goes over both saddle points is also shown.

$$f(z) \underset{\text{close to } z_2}{\simeq} f_1^* - \frac{i}{2}|f_1''|\left\{\left[(x-x_0)^2-(y-y_0)^2\right]+2i(x-x_0)(y-y_0)\right\} \qquad (33b)$$

where x_0 and y_0 are defined by $z_1 = x_0 + iy_0$. Fig. II4 shows a sketch of the equipotentials of $Real\left(\frac{i}{\hbar}f\right)$ in this case. It is clear that the integration path in this case can only go over one saddle point (the one which is lower), and so only one saddle point contributes to the integral. If the saddle point at z_1 is the saddle which contributes to the integral, then the result (in the classically forbidden case) is:

$$I \simeq g_1\sqrt{\frac{2\pi i\hbar}{f_1''}}\, e^{i\frac{f_1}{\hbar}} \qquad (34)$$

There is also a physical reason, as we shall see later, why the other saddle point does not contribute. Let's note at this point that the lower saddle (that is, the saddle whose height is lower) is the saddle point for which $f(z_1) = f_1$ has a positive imaginary part.

c) Uniform Airy Approximation. When the two saddle points x_1 and x_2 are close together, then the approximations leading to eq. (31) can not be made. That is, one cannot treat one saddle point as being completely independent of the other. When the saddle points move together, then $|f_1''|$ and $|f_2''|$ become very small (zero in the limit that the two saddle points coincide) and eq. (31) is no longer a good approximation to the integral I. Also, from Fig. II1 it is clear that when the two saddle points come close together a quadratic expansion around the maximum

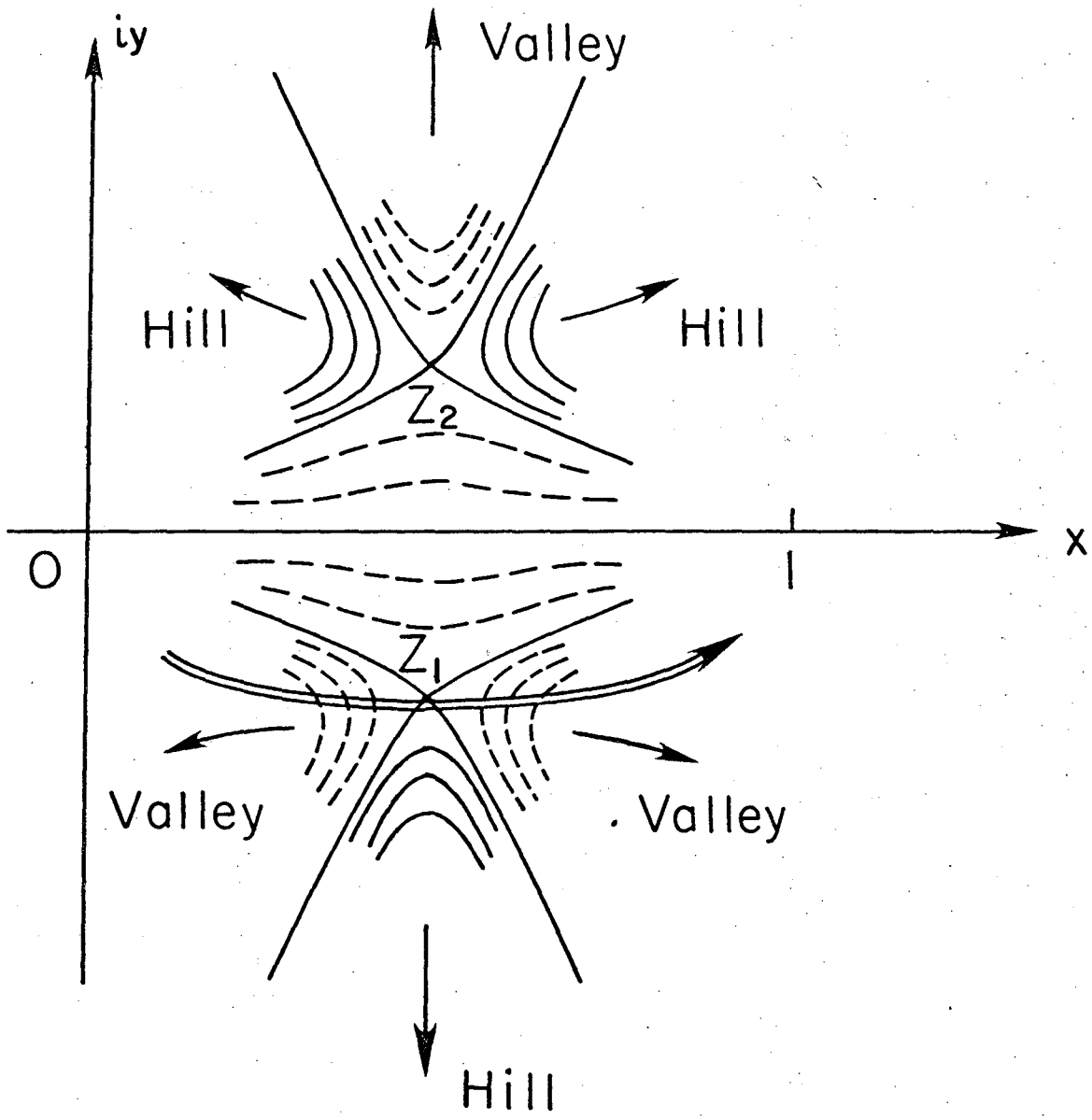

XBL759-4066

Fig. II-4 Same as Fig. II-3 but for the classically inaccessible case. The saddle points are now in the complex plane and the integration path goes only over one saddle (the lower one).

and minimum is not adequate, and that a better expansion would be a cubic expansion around the turning point. A still better way[16,20] is to map the phase f onto a cubic in such a way that the stationary points of f and the cubic correspond. In that case the mapping is uniformly analytic and one-to-one. The advantage of using the mapping procedure is that the results so obtained are valid for all cases, when the two saddle points are close together and far apart, and also for the case where $f(x)$ is a complex function.

Let the new variable y be implicitly defined by

$$f(z) = \frac{1}{3}u^3 - \xi u + A \equiv h(u) \tag{35}$$

The constants ξ and A are chosen so that the saddle points z_1 and z_2 of $f(z)$ correspond to the saddle points u_1 and u_2 of $h(u)$, that is

$$z_1 \longleftrightarrow u_1 = \sqrt{\xi} \tag{36a}$$

$$z_2 \longleftrightarrow u_2 = -\sqrt{\xi} \tag{36b}$$

one finds

$$2A = f_1 + f_2 \tag{37}$$

$$\frac{4}{3}\xi^{3/2} = f_2 - f_1 \tag{38}$$

After substituting eq. (35) into eq. (28) one finds for the integral

$$I \simeq e^{iA} \int_{-\infty}^{+\infty} du \left(\frac{dz}{du}\right) g(z)\, e^{i\left(-\xi u + \frac{1}{3}u^3\right)} \tag{39}$$

The symbol $\simeq$ is used because, as before, the limits of the integral were extended from $-\infty$ to $+\infty$. Only the region around the origin in u will contribute to the integral in eq. (39), so one may expand:

$$\frac{dz}{du}\, g(z) \simeq \alpha_o + \alpha_1 u \tag{40}$$

Using eq. (36) we find

$$\left(\frac{dz}{du}\right)_1 g_1 \simeq \alpha_o + \alpha_1 \sqrt{\xi}$$

$$\left(\frac{dz}{du}\right)_2 g_2 \simeq \alpha_o - \alpha_1 \sqrt{\xi}$$

from which

$$\alpha_o = \frac{1}{2}\left[\left(\frac{dz}{du}\right)_1 g_1 + \left(\frac{dz}{du}\right)_2 g_2\right] \tag{41a}$$

$$\alpha_1 = \frac{1}{2\sqrt{\xi}}\left[\left(\frac{dz}{du}\right)_1 g_1 - \left(\frac{dz}{du}\right)_2 g_2\right] \tag{41b}$$

The value of the derivatives in eq. (41) can be found by differentiating eq. (35) twice

$$f'(z) = (u^2 - \xi)\frac{du}{dz}$$

$$f''(z) = 2u\left(\frac{du}{dz}\right)^2 + (u^2 - \xi)\frac{d^2u}{dz^2}$$

For $z = z_1$, or z_2, one has from eq. (36) that $(u^2 - \xi) = 0$, therefore:

$$\left(\frac{dz}{du}\right)_1 = \left(\frac{2\sqrt{\xi}}{f_1''}\right)^{1/2} \tag{42a}$$

$$\left(\frac{dz}{du}\right)_2 = \left(\frac{-2\sqrt{\xi}}{f_2''}\right)^{1/2} \tag{42b}$$

Substituting the expansion (40) into eq. (39), one has for I

$$I \simeq e^{iA}\int_{-\infty}^{+\infty} du\,(\alpha_0 + \alpha_1 u)\, e^{i\left(-\xi u + \frac{1}{3}u^3\right)} \tag{43}$$

An integral representation of the regular Airy function is[23]

$$Ai(\lambda) = \frac{1}{2\pi}\int_{-\infty}^{+\infty} e^{i\left(\lambda u + \frac{1}{3}u^3\right)}\, du \tag{44a}$$

taking the derivative with respect to λ one has

$$Ai'(\lambda) = \frac{i}{2\pi}\int_{-\infty}^{+\infty} u\, e^{i\left(\lambda u + \frac{1}{3}u^3\right)}\, du \tag{44b}$$

Using eq. (44), eq. (43) becomes:

$$I = 2\pi e^{iA}\left[\alpha_0 Ai(-\xi) - i\alpha_1 Ai'(-\xi)\right] \tag{45}$$

The final expression for I is obtained if α_0 and α_1 in eq. (45) are replaced by their expression eq. (41) together with (42)

$$I \simeq \sqrt{2}\,\pi e^{\frac{i}{2}(f_1+f_2)}\left\{\left(\frac{g_1}{\sqrt{f_1''}}+\frac{g_2}{\sqrt{-f_2''}}\right)\xi^{1/4}\,Ai(-\xi)+\right.$$

$$\left.+(-i)\left(\frac{g_1}{\sqrt{f_1''}}-\frac{g_2}{\sqrt{-f_2''}}\right)\frac{1}{\xi^{1/4}}\,Ai'(-\xi)\right\} \qquad (46)$$

with (from eq. (38)

$$\xi^{1/2} = \left[\frac{3}{4}(f_2-f_1)\right]^{1/3} \qquad (47)$$

When using eq. (46), great care has to be taken to assure that one is on the correct branch when taking the square roots.

The mapping used in this section is one of many possibilities and in some cases a different mapping can give a better approximation. In chapter IV a different mapping will be used. The more general case in which three or more saddle points contribute to the integral (several of which could be close together or coinciding) has been investigated by Connor.[20] For the asymptotic evaluation of the multidimensional integrals for the S-matrix we refer to reference.[21]

Let us now apply the general result obtained in c) to the evaluation of The S-matrix for the case of one internal degree of freedom (this is the only case we will need in the next chapters). From the integral expression of the S-matrix (eq. (25)) one has for only one degree of freedom:

$$S_{\nu\mu} = \int_0^1 \sqrt{\frac{v^{(\nu)}}{v}} \left(\frac{dq}{dq^{(\mu)}} \right)^{-\frac{1}{2}} e^{\frac{i}{\hbar}\Delta} \, dq \tag{48}$$

with

$$\Delta = \left(\int_{t_o}^{t} K(t') \dot{R}(t') dt' - K_{n^{(\mu)}} R^{(o)} - K_{n^{(\nu)}} R \right) + \frac{\pi}{2} +$$

$$+ 2\pi \left(\int_{t_o}^{t} \dot{q}(t') n(t') dt' + n^{(\mu)} q^{(o)} - n^{(\nu)} q \right) \tag{49}$$

Integrating by parts one finds:

$$\Delta = -\int_{t_o}^{t} \dot{K}(t') R(t') dt' + \left(K(t) - K_{n^{(\nu)}} \right) R + \frac{\pi}{2} +$$

$$+ 2\pi \left(\left(n(t) - n^{(\nu)} \right) q - \int_{t_o}^{t} q(t') \dot{n}(t') dt' \right) \tag{50}$$

The saddle points are found from:

$$\frac{d\Delta}{dq} = 2\pi \left(n - n^{(\nu)} \right) = 0 \tag{51}$$

That is, only those trajectories for which the system after the interaction is in an internal state with quantum number $n^{(\nu)}$ will contribute. From eq. (50) one then has that, for the trajectories that contribute to the S-matrix, the phase Δ is

$$\Delta = \frac{\pi}{2} - \int_{t_o}^{t} \left(R(t')\dot{K}(t') + q(t')\dot{n}(t') \right) dt' \tag{52}$$

The second derivative of Δ can be found from eq. (51)

$$\frac{d^2\Delta}{dq^2} = 2\pi \frac{dn}{dq} \tag{53}$$

Applying the Airy Uniform Approximation (eq. (46)) to the S-matrix integral eq. (48) we find:

$$S_{\nu\mu} = \sqrt{\pi}\, e^{\frac{i}{2}(\Delta_1+\Delta_2)} \left\{ \left(\sqrt{P_1} + \sqrt{-P_2}\right) \xi^{1/4} Ai(-\xi) + \right.$$
$$\left. + (-i)\left(\sqrt{P_1} - \sqrt{-P_2}\right) \frac{1}{\xi^{1/4}} Ai'(-\xi) \right\} \tag{54}$$

where ξ and the "classical" probabilities p_j are given by

$$P_j = \frac{1}{\left(\frac{dn}{dq(\mu)}\right)_j} \qquad j = 1,2 \tag{55}$$

$$\xi^{1/2} = \left(\frac{3}{4}(\Delta_2 - \Delta_1)\right)^{1/3} \tag{56}$$

The excitation probability $P_{\nu\mu}$, which gives the probability of finding the system with internal quantum number $n^{(\nu)}$ after the interaction if initially it was $n^{(\mu)}$, is given by the absolute square modulus of the S-matrix element (eq. (54)).

In two important special cases the excitation probability takes a simple form:

i) If Δ and its derivatives are real for the two trajectories satisfying the boundary conditions, one finds

$$P_{\nu\mu} = \pi\sqrt{\xi}\left[\left(\sqrt{P_1}+\sqrt{-P_2}\right)^2 Ai^2(-\xi) + \left(\sqrt{P_1}-\sqrt{-P_2}\right)^2 \frac{Ai'^2(-\xi)}{\xi}\right] \qquad (57)$$

If in eq. (57) $Ai'^2(-\xi)/\xi$ is replaced by $Bi^2(-\xi)$, where Bi is the irregular Airy function, then one obtains the uniform approximation for the transition probability which was derived by Miller:[1]

$$P_{\nu\mu} = \pi\sqrt{\xi}\left[\left(\sqrt{P_1}+\sqrt{-P_2}\right)^2 Ai^2(-\xi) + \left(\sqrt{P_1}-\sqrt{-P_2}\right)^2 Bi^2(-\xi)\right] \qquad (58)$$

Only for large ξ does the second term in eq. (57) and (58) contribute significantly to the excitation probability (for small ξ the first terms dominate), but in this limit both expressions become equivalent. This can be seen from the asymptotic expressions for $Bi(-\xi)$ and $Ai'(-\xi)$ taken for large values of ξ.[23]

ii) If Δ and its derivatives are complex conjugate for the two trajectories satisfying the boundary conditions, one finds:

$$P_{\nu\mu} = 4\pi p\sqrt{|\xi|}\, Ai^2(|\xi|) \qquad (59)$$

where $p \equiv |p_1| = |p_2|$.

5) Summary

In order to solve a problem using the USCA method one has to perform

the following steps (for the case of one "macroscopic" and one "internal" coordinate):

i) Write down the Hamiltonian for the system using for the internal degree of freedom action-angle coordinates.

ii) Integrate (numerically) the exact classical equations of motion, subject to proper boundary conditions also evaluating along the classical trajectory the phase Δ for a set of initial values of the angle variable $q^{(\mu)}$. Find the "quantum number function", that is the value of $n(q^{(\mu)})$ (usually not an integer) obtained at the *end of the integration* as a function of the initial angle variable $q^{(\mu)}$.

iii) Find the initial orientations for which the quantum number function is equal to the final quantum number $n^{(\nu)}$. Find also the phase Δ and the derivatives $dn/dq^{(\mu)}$ for those trajectories.

iv) Evaluate $S_{\nu\mu}$ and $P_{\nu\mu}$.

All these steps will become clear when this procedure is carried out for the specific applications in the next chapters.

Let's summarize the main features of the USCA. In this semi-classical approximation the full classical dynamics of the problem is maintained (one is solving the exact classical equations of motion); that is, one does not introduce any explicit dynamical approximations. The quantum mechanical superposition principle is also included in this theory. One keeps the information of phase along the trajectory, and the contributions to the S-matrix of different trajectories satisfying the same boundary condition are not added incoherently but coherently. In other words,

for indistinguishable processes one adds probability amplitudes rather than probabilities. Since many intrinsically quantum effects, like the quantization or interference effects are a consequence of the superposition principle, many of these phenomena are at least qualitatively included in this semiclassical limit. Also, since in this theory one has to find classical trajectories which satisfy certain boundary conditions, Heisenberg's uncertainty principle is not violated. Several additional features of the USCA will come to light in the chapters to follow.

III BACKSCATTERING FROM A DEFORMED NUCLEUS

1) Introduction

In this chapter the application of the USCA to heavy-ion backscattering from a doubly even deformed target at energies below and up to the Coulomb barrier* will be considered. The type of collisions between a heavy-ion projectile (heavier than α particles) on a heavy deformed target range from elastic scattering and pure Coulomb excitation below the Coulomb barrier to one and multinucleon transfer and compound reactions for higher bombarding energies. At energies well below the Coulomb barrier, only the electromagnetic interaction between the two heavy-ions needs to be considered. At these low energies, the only important processes are elastic scattering and the Coulomb excitation of collective states of the target and projectile. In section 2 the Coulomb excitation of the rotational ground band of a doubly even deformed target will be considered. In later sections the modifications introduced by a nuclear potential will be included.

To insure that the projectile does not penetrate into the nucleus (for energies below the Coulomb barrier), one has to demand that the wave length λ of the projectile be much smaller than the distance of closest approach in a head-on-collision, i.e. that :

* For very heavy nuclei the Coulomb barrier does not always exist, since the Coulomb repulsion may be so strong that the nuclear force is not able to produce a Coulomb barrier. The energies we want to consider shall, in all cases, be low enough so that nucleon transfer and processes that occur at higher energies be neglibible.

$$\eta \equiv \frac{a}{\lambda\!\!\!^{-}} = \frac{Z_T Z_P e^2}{\hbar v} \gg 1 \qquad (1)$$

The parameter η is the so-called Sommerfeld parameter. In eq. (1) Z_T and Z_P are the charge numbers of the target and projectile respectively, v is the relative velocity in the asymptotic region and a is half the distance of closest approach in a head-on-collision (for a pure monopole-monopole interaction), i.e.

$$a = \frac{Z_T Z_P e^2}{m v^2} \qquad (2)$$

where m is the reduce mass of the system. For heavy-ion collisions with bombarding energies such that the distance of closest approach is larger than the sum of the radii of the target and projectile, i.e.

$$2a > r_0 \left(A_T^{1/3} + A_P^{1/3} \right) \qquad \cdot \left(r_0 \simeq 1.2 \text{ Fm} \right) \qquad (3)$$

one has that the inequality eq. (1) is always satisfied. N. Bohr[25] has shown that if $\eta \gg 1$, the collision may then be approximately described by considering the system as moving along a classical trajectory. The parameter η is a measure of the strength of the monopole-monopole interaction. If $\eta \gg 1$, the classical orbit will be very close to the hyperbolic orbit the system would follow if only the monopole-monopole interaction were present.

In this chapter we will restrict the analysis to backward scattering

only (this will introduce a great simplification in the geometry of the problem). This is not of pure academic interest, since in Coulomb excitation experiments one usually measures at backward scattering angles since at those angles the excitation probability of high spin states is highest (as long as the center-of-mass is below the Coulomb barrier). Table III 1 hows the excitation probability P(I) for multiple Coulomb excitation of the ground rotational band of ^{238}U with the reaction $^{40}Ar + ^{238}U$ for the laboratory bombarding energies of 170 MeV and 200 MeV. The calculations were done using the semi-classical de Boer-Winther code[15] for multiple Coulomb excitation (see Appendix A). The second and third column in Table III 1 show the results for the cases where the projectile is scattered to the center-of-mass scattering angles $\theta_{CM} = 180°$ and $\theta_{CM} = 165°$ respectively. The difference between the excitation probability for these two angles is small compared to the variations of the excitation probability with spin, and therefore excitation probabilities at 180° are useful to interpret experimental results at backscattering angles. Figure III 1 shows graphically the excitation probability for the various final spin states of the target for the two scattering angles. A systematical improvement is obtained if the bombarding energy is adjusted in such a way that the classical turning point of the trajectories occur at the same distance*. Column four in Table III 1 shows the excitation probability at $\theta_{CM} = 165°$ for an energy such that the truning point is the same as the turning point for the calculations at $\theta_{CM} = 180°$ shown in

*The distance of closest approach for a hyperbolic orbit of excentricity ε is given by (see appendix A) $r_{ca} = a\ (1 + \varepsilon)$. Using the relation $\varepsilon = 1/\sin\ (\theta_{cn}/2)$ we find how the bombarding energies for the two trajectories whose scattering angles are 180° and θ_{cn} have to be related to give the same turning point:

Table III 1. Probability to excite a rotational state of angular momentum I calculated with the de Boer - Winther code for $^{40}Ar + ^{238}U$ with $Q_o^{(2)}$=11.12 eb and $Q_o^{(4)}$= 0.0 eb^2.

I	E_{lab} = 170 MeV θ_{cm} = 180° E_I = exp.	E_{lab} = 170 MeV θ_{cm} = 165° E_I = exp.	E_{lab} = 170.733 MeV θ_{cm} = 165° E_I = exp.	E_{lab} = 170 MeV θ_{cm} = 180° E_I = rotational formula
0	0.07407	0.07654	0.07521	0.07401
2	0.17104	0.17089	0.17100	0.17135
4	0.05737	0.06448	0.05528	0.05797
6	0.17766	0.10540	0.18770	0.18048
8	0.29148	0.29121	0.29170	0.29362
10	0.16783	0.15769	0.16231	0.16581
12	0.05006	0.04483	0.04717	0.04756
14	0.009186	0.007888	0.008470	0.008158
16	0.001139	0.000941	0.001030	0.000911
18	0.000102	0.000082	0.000091	0.000071
20	0.000007	0.000005	0.000006	0.000004

I	E_{lab} = 200 MeV θ_{cm} = 180° E_I = exp.	E_{lab} = 200 MeV θ_{cm} = 165° E_I = exp.	E_{lab} = 200.863 MeV θ_{cm} = 180° E_I = exp.	E_{lab} = 200 MeV θ_{cm} = 180° E_I = rotational formula
0	0.08550	0.08434	0.08456	0.08498
2	0.05809	0.06134	0.05967	0.05826
4	0.14832	0.15158	0.15037	0.14916
6	0.06170	0.05305	0.05642	0.06229
8	0.08977	0.10628	0.09892	0.09329
10	0.23935	0.24745	0.24428	0.24374
12	0.20190	0.10286	0.19709	0.22050
14	0.08734	0.07877	0.08261	0.08301
16	0.02345	0.02017	0.02162	0.02080
18	0.00443	0.00364	0.00399	0.00358
20	0.000642	0.000508	0.000568	0.000416

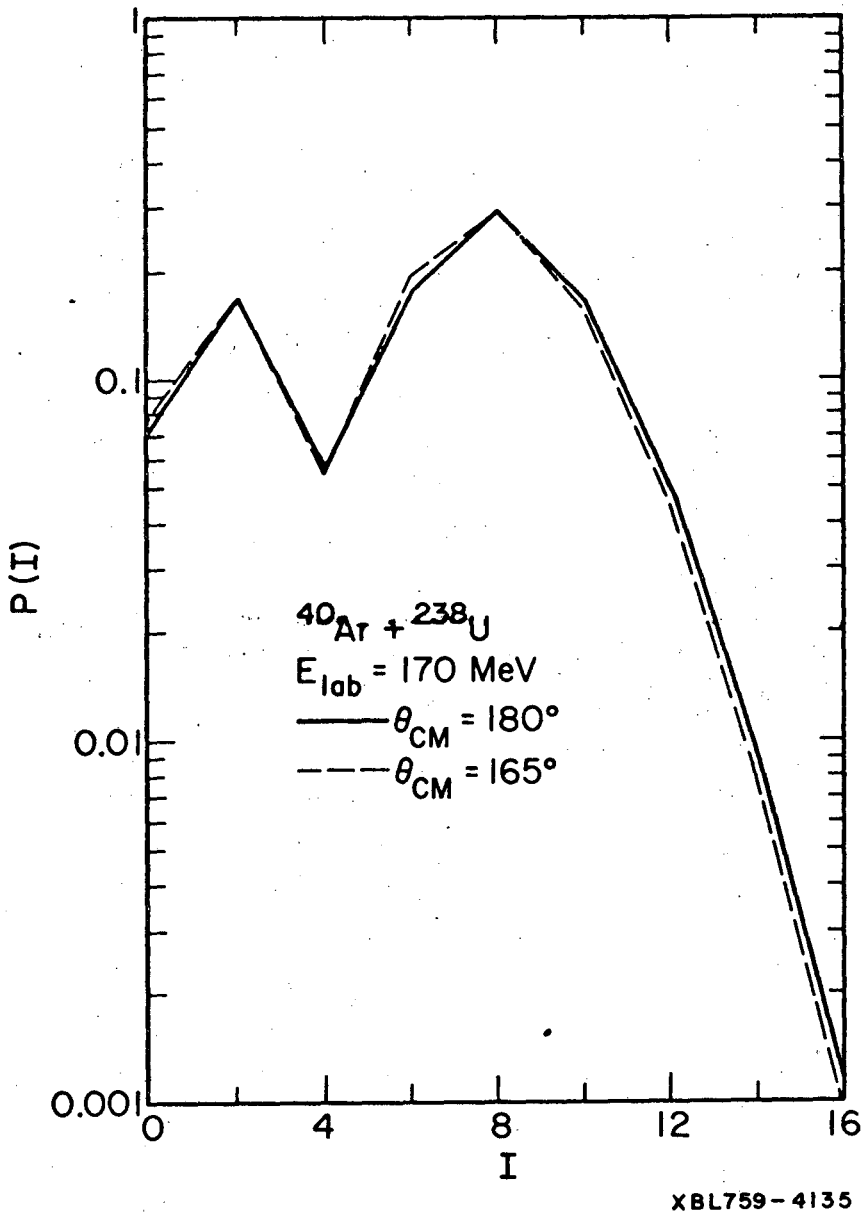

Fig. III-1 Probability to excite rotational states of angular momentum I, calculated with the de Boer-Winther code for $^{40}Ar + ^{238}U$ at E_{lab} = 170. MeV, ($Q_o^{(2)}$ = 11.12eb^2, $Q_o^{(4)}$ = 0. Shown are the results at two different scattering angles Θ_{CM} = 180° (solid line) and Θ_{CM} = 165° (dashed line). The similarity is even more striking if the bombarding energy is adjusted so that for both calculations the turning points are the same (see Table III 1).

the second column. The agreement is now better by at least a factor two.

Since the scattering angle, and therefore the exact initial orbital angular momentum is not so critical in the heavy-ion scattering case (as long as the scattering angle is in the backward direction), we chose here the case for which the problem simplifies considerably; namely, we consider the case in which the projectile moves in on the target with zero impact parameter. In this case, classically the collision takes place in a plane (defined by the projectile position and the symmetry axis of the target), and only two degrees of freedom are relevant. Therefore, one can use the USCA method to solve a much simpler problem, the backscattering from a planar rotor. Afterwards, by properly weighting the probability amplitudes (see section III2d), we then obtain the excitation probabilities for the backscattering from a three dimensional rotor.

Independently, a similar application to Coulomb excitation of the USCA method was done by Levit, Smilansky and Pelte.[25] However there are several significant differences between their and our approach which will be indicated in due time.

2) The USCA applied to multiple Coulomb excitation

a) The Hamiltonian and the classical equations of motion

We will now follow the steps outlined in section II 5 in applying the USCA to the problem of backscattering problem from deformed nuclei.[26] As already mentioned in the introduction, we will consider only the case in which the projectile moves in on the target with zero impact parameter. In this case, the problem reduces classically to a two-dimensional problem. Figure III 2 shows the geometry of the problem. Let the z-axis

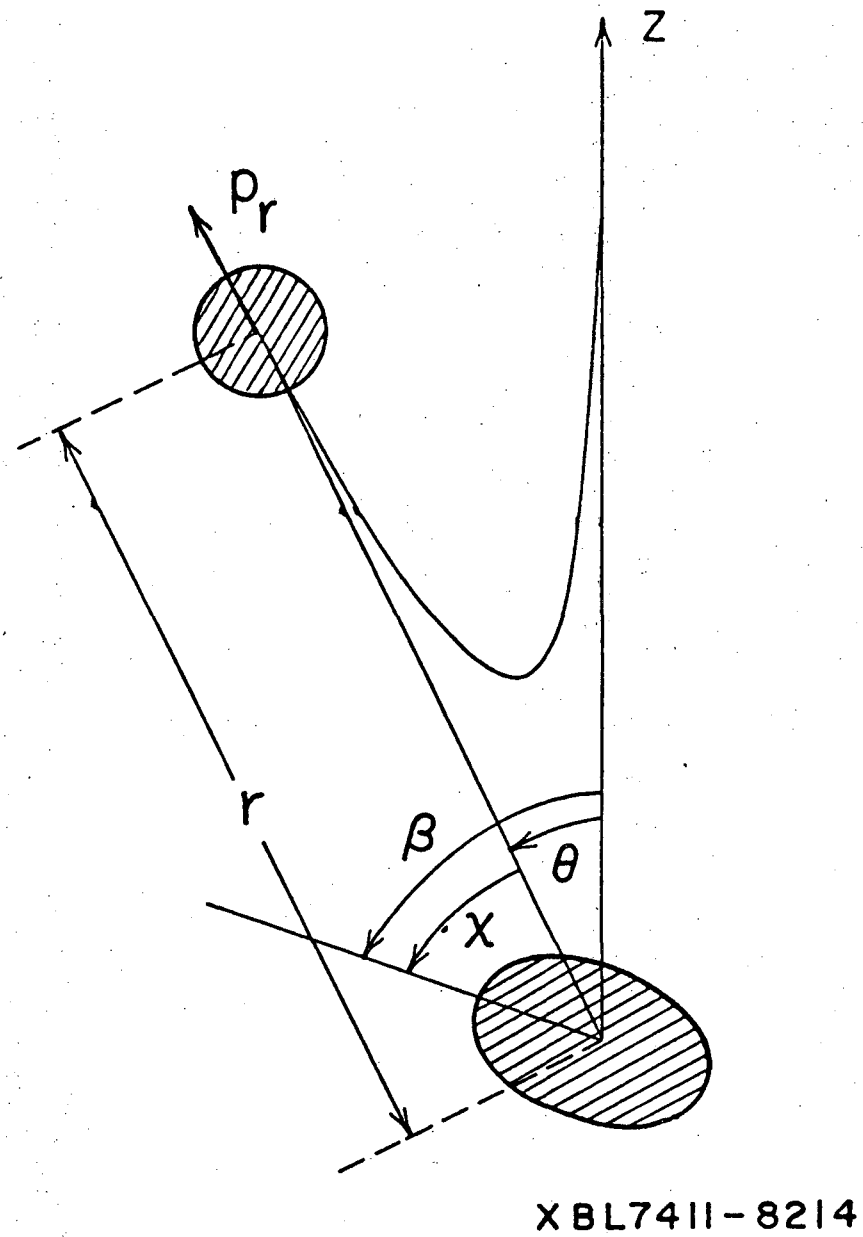

Fig. III-2 Diagram showing the geometry for the projectile-target system.

be the initial beam axis and let θ and β be the azimuthal angles of the projectile and the symmetry axis of the target respectively. It is convenient to introduce the angles (see Fig. III 2)

$$\chi \equiv \beta - \theta \tag{22a}$$

$$\gamma \equiv \beta + \theta \tag{22b}$$

If r is the distance between the nuclear centers and p_r, p_χ, p_γ are the canonically conjugate momenta to the generalized coordinates r, χ, γ then we can write the classical Hamiltonian for the system as:

$$H(r,\chi;p_r,p_\chi) = \frac{p_r^2}{2m} + p_\chi^2\left(\frac{1}{2mr^2} + \frac{1}{2\mathcal{I}}\right) + \frac{Z_T Z_p e^2}{r} + \frac{Z_p e^2 Q_o^{(2)}}{2r^3} P_2(\cos\chi) \tag{23}$$

Here we have explicitly made use of the fact that $\ell_{in} = 0$ and that initially the rotational angular momentum of the target is zero (ground state of an even-even nucleus), i.e. that the total angular momentum of the system is zero. In the expression for the Hamiltonian, m is the reduced mass of the target-projectile system, $\mathcal{I}$ is the nuclear moment of inertia of the target, Z_T, Z_p are the charge numbers of the target and projectile, respectively, and $Q_o^{(2)}$ is the intrinsic quadrupole moment of the target. This Hamiltonian does not take into account any interaction between the target and the projectile due to the nuclear force nor any higher electric and magnetic multipole moments. Also we are not taking

into account any excitation of the projectile nor any excitation of the target besides the excitation of the collective rotational degree of freedom. The intrinsic electric moments $Q_o^{(\lambda)}$ are defined by:

$$Q_o^{(\lambda)} = \sqrt{\frac{16\pi}{2\lambda+1}} \frac{\mathcal{M}(E\lambda,0)}{e} \tag{24}$$

where $\mathcal{M}(E\lambda,\mu)$ is given by

$$\mathcal{M}(E\lambda,\mu) = \int r^{\lambda} Y_{\lambda\mu}(\theta,\phi)\, \rho(\vec{r})\, d^3r \tag{25}$$

In writing the Hamiltonian (eq.(23)) it was also assumed that the target nucleus is a perfect quantum mechanical rotor. In Table III 1 the excitation probability is also shown for the case where instead of the experimental energy levels, the energy levels given by the rotational formula

$$E_I = \frac{E_2}{6} I(I+1) \tag{26}$$

(E_2 being the experimental energy of the I = 2 member of the ground rotational band) are used in the de Boer-Winther code. Except for the highest spins, the difference is negligible. Still, when comparing the USCA results to the results using the conventional semiclassical method, we will use in the de Boer-Winther code the same energy levels as in the USCA, that is, the energy levels given by the rotational formula eq. (26).

The Hamiltonian depends only on two coordinates (r, the distance between the centers of the target and the projectile and χ, the angle

between the projectile and the target's symmetry axis) and their canonically conjugate momenta. The canonically conjugate variables χ and p_χ actually are not action-angle variables for this problem, since the angle variable lies not in the interval $[0,1]$ but $[0,2\pi]$. The action-angle variables are proportional to χ and p_χ, the angle variable being $q = \chi/2\pi$, and the action variable being $J = 2\pi p_\chi$. We will however use χ and p_χ, because they are more convenient, keeping in mind the relations to the action-angle variables when using formulas from chapter II. The four equations of motion are*

$$\dot{r} = p_r/m \tag{27a}$$

$$\dot{p}_r = \frac{p_\chi^2}{m r^3} + \frac{Z_T Z_p e^2}{r^2} + \frac{3 Z_p e^2 Q_0^{(2)}}{2 r^4} P_2(\cos\chi') \tag{27b}$$

$$\dot{\chi} = \left(\frac{1}{m r^2} + \frac{1}{\mathcal{I}}\right) p_\chi \tag{27c}$$

$$\dot{p}_\chi = -\frac{Z_p e^2 Q_0^{(2)}}{2 r^3} \frac{\partial}{\partial \chi} P_2(\cos\chi) \tag{27d}$$

If one is interested in the angles β and θ, then the value of γ is needed, and it can be found by integrating

$$\dot{\gamma} = \left(-\frac{1}{m r^2} + \frac{1}{\mathcal{I}}\right) p_\chi \tag{27e}$$

*The work of Levit et al.[25] differs at this point from our approach in that they constrain the projectile to move on a straight line, therefore in their work the total angular momentum is not conserved.

Another quantity of interest is the phase Φ. The phase Φ is related to the phase Δ of (eq. II 52) through $\Phi = \Delta - \pi/2$ that is:

$$\Phi = -\frac{1}{\hbar}\int_{t_i}^{t_f}\left(r\dot{P}_r + \chi\dot{P}_\chi\right)dt \tag{28}$$

The differential equation for Φ is therefore

$$\dot{\Phi} = -\frac{1}{\hbar}\left(r\dot{P}_r + \chi\dot{P}_\chi\right) \tag{29}$$

The eqs. (25) have to be integrated numerically with the initial conditions:

$$r_i = \text{large} \tag{30a}$$

$$P_{r_i} = \sqrt{2m\left(E_{cm} - \frac{Z_p Z_T e^2}{r_i}\right)} \tag{30b}$$

$$\chi_i = \beta_o \quad \text{(arbitrary)} \tag{30c}$$

$$\gamma_i = \beta_o \tag{30d}$$

$$P_{\chi_i} = 0 \tag{30e}$$

$$\Phi_i = 0 \tag{30f}$$

The initial distance, r_i, was taken to be 40 times the distance of

closest approach. The quantity p_χ is the classical angular momentum of the target; the rotational energy of the planar rotor is given (classically) by:

$$E = \frac{p_\chi^2}{2\mathcal{I}} \tag{31}$$

b) The excitation probability

Integrating the equations of motion with the initial condition $\chi_i = \beta_o$ for several values of β_o, the "quantum number" function $\hat{I}(\beta_o)$ is found, where $\hat{I}$ is the value of $p_\chi/\hbar$ after the integration.

Initially the target is in the ground state, I = 0; we want to find the excitation probability $P(I) = P_{I\leftarrow 0}$, that is, the probability of finding the target in a rotational state with angular momentum I after the integration. In order to find the trajectories which contribute to the S-matrix, we have to find the trajectories for which, after the integration, the angular momentum of the target is I. In other words, we have to find the orientations of the target before the interaction (the so-called "initial orientations") which leave the target after the interaction with spin I. These initial orientations are found by solving for the roots of the equation

$$\hat{I}(\beta_o) = I \tag{32}$$

For a typical case, $^{40}Ar + ^{238}U$ at E_{lab} = 170.0 MeV, the quantum number function $\hat{I}(\beta_o)$ is shown in Fig. III 3. For β_o = 0° and 90°, $\hat{I}(\beta_o)$ goes through zero, since for those initial orientations no torque will

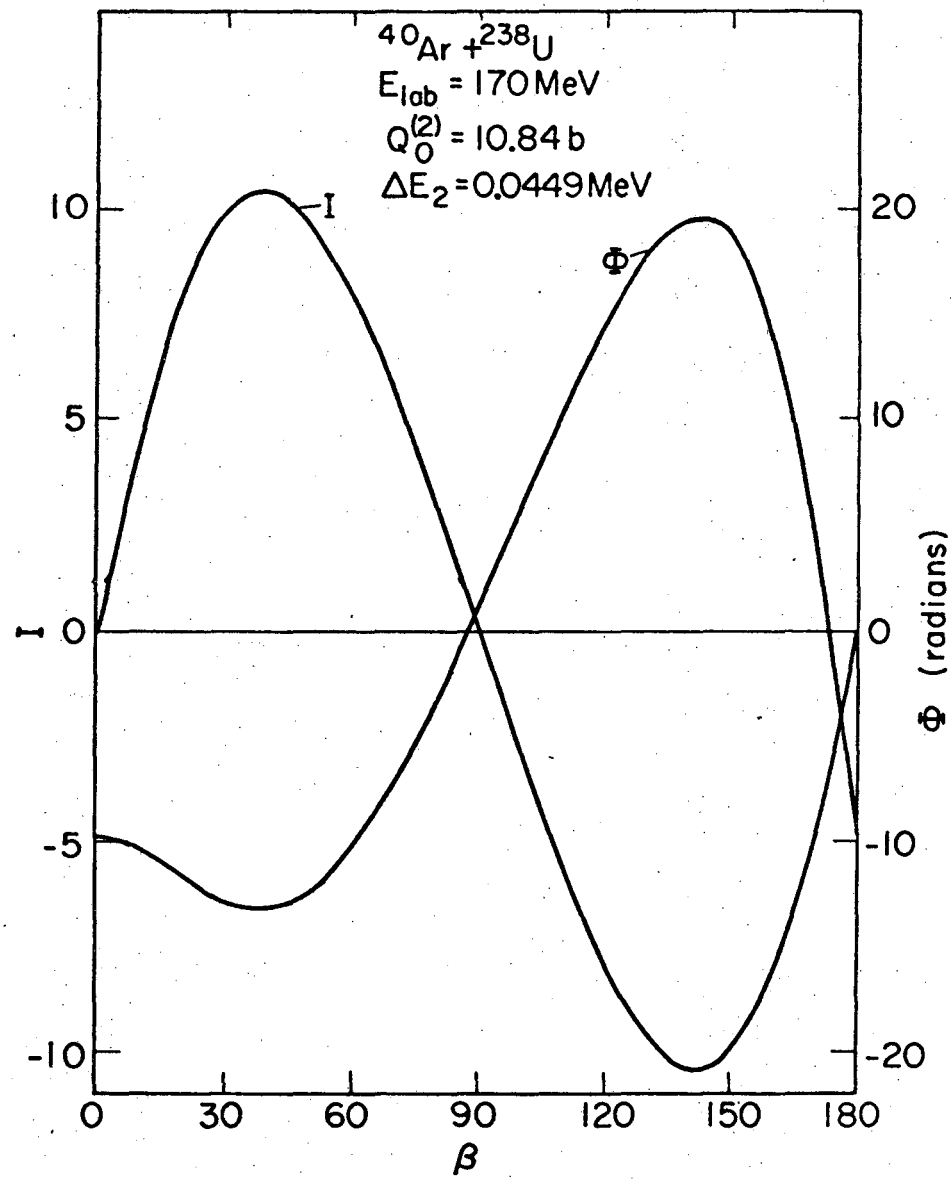

Fig. III-3 Graphs of the quantum number function $\hat{I}(\beta_\infty)$ and the phase $\Phi(\beta_\infty)$ for the case $^{40}Ar + ^{238}U$ at E_{lab} = 170 MeV.

act on the target (remember that the projectile is moving in with zero impact parameter and that initially the planar rotor is not rotating). Let's note also that $\hat{I}(\beta_0)$ is a periodic function with period π, since the force from a monopole-quadrupole potential has this periodicity. Fig. III 3 also shows the final value of the phase Φ as a function of the initial orientation angle (for convenience a large constant value Φ_0 was subtracted; this has no physical consequence since an overall phase in the S-matrix is not observable). The function $\Phi(\beta_0)$ is not a periodic function. From eq. (28) we find

$$\Phi(\beta_0+\pi) = -\frac{1}{\hbar}\int_{t_i}^{t_f}\left(r\dot{p}_r + (\chi+\pi)\dot{p}_\chi\right)dt$$

$$= \Phi(\beta_0) - \frac{1}{\hbar}\pi\int_{t_i}^{t_f}\dot{p}_\chi\,dt$$

$$= \Phi(\beta_0) - \frac{\pi}{\hbar}\left[p_{\chi_f}(\beta_0) - p_{\chi_i}(\beta_0)\right] \qquad (33)$$

Since the initial orientations β_0 and $\beta_0+\pi$ are physically equivalent, one must have for the trajectories which contribute to the S-matrix that the phases $\Phi(\beta_0)$ and $\Phi(\beta_0+\pi)$ be equivalent, that is, they should differ at most by an integer times 2π. From eq. (33) one finds that for the physically acceptable trajectories

$$\frac{1}{\hbar}\left(p_{\chi_f} - p_{\chi_i}\right) = I_f - I_i = \Delta I = \text{even integer} \qquad (34)$$

We find that the symmetry of the problem introduces selection rules. Selection rules, as can be seen from this example, are naturally included

in the USCA.

Let $\hat{I}_{max}$ be the maximum of $\hat{I}(\beta_o)$, for $|I| < \hat{I}_{max}$ one has that in the interval $[0, \pi]$ there are always two real solutions to equation (32). Let us call them β_1 and β_2. Since $\hat{I}(\beta_o)$ is periodic with period π one also has that $\beta_1+\pi$ and $\beta_2+\pi$ are also solutions. The primitive semiclassical expression for the S-matrix is (see eq. II 31)

$$S = \sum_j A_j e^{i\Phi_j} \tag{35}$$

where A_j is a preexponential factor; the index j goes over all the solutions of equation (32) in the interval $[0, 2\pi]$. There are two pairs of solutions of eq. (32), ($\beta_1, \beta_1+\pi$) and ($\beta_2, \beta_2+\pi$). The solutions of each pair have the same pre-exponential factor A in the expression for the S-matrix. One finds (using eq. (33)):

$$S = A_1\left(e^{i\Phi_1} + e^{i(\Phi_1 - \pi\Delta I)}\right) + A_2\left(e^{i\Phi_2} + e^{i(\Phi_2 + \pi\Delta I)}\right)$$

$$= \left(A_1 e^{i\Phi_1} + A_2 e^{i\Phi_2}\right)\left(1 + e^{-i\pi\Delta I}\right) \tag{36}$$

Also from eq. (35) it is clear that ΔI has to be an even integer.

The function $\hat{I}(\beta_o)$ has also the symmetry $\hat{I}(\beta_o) = -\hat{I}(\beta_o - \pi)$, since the quadrupole potential has this symmetry. Therefore when finding the roots of $\hat{I}(\beta_o) = I$, we also find the initial orientations $\bar{\beta}_o$, for which $\hat{I}(\bar{\beta}_o) = -I$. A negative value of I just means that the rotor is turning in the opposite direction. In a three-dimensional symmetric

rotor, the angular momentum quantum number I is always zero or an even positive integer; a rotation in the opposite direction manifests itself through the fact that the projection M of I on the axis perpendicular to the scattering plane has the opposite sign (that is, has a different quantum number). In the two dimensional case one does not have the quantum number M, and a rotation in the opposite direction manifests itself by the change of the sign of I. Therefore, when evaluating the excitation probability P_I of finding the system in a state with angular momentum I ($I = 0$ or positive even integer), one also has to include in the analysis the roots of $\hat{I}(\beta_0) = -I$, but since they correspond to a different physical situation, their contribution to the excitation probability is not added coherently with the contribution from the roots of $\hat{I}(\beta_0) = I$. In other words, we may restrict the analysis of the problem to the interval $[0, \pi/2]$ and multiply the excitation probability at the end by 2, or the S-matrix by $\sqrt{2}$. This $\sqrt{2}$ together with the factor 2 due to the reflection symmetry of the target (see eq. (36)) gives the factor $\sqrt{8}$ by which we have to multiply the S-matrix if we restrict ourselves to the interval $[0, \pi/2]$. In actual calculations the uniform semiclassical S-matrix (eq. II 54) will be used, but in order to gain some physical insight, the primitive semiclassical S-matrix is useful and will be considered briefly.

For $I < \hat{I}_{max}$ eq. (32) has two real solutions in the interval $[0, \pi/2]$. Let's call the two roots β_1 and β_2. Since also the phases Φ_1 and Φ_2 corresponding to these roots are also real, we can use the results of section II 4a to write the primitive expression for the S-matrix (see eq. II 31):

$$S = i\sqrt{\frac{8}{2\pi}}\left\{\sqrt{\left(\frac{\partial^2\Phi}{\partial I_i \partial I_f}\right)_1}\, e^{i\left(\Phi_1 + \frac{\pi}{4}\right)} + \sqrt{-\left(\frac{\partial^2\Phi}{\partial I_i \partial I_f}\right)_2}\, e^{i\left(\Phi_2 - \frac{\pi}{4}\right)}\right\} \tag{37}$$

In deriving eq. (37) the relation between I and action variable J, $J = 2\pi\hbar I = 2\pi p_\chi$, was used (see eq. II 6). The phase Φ is given by eq. (26). Writing it in a different form, we have

$$\Phi = -\frac{1}{\hbar}\int_{t_i}^{t_f} r\,\dot{p}_r\, dt - \int_{I_i}^{I_f} \chi\, dI \tag{38}$$

From eq. (38) the derivative $\partial\Phi/\partial I_i$ can be evaluated

$$\frac{\partial\Phi}{\partial I_i} = \chi_i = \beta_o \tag{39}$$

Introducing the definition

$$P_\kappa \equiv \frac{8}{2\pi}\left(\frac{\partial^2\Phi}{\partial I_i \partial I_f}\right)_\kappa = \frac{4}{\pi\left(\frac{\partial I_f}{\partial \beta_o}\right)_\kappa} = \frac{4}{\pi}\left(\left(\frac{\partial \hat{I}(\beta_o)}{\partial \beta_o}\right)_\kappa\right)^{-1} \quad (\kappa = 1,2) \tag{40}$$

one can write the S-matrix in a more useful way

$$S_{I\leftarrow 0}(E) = i\left\{\sqrt{|P_1|}\, e^{i\left(\Phi_1 + \frac{\pi}{4}\right)} + \sqrt{|P_2|}\, e^{i\left(\Phi_2 - \frac{\pi}{4}\right)}\right\} \tag{41}$$

where the root 1 is the one for which $(\partial \hat{I}(\beta_o)/\partial\beta_o) > 0$. For I = 0, the evaluation of the S-matrix integral equation by the stationary phase method (as in chapter II) has to be modified slightly. The problem is

that in this case the stationary phase points are at the extremes of the interval of integration. As one might guess, in this case the result has to be divided by 2. This is related closely to the fact that for a planar rotor the "space" of initial orientations leading to I = 0 is half as large than for I ≠ 0. The meaning of this statement will become clearer in the next section.

From the S-matrix (eq. (41)) one obtains the primitive excitation probability for backward scattering angles:

$$P_{prim}(I) = \left| S_{I \leftarrow 0}(E) \right|^2 = |P_1| + |P_2| + 2\sqrt{|P_1 P_2|}\sin(|\Delta\Phi|) \qquad (42)$$

where

$$\Delta\Phi = \Phi_2 - \Phi_1 \qquad (43)$$

If $I > \hat{I}_{max}$, then eq. (32) has no real solutions, and one says that the spin I is classically inaccessible or that the transition is classically forbidden. There are, of course, complex solutions of $\hat{I}(\beta_o) = I$ for $I > \hat{I}_{max}$. All the solutions will come in pairs; if β is a solution then β^* will also be a solution. Let's consider only the pair $(\beta_1, \beta_2 = \beta_1^*)$ of solutions which lie closest to the real axis. Since in this problem the interaction potential is a real potential, one also has $\Phi_2 = \Phi_1^*$ and all its derivatives at the stationary phase points β_1, β_2 are complex conjugates of each other. We are therefore in the situation described in section II4b. If the root 1 is the root for which $Im(\Phi) = Im(\Phi_R + i\Phi_I) = \Phi_I$ is positive, one obtains for the primitive S-matrix

$$S_{I\leftarrow O}(E) = i\sqrt{|p|}\, e^{i\Phi_R} e^{-\Phi_I} \tag{44}$$

Since p_1 and p_2 are complex conjugates $|p_1| = |p_2| \equiv p$. The primitive excitation amplitude is then

$$P_{prim}(I) = |p| e^{-2\Phi_I} \tag{45}$$

For very forbidden transitions, Φ_I will be very large and from eq. (45) it follows that the excitation probability will be exponentially vanishing. For this reason, other pairs of roots with larger imaginary parts may be ignored. In chapter II we found that only one saddle point contributes to the S-matrix in the classically forbidden case. If the other would contribute, it would give an exponentially increasing contribution to the S-matrix for more and more forbidden transitions. This, of course, would be physically unacceptable.

According to the theory in chapter II, there is no reason to exclude the cases where the stationary phase points are in the complex plane. So there are no reasons for not considering complex initial orientations. According to general quantum mechanical principles, only observables must be real; all other variables may be complex. The initial orientation of the target is not an observable and therefore may be complex. In order to find the classically forbidden transitions, one has to start the integration with complex initial orientations. Continuing analytically the potential and the equations of motion into the complex plane, the

now complex trajectory that the system traces is found. All the variables become complex during the integration. Since one will observe the projectile at a real distance from the target, r should be real. This is easily achieved by moving the time path in the asymptotic region from the real time axis into the complex plane, that is by using, after the interaction has taken place, complex time increments until r becomes real. In the asymptotic region, since there is no coupling between the two degrees of freedom, the angular momentum I of the target will be a constant of motion and so an excursion of the time path during the integration into the complex time plane will not affect it.

As already mentioned in chapter II, the primitive expressions for the excitation probabilities fail if the two stationary points are close together, i.e. if I is close to $\hat{I}_{max}$ or equivalently if $\Delta\Phi$ is small. In this case the uniform expressions have to be used. Using the results of section 114c we find

$$P_{unif}(I) = \pi\sqrt{\xi}\left[\left(\sqrt{|P_1|}+\sqrt{|P_2|}\right)^2 Ai^2(-\xi) + \left(\sqrt{|P_1|}-\sqrt{|P_2|}\right)^2 Bi^2(-\xi)\right] \qquad I \leq \hat{I}_{max} \tag{46}$$

$$P_{unif}(I) = 4\pi|P|\sqrt{|\xi|}\,Ai^2(|\xi|) \qquad I \geq \hat{I}_{max} \tag{47}$$

with ξ defined by

$$\xi = \left(\frac{3}{4}|\Delta\Phi|\right)^{2/3} \tag{48}$$

If the transition is not too forbidden and if the function $\hat{I}(\beta_o)$ can be represented by a parabola around its maximum $\hat{I}_{max}$, then it is possible to sidestep all the complications of integrating complex trajectories with complex initial orientations for the classically forbidden transitions by Taylor expanding about the extremum.[2] Approximating $\hat{I}(\beta_o)$ as a quadratic and Φ as a cubic about β_{max}, one finds the following approximate expression for the excitation probability (for the classically forbidden transitions)

$$P_{unif}(I) \simeq 4 \frac{Ai^2\left(\frac{I-\hat{I}_{max}}{A}\right)}{A^2\left|\left(\frac{\partial \bar{\chi}_f}{\partial \beta_o}\right)_{\beta_o=\beta_{max}}\right|} \tag{49}$$

with A and $\bar{\chi}_f$ defined by

$$A \equiv \left\{\left(\frac{\partial^2 \hat{I}(\beta_o)}{\partial \beta_o^2}\right) \Big/ \left(2\left(\frac{\partial \bar{\chi}_f}{\partial \beta_o}\right)^2\right)\right\}^{1/3}_{\beta_o=\beta_{max}} \tag{50}$$

$$\bar{\chi}_f \equiv -\frac{\partial \Phi}{\partial I_f} = -\frac{m\hbar}{\mathcal{I}}\left(\frac{rI}{P_r}\right)_f + \chi_f \tag{51}$$

c) Backscattering from a three-dimensional rotor.

So far the problem considered has been the backscattering from a rotor in two dimesnions (2D). In this subsection we will show how to modify the previous equations so that they correspond to the three dimensional (3D) backscattering from a rotor, without integrating the full three dimensional equations of motion.

The energy levels of a quantum mechanical rotor in 3D are given by

$$E_I = \frac{\hbar^2}{2\mathcal{I}} I(I+1) \tag{52}$$

Using eq. (31), one would like to make the identification

$$P_\chi = \hbar \sqrt{I(I+1)} \tag{53}$$

but this generates a small problem. From eq. (34) one has that the quantity $P_\chi/\hbar$ has to differ by an integer for different quantum states. The identification eq. (53) does not satisfy this criterion and therefore has to be abandoned. The next best suggestion, and the one adopted here, is to make the usual semiclassical identification

$$P_\chi = \hbar\left(I + 1/2\right) \tag{54}$$

which also gives the correct energy spacings when using eq. (31). Therefore, one of the modifications that has to be introduced in the generalization to 3D is to look for roots of the equation

$$\hat{I}(\beta_o) = I + 1/2 \tag{55}$$

where I is, as before, an even integer, and $\hat{I}(\beta_o)$ is the quantum number function of the 2D planar rotor.

Even though one uses the identification equation (54), we will use equation (52), to find the moment of inertia $\mathcal{I}$ of the target, that is

$$\mathcal{I} = \frac{3\hbar^2}{E_2} \tag{56}$$

where E_2 is the energy of the first excited rotational state of the target.

In order to find out how to modify the p's (defined in eq. (40)) for the 3D case, it is useful to consider the 2D case in more detail.

In the 2D case one has for $I \neq 0$ that

$$|P_1| \equiv \frac{2}{\frac{\pi}{2}\left|\left(\partial \hat{I}(\beta_0)/\partial\beta_0\right)_1\right|} \simeq \frac{|\beta_1^< - \beta_1^>|}{\frac{\pi}{2}} \tag{57}$$

where $\beta_1^<$ and $\beta_1^>$ are defined in Fig. III 4. Now the physical meaning of eq. (41) for the primitive expression of the excitation probability P(I) becomes very clear. The quantity p_1 has a geometrical meaning; it is the probability that the initially randomly oriented target has an initial orientation β_0 such that the angular momentum of the target after the interaction $\hat{I}(\beta_0) = p_x/\hbar$ is in the interval [I-1, I+1]. There are two such groups of initial orientations. The excitation probability is then given by the probability that the initial orientation angle is in one of the groups, plus a term describing their interference.

In the 3D case, we will denote the p's with a bar on top. In an analogous way to the 2D case, the p's in the 3D case will approximately be the probability that the initial azimuthal angle of the rotor is such that the angular momentum of the target $\hat{I}(\beta_0) = p_x/\hbar$ after the interaction be in the interval $[\, I-1+\tfrac{1}{2}\,,\ I+1+\tfrac{1}{2}\,]$ (see also eq. (54)). We find (see

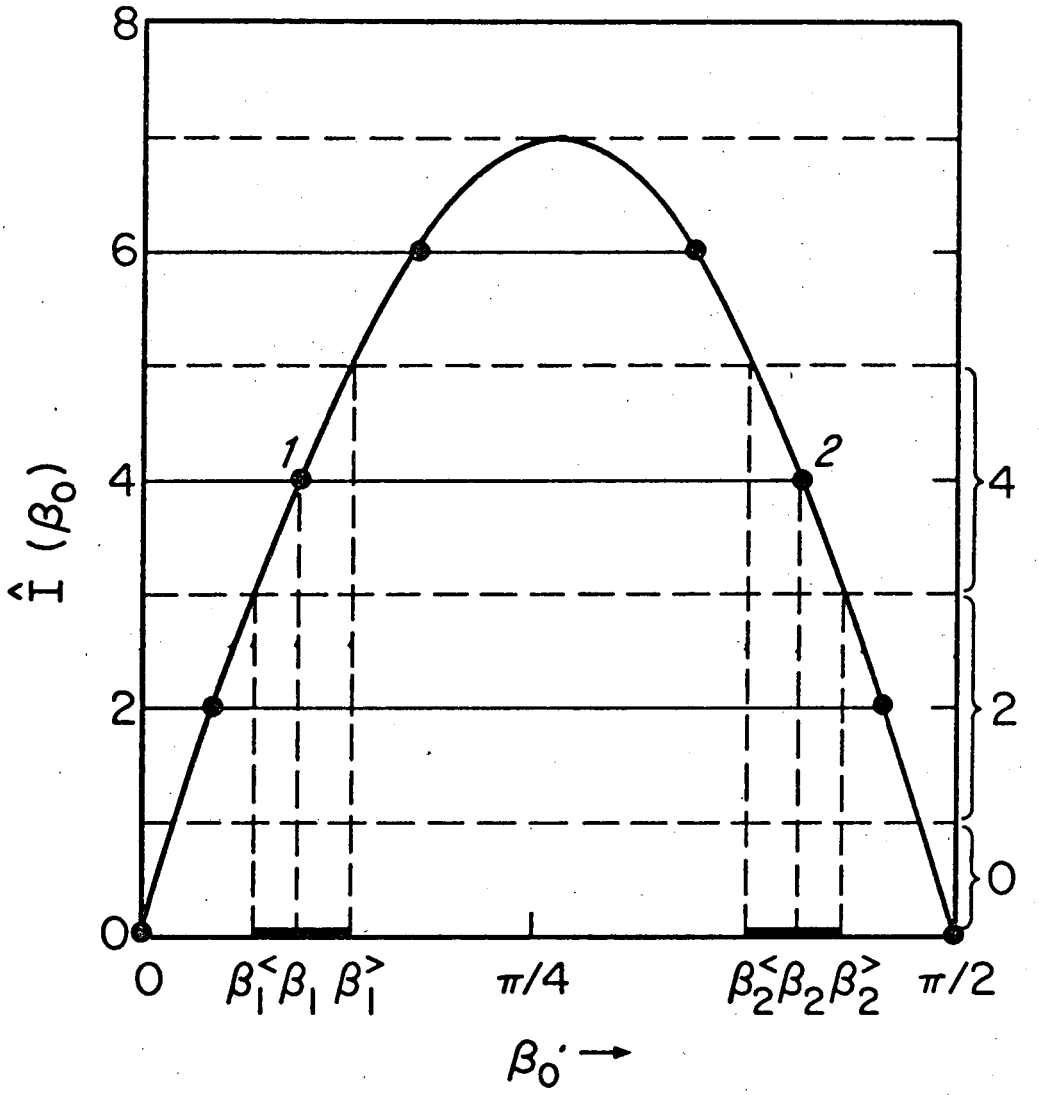

XBL759-4134

Fig. III-4 Graph of the quantum number function $\hat{I}(\beta_0)$ versus β_0 for the backscattering from a planar rotor. The two roots β_1 β_2 of $\hat{I}(\beta_0) = I$ are shown for $I = 4$. Note that the "initial orientation space" leading to $I = 0$ is half as large as the one leading to $I \neq 0$.

fig. II 6)

$$|\bar{P}_1| \simeq \left(\frac{\pi}{2}|\sin\bar{\beta}_1|\right)\frac{|\bar{\beta}_1^{<} - \bar{\beta}_1^{>}|}{\frac{\pi}{2}} \qquad (58)$$

where $\bar{\beta}_1^{<}$ and $\bar{\beta}_1^{>}$ are defined in Fig. III 5, which is the analogous figure to Fig. III 4 but for the 3D case. Comparing eqs. (57) and (58), one finds

$$\bar{P}_\kappa \equiv \frac{2\sin\bar{\beta}_\kappa}{\left(\frac{\partial\hat{I}(\beta_0)}{\partial\beta_0}\right)_\kappa} \qquad (\kappa = 1,2) \qquad (59)$$

The $\sin\bar{\beta}_\kappa$ factor arises from a purely geometric argument (see Fig. III 6). The excitation probabilities for the 3D backscattering problem are obtained when, in the expression of the previous section, the p's are replaced by the $\bar{p}$'s. For the forbidden transitions $\bar{\beta}_k$ will be a complex angle; for those cases, in equation (59) the sine of a complex angle is used.

One final aspect in converting the 2D equations to the 3D case concerns the special case I = 0. In the 2D case, the p's for I = 0 had to be divided by two. In the 3D case, the stationary points are not quite at the extremes of the integration interval (this because one looks for solutions of $\hat{I}(\beta_0) = 0 + \frac{1}{2}$). From Fig. III-5 we find that in the 3D case the initial orientation space leading to I = 0 is only 3/4 as large as the one leading to $I \neq 0$. Therefore, for I = 0 one has to multiply $\bar{p}$ by 0.75.

As already mentioned, in reference 25 the USCA was also applied to backscattering Coulomb excitation. The main difference between the work

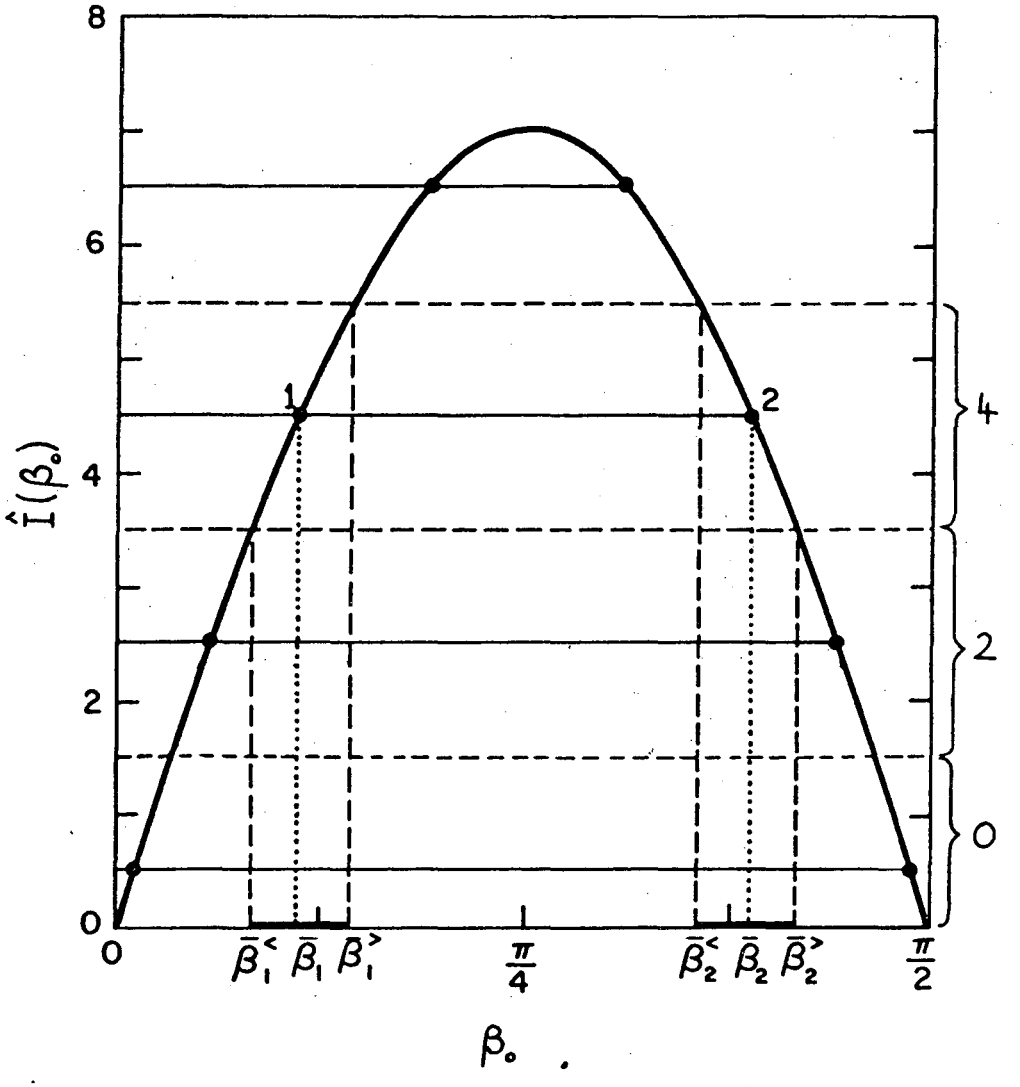

XBL759-4133

Fig. III-5 Same as Fig. III-4, but now looking for roots of $\hat{I}(\beta_o) = I + 1/2$ in order to make it correspondent to the backscattering from a three-dimensional rotor. Note that now the "initial orientation space" leading to $I = 0$ is 3/4 as large as the one leading to $I \neq 0$.

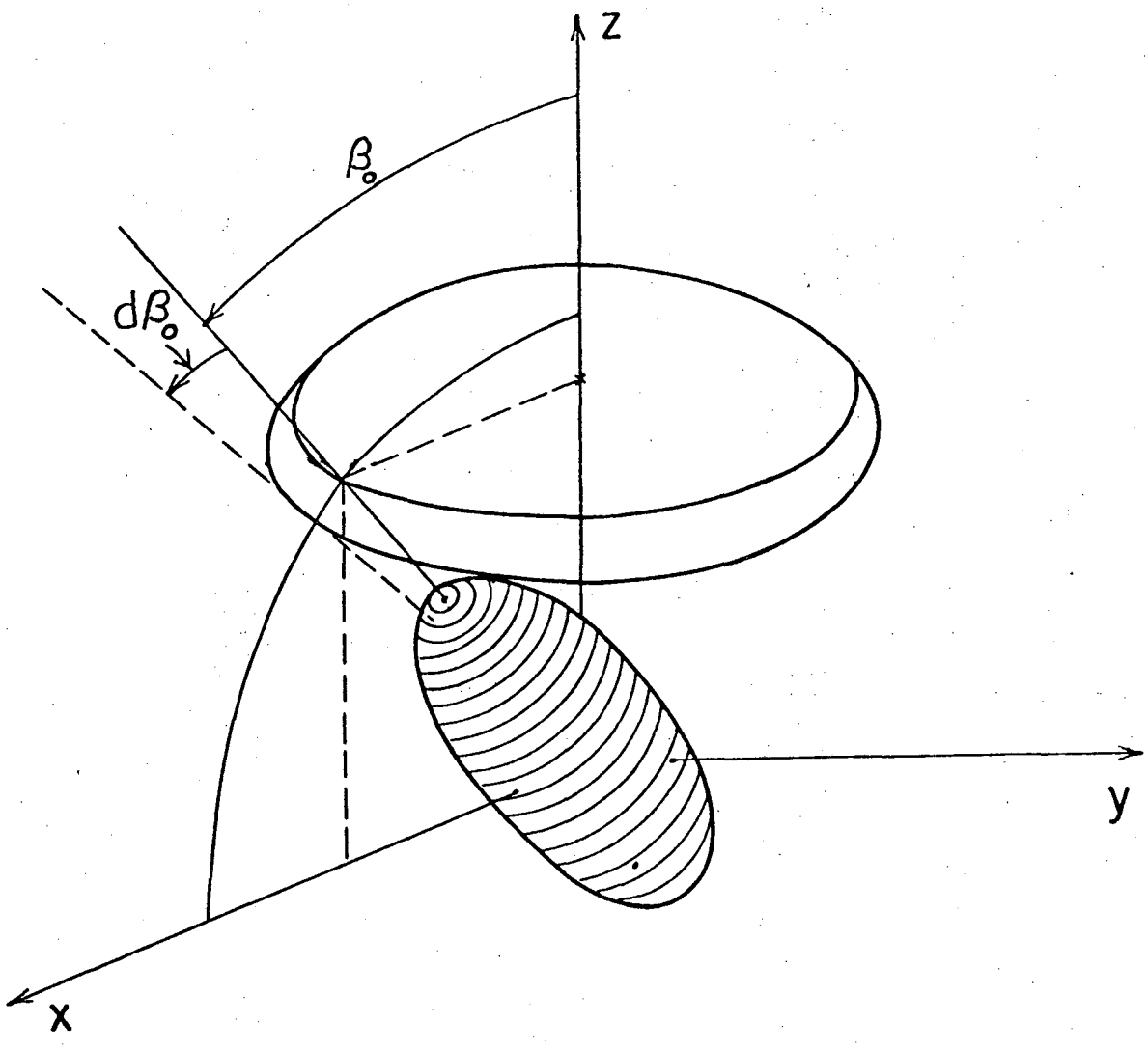

XBL7411-8213

Fig. III-6 Diagram showing the initial configuration of the system. The probability that the azimuthal angle of the symmetry axis of the target lies between β_o and $\beta_o + d\beta_o$ is clearly proportional to $\sin\beta_o$ in the 3-D case.

by Levit et. al.[25] is that they do not perform the modifications indicated in this subsection, that is they only solve the problem of backscattering from a planar rotor, although they compare their results to the 3D de Boer-Winther code for multiple Coulomb excitation.

d) Numerical considerations.

In order to find the excitation probabilities of Coulomb exciting a rotational band in a doubly even target, two computer codes were developed.

One computer code, let's call it code A, is very efficient and easy to use. In code A the quantum number function $\hat{I}(\beta_\circ)$ and the phase $\Phi(\beta_\circ)$ are found by solving the classical equations of motion (eqs. (27) and (29)) with the initial conditions eq. (30) (the initial orientation $\beta_\circ$ was varied in steps of 5°). After finding the function $\hat{I}(\beta_\circ)$ and $\Phi(\beta_\circ)$ every 5°, a simple three-point quadratic interpolation between the discrete points is used to find the roots of equation $\hat{I}(\beta_\circ) = I + \frac{1}{2}$. The derivatives $\left(\partial\hat{I}(\beta_\circ)/\partial\beta_\circ\right)_k$ (and therefore $\bar{p}_k$) are also immediately found by using the fitting coefficients of the function $\hat{I}(\beta_\circ)$. For $I + \frac{1}{2} \leq \hat{I}_{max}$ the excitation probability is evaluated using eq. (46). For $I + \frac{1}{2} > \hat{I}_{max}$ the procedure outlined in eqs. (49)-(51) is used to find approximately the excitation probability for the classically forbidden transitions. Code A also allows for the inclusion of an hexadecupole-monopole potential.

The other computer code, code B, on the other hand is much more complicated to use, but therefore relinquishes many approximations used in code A and also is applicable to more general potentials, for example, it does allow for the inclusion of a complex optical nuclear potential. In

code B the roots of equation $\hat{I}(\beta_0) = I + \frac{1}{2}$ are found "exactly", that is by running trajectories until, by an iteration procedure, a trajectory is found very close to the root. The S-matrix (eq. (II53)) is then evaluated. By taking the absolute square of the S-matrix, the excitation probabilities for both the classically accessible and forbidden transitions are found. Since for forbidden transitions β_∞ is complex, code B is set up to solve the classical equations of motion for the case where all the variables become complex (including the time). A complex nuclear optical potential of the Wood-Saxon type is also included in code B; a more detailed discussion of this is presented in a later section.

In both codes, the integration is started at a distance r equal to 40 times the distance of closest approach and is stopped when r again, after the integration, is 40 times the distance of closest approach. At $r = 80\ a$ (a = half distance of closest approach, see eq. (2)), the quadrupole potential, which is the non-central potential of longest range we will be dealing with and which goes to zero as $1/r^3$, is negligible and thereafter there will be no significant change in the quantum number function $\hat{I}(\beta_\infty)$. The long range $1/r$ pure Coulomb interaction of course still affects the trajectory of the projectile and the phase Φ, for $r > 80a$, but it does not affect in any way the excitation probability. This is so because it is not the absolute phase which is important in our zero impact parameter calculation, but rather the phase difference $\Delta\Phi$ between the two trajectories, which have the same initial and final asymptotic quantum numbers. For two such trajectories, which have the same quantum numbers in the asymptotic region, there will be contribution to $\Delta\Phi$ only as long as the non-central part of the interaction potential

is non-negligible. For all practical purposes, $r_{ini} = 80\ a$ is a "safe" distance to start the integration.

e) Example

When the classical equations of motion (eqs. (25)) are written in terms of dimensionless quantities, one finds that the evolution of the system depends only on the following dimensionless parameters:

$$\eta = \frac{Z_T Z_p e^2}{\hbar v_o} \qquad \text{(Sommerfeld parameter)} \qquad (60)$$

$$\xi_{o2} = \eta \frac{E_2}{2E_{CM}} \qquad \text{(Adiabaticity parameter)} \qquad (61)$$

$$\bar{q}_2 = \frac{Z_p e^2 Q_o^{(2)}}{4\hbar v_o a^2} \qquad \text{(Quadrupole interaction strength parameter)} \qquad (62)$$

where v_o is the velocity of the incoming projectile and a is half the distance of closest approach (eq.(2)).

In a Coulomb field the Sommerfeld parameter η is a measure of how classical the system is. The larger η ($\eta \gg 1$), the more classically the system will behave.

The adiabaticity parameter ξ_{o2} is a measure of how sudden or adiabatic the collision is with respect to the rotational period. If ξ_{o2} is small ($\xi_{o2} \ll 1$) the collision is more or less sudden, that is, the target does not rotate appreciably during the time the projectile is close to the target. $\xi_{o2} = 0$ is the sudden collision limit, this limit can be achieved for example by taking the moment of inertia as infinite, then E_2 and

therefore ξ_{o2} will be zero. In the limit of large ξ_{o2} $(\xi_{o2} \gg 1)$ the collision is said to be adiabatic. In that limit the target, if excited to $I = 2$, will rotate very fast, which has a consequence the averaging to zero of the quadrupole-monopole interaction. Consequently higher spins are very unlikely to be excited in the target.

The parameter $\bar{q}_2$ is a measure of the quadrupole-monopole interaction strength. If $\bar{q}_2 << 1$ the target will remain in its ground state and no rotational states will be excited. If $\bar{q}_2 >> 1$ many rotation states will be excited (unless the collision is extremely adiabatic). A rough rule-of-thumb is that the largest rotational angular momentum that will be excited in the target is approximately $2\bar{q}_2$. The ratio $\bar{q}_2/\eta$ gives a measurement of how much the orbit of the projectile, which is mainly a pure hyperbolic orbit, is disturbed by the presence of the non-central quadrupole field. If $\bar{q}_2/\eta << 1$ then the orbit is close to a hyperbolic orbit. In reference 20 it is shown that the scattering angle of the projectile, for zero impact parameter, can deviate at most by $2\bar{q}_2/\eta$ from π. If $\bar{q}_2/\eta >> 1$ the trajectory will be very different from a hyperbola. Figure III 7 shows the values of the parameters η and $\bar{q}_2$ for various target-projectile systems at several energies (in MeV).

The theoretical developments of the previous sections will now be illustrated with an example. We will consider the backscattering of ^{40}Ar from ^{238}U with bombarding energies between 150 and 210 MeV in the laboratory. Table III 2 shows the relevant parameters for the example at the various energies. We will for the moment neglect the hexadecupole moment of the target; it will be included in a later subsection.

In figure III 8 the quantum number functions for the bombarding

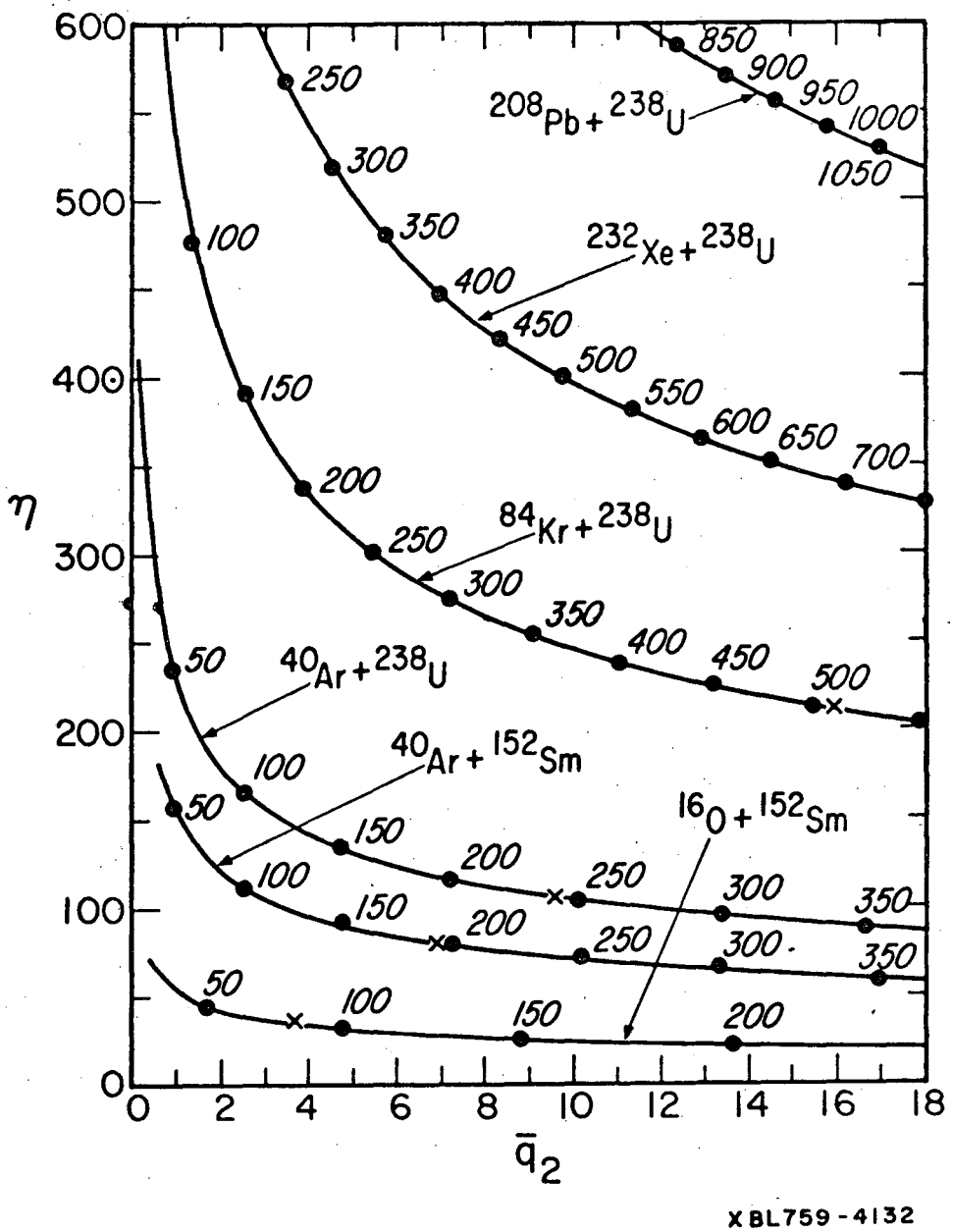

Fig. III-7 The value of the dimensionless parameters η and $\bar{q}_2$ are shown for various target-projectile systems at several laboratory energies (in MeV). The crosses indicate the places for which 2a = distance of closest approach $= 1.4\ (A_T^{1/3} + A_p^{1/3})$.

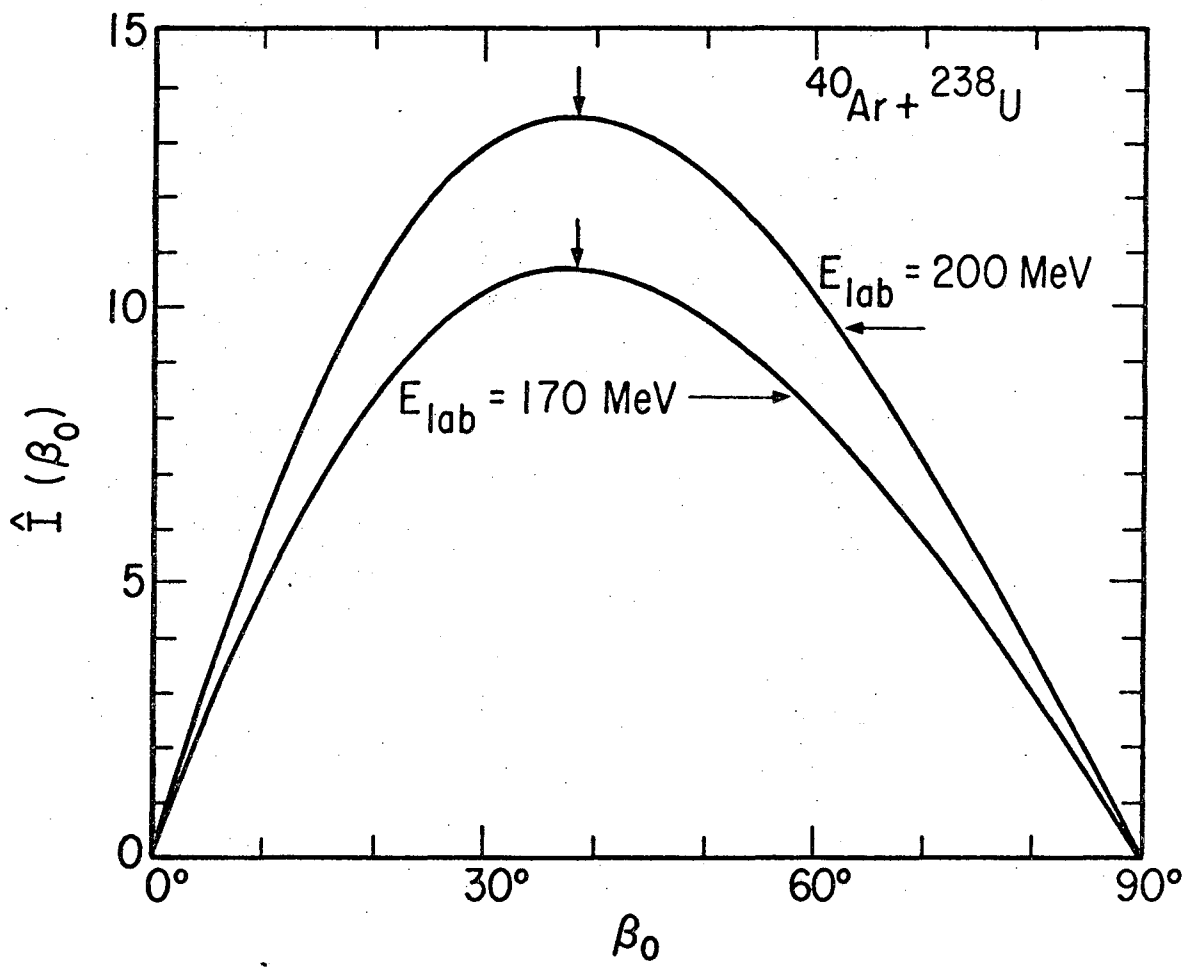

XBL759-4131

Fig. III-8 The quantum number function $\hat{I}(\beta_0)$ vs. β_0 is shown for the backscattering of ^{40}Ar on ^{238}U at E_{lab} = 170 and 200 MeV. The parameters for this example are shown in Table III-2.

Table III 2. Value of several parameters for the scattering of ^{40}Ar on ^{238}U for several bombarding energies.

E_{lab} (MeV)	$\bar{q}_2$	η	σ_2	β_{max}	I_{max}	a (fm)
150	4.739	135.2	0.0236	38.05	8.911	9.284
155	4.978	133.0	0.0225	38.05	9.346	8.985
160	5.221	130.9	0.0215	38.05	9.786	8.704
165	5.467	128.9	0.0205	38.05	10.231	8.400
170	5.718	127.0	0.0196	38.05	10.681	8.192
175	5.972	125.1	0.0188	38.06	11.136	7.960
180	6.230	123.4	0.0180	38.06	11.595	7.737
185	6.491	121.7	0.0173	38.06	12.058	7.528
190	6.756	120.1	0.0166	38.06	12.526	7.330
195	7.024	118.6	0.0159	38.06	12.999	7.142
200	7.296	117.1	0.0153	38.05	13.473	6.963
205	7.571	115.6	0.0148	38.05	13.952	6.793
210	7.850	114.2	0.0143	38.05	14.434	6.632

$Q_o^{(2)} = 11.12$ eb

$Q_o^{(4)} = 0.0$ eb^2

$mc^2 = 3.21377\ 10^4$ MeV

$E_2 = 0.0449$ MeV

$\xi = \xi_{o2}\,\bar{q}_{t2} = 0.112$

energies E_{lab} = 170 and 200 MeV are shown. For a target with an infinite moment of inertia, or in other words, if the target would not rotate during the time the collision takes place, one would expect that β_{max} (the value of β_∞ for which $\hat{I}(\beta_\infty) = \hat{I}_{max}$) occurs at 45°. However, since the collision is not completely sudden, the value of β_{max} is shifted to smaller values. The value of β_{max} is quite independent of energy (see table III-2). The reason for this is easy to find. For higher energies the collision will occur faster, but also higher spins will be excited and the target will rotate faster; the ratio between the collision time and the period of rotation of the target is roughly independent of energy. A parameter which should describe much better than ξ_{02} whether a collision is adiabatic or sudden is the parameter ζ defined by

$$\zeta \equiv \xi_{02}\,\bar{q}_2 . \tag{63}$$

Rembmber that $I = 2\bar{q}_2$ will roughly be the largest angular momentum that can classically be transferred to the target (see also subsection III f)). From eqs. (61) and (62) we find

$$\zeta = \frac{3}{2}\left(\frac{Q_o^{(2)}}{Z_T}\right)\Big/\left(\frac{\mathcal{I}}{m}\right) \tag{64}$$

that is, ζ is independent of energy. Table III 3 shows the value of ζ for the target-projectile systems shown in Fig. III 7. If $\zeta \ll 1$ then the collision is sudden; if $\zeta \ll 1$ then the collision is more or less adiabatic.

In Fig. III 9, $\Delta\Phi$ and $\sqrt{\bar{p}}$ are plotted for the classically allowed values of the final angular momentum of the target I. Figures III 10 and

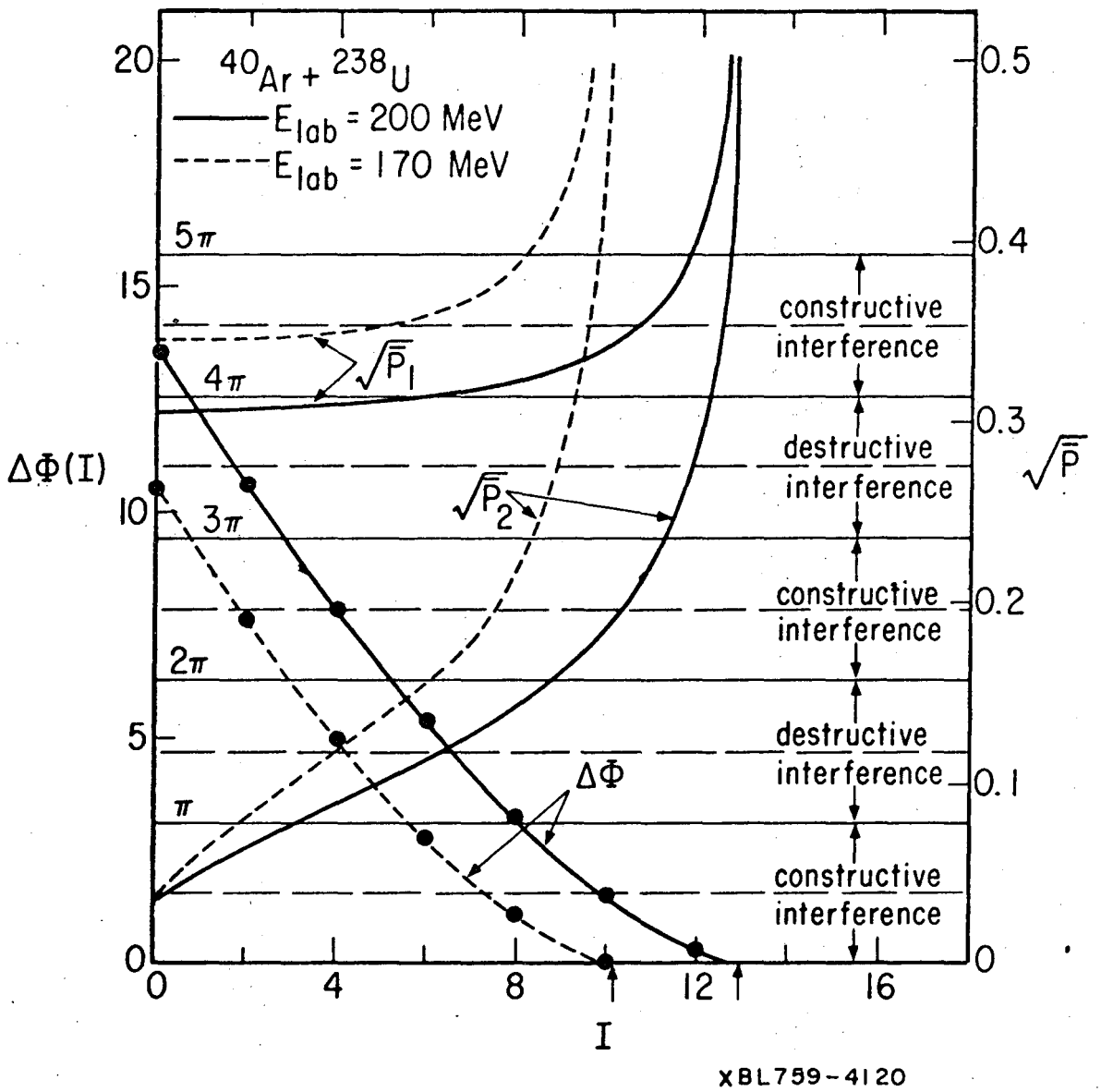

Fig. III-9 Graphs of $\Delta\Phi$, $\sqrt{\bar{p}_1}$ and $\sqrt{\bar{p}_2}$ versus I for the same examples shown in Fig. III-8.

Table III 3. Value of the parameter ξ for several target-projectile systems.

System	ξ
$^{16}O + ^{152}Sm$	0.1010
$^{40}Ar + ^{152}Sm$	0.2209
$^{16}O + ^{238}U$	0.0485
$^{40}Ar + ^{238}U$	0.1108
$^{84}Kr + ^{238}U$	0.2008
$^{132}Xe + ^{238}U$	0.2746
$^{208}Pb + ^{238}U$	0.3589

III 11 show the excitation probabilities obtained for these examples. The USCA results are shown by the black dots. For comparison, the result using the conventional semiclassical de Boer-Winther code for multiple Coulomb excitation is also shown (by open circles). The agreement is very reasonable. In Fig. III 10 also shown (by open squares) is the so called classical excitation probability

$$P_{cl}(I) = \bar{P}_1 + \bar{P}_2 \qquad \left(\text{for } I+\tfrac{1}{2} < \hat{I}_{max}\right) \qquad (65)$$

The classical excitation probability $P_{cl}(I)$ shows no interference structure (i.e. is a smooth function of I) and goes only up to spin I = 8, which is the largest spin allowed by classical dynamics for this energy (see Fig. III 8). For I = 0 the excitation probability is roughly 3/4 of what it is for I = 2; this is not related to an interference effect but rather has to do with the fact that the space of initial orientations leading to I = 0 is about 3/4 as large as the one leading to I = 2.

In Fig. III 11 also the 2D-USCA results are shown (crosses); these are the results obtained if the modifications described in section III 2e are ignored. Note that the interference pattern in the 2D-USCA is much larger for low spins, in disagreement with the de Boer-Winther code.

In table III 4, all the different ways of evaluating the excitation probabilities for the bombarding energies E_{lab} = 170 and 200 MeV are shown; namely the classical, primitive semiclassical, USCA-2D and USCA-3D results, (compare also with table III 1). The main features of the interference pattern of the 3D-USCA calculations can be understood by using Fig. III 9 and remembering that for I not too close to $\hat{I}_{max}$ the

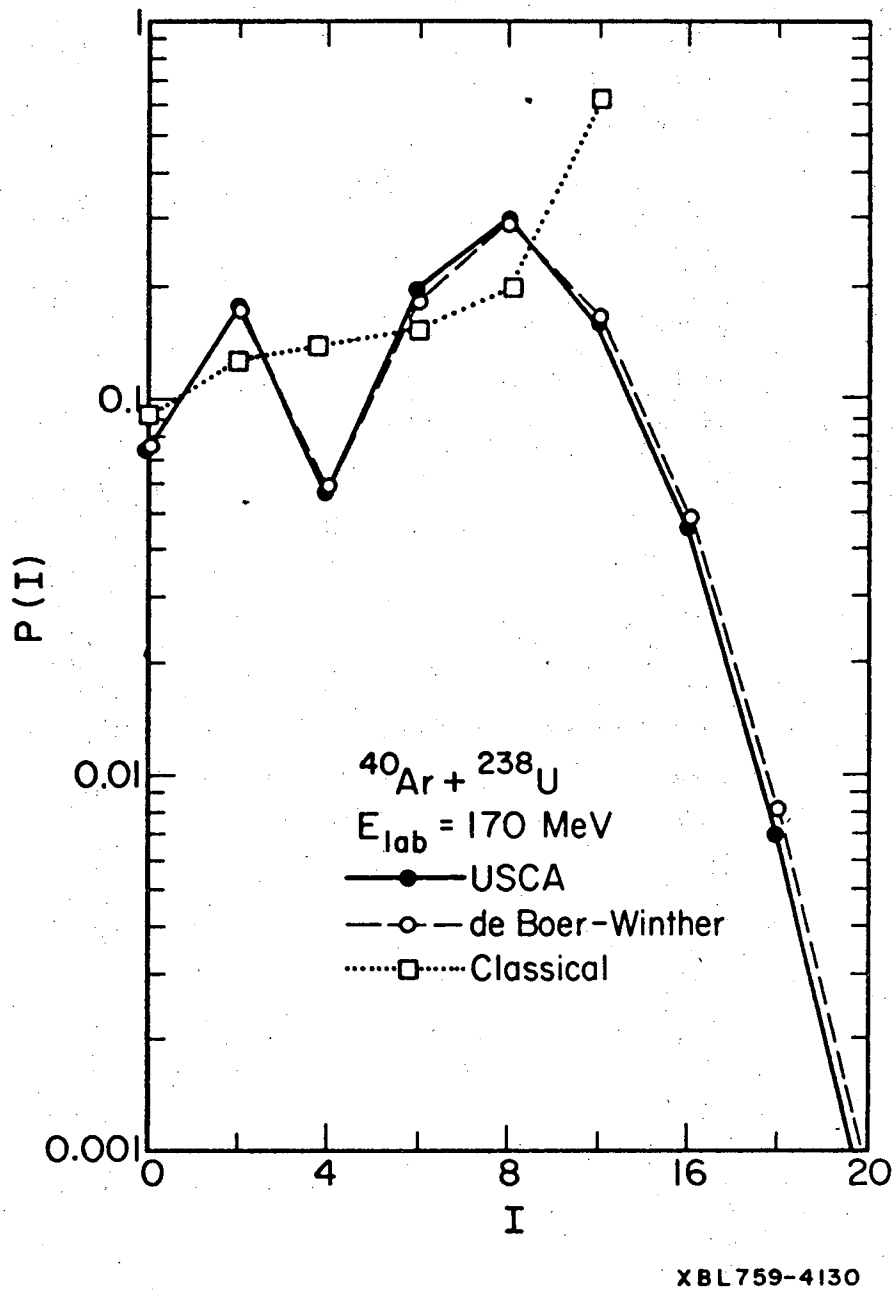

Fig. III-10 Calculations of Coulomb excitation probabilities to excite members of the rotational ground band in ^{238}U (target) with the backscattering of ^{40}Ar at E_{lab} = 170.0 MeV. The parameters for this example are shown in Table III-2. In addition to the USCA results (solid line) and the results using the de Boer-Winther code (dashed line), the classical results (dotted line) which shows no interference is shown.

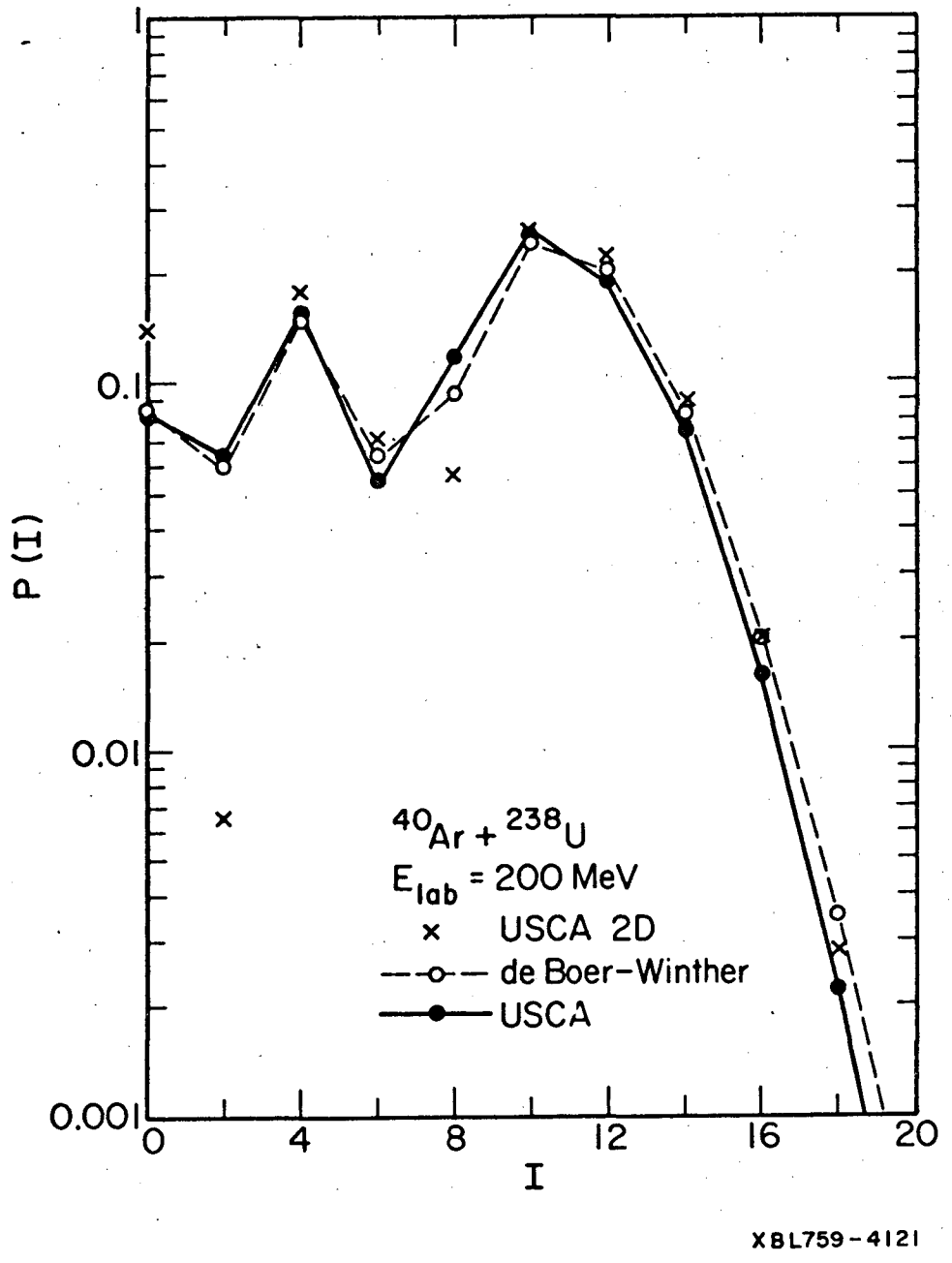

Fig. III-11 Same as Fig. III-10, but at E_{lab} = 200 MeV. Also, instead of the classical excitation probability, the results obtained if the modification discussed in section III-1c are not included, i.e. the 2D-USCA results are shown (crosses).

primitive semiclassical approximation (eq. (42)) gives almost the correct result. From eq. (42) one finds that if $\Delta\Phi$ is in the interval $[2n\pi, (2n+1)\pi]$ the interference is constructive and if $\Delta\Phi$ is in the interval $[(2n-1)\pi, 2n\pi]$, the interference is destructive. In Fig. III 9 the regions where the interference is constructive or destructive are indicated. For E_{lab} = 170 MeV and I = 4, for example, $\Delta\Phi$ is in a region of destructive interference. Hence, $P_{uni}(I = 4)$ is much smaller than $P_{cl}(I = 4)$. For I = 6 (E_{lab} = 170 MeV), $\Delta\Phi$ is only slightly into a region of constructive interference, therefore P_{uni} is a little larger than P_{cl}. The fact that $\sqrt{\bar{p}_1}$ goes to zero for small $I + \frac{1}{2}$ in the 3D case (due to the $\sin\beta_1$ in eq. (59)) has the consequence that the interference pattern becomes progressively weaker going to small I. In the 2D USCA $\sqrt{p_1}$ does not tend to zero for low I (as a matter of fact the graphs of $\sqrt{p_1}$ and $\sqrt{p_2}$ are fairly similar and lie between the graphs of $\sqrt{\bar{p}_1}$ and $\sqrt{\bar{p}_2}$ in Fig. III 9); this explains why the interference pattern is much stronger for the 2D-USCA.

In figure III 12 the excitation probability for a few selected states (I = 4,6 and 10) of the rotational band in ^{238}U in the backward scattering of ^{40}Ar ions with E_{lab} = 150-210 MeV is shown. The agreement between the USCA and the conventional semicalssical approximation is very reasonable, although there seems to be a small systematic shift. The agreement is less good for the higher energies. It is not clear which of the two semiclassical methods would be closer to an exact quantum mechanical calculation if such a calculation could be performed. If the difference of the two semiclassical calculations were solely due to the fact that in the USCA the dynamics of the problem is included correctly, but in the

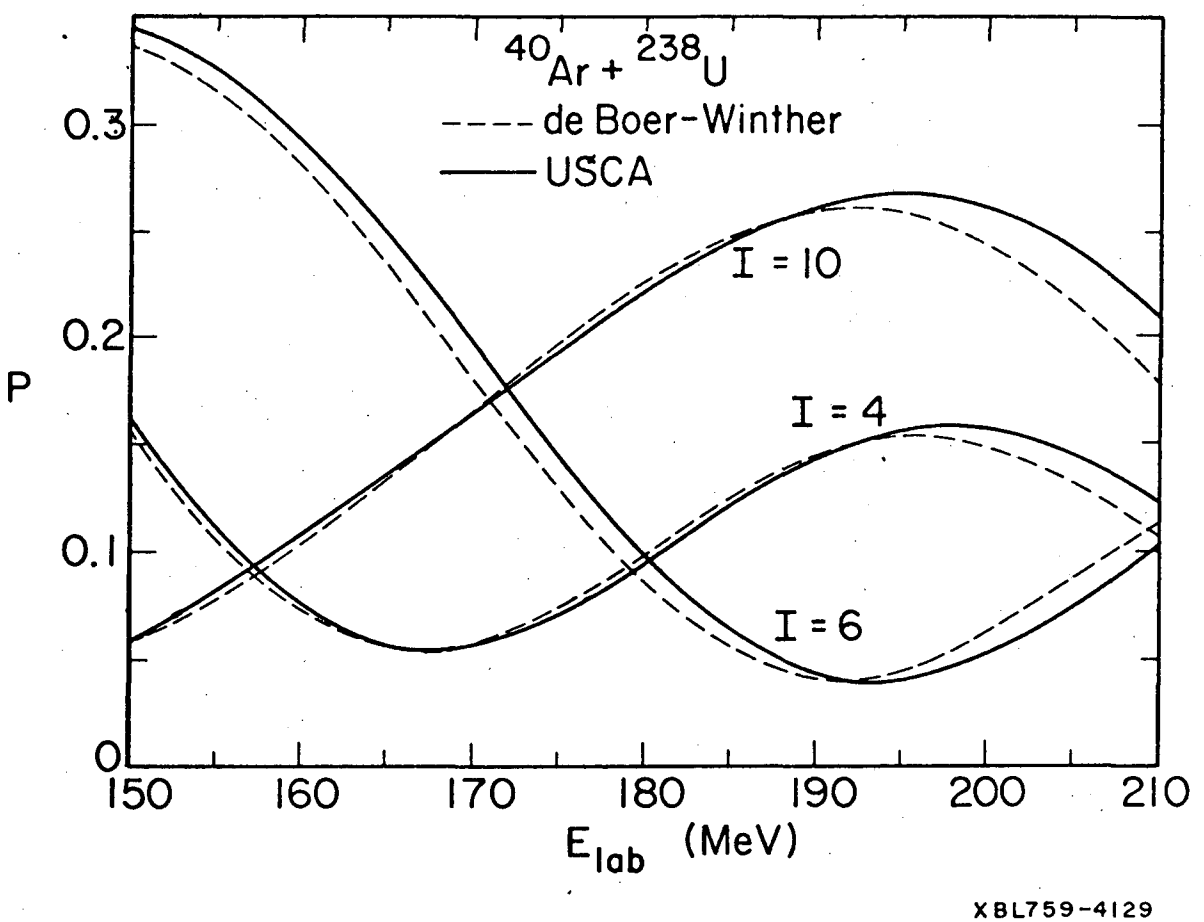

Fig. III-12 Calculations of the probability to excite the rotational states I = 4, 6 and 10 of ^{238}U in the backscattering of ^{40}Ar are shown versus the laboratory bombarding energy.

Table III 4. The probabilities of excitation of rotational states calculated in different ways for the reaction $^{40}Ar + ^{238}U$ with bombarding energies E_{lab} = 170 and 200 MeV.

I	P_{cl}	P_{prim}	P^{2D}_{unif}	P_{unif}	E_{lab}
0	0.0900	0.0743	0.00570	0.0743	
2	0.1260	0.1797	0.2311	0.1783	
4	0.1356	0.0592	0.04596	0.0566	
6	0.1535	0.1920	0.1300	0.1960	
8	0.1968	0.3428	0.3315	0.2992	
10	0.6306	0.6480	0.1999	0.1548	170
12	---	0.0552	0.05676	0.0457	
14	---	0.00755	0.00910	0.00694	
16	---	0.00071	0.00092	0.00067	
18	---		0.00006		
0	0.0713	0.0818	0.1401	0.0815	
2	0.0985	0.0633	0.00656	0.0635	
4	0.1033	0.1578	0.1785	0.1571	
6	0.1110	0.0576	0.07035	0.0532	
8	0.1243	0.1131	0.05554	0.1177	
10	0.1513	0.2785	0.2588	0.2600	200
12	0.2483	0.3163	0.2247	0.1876	
14	---	0.1045	0.08901	0.0747	
16	---	0.0178	0.01996	0.0158	
18	---	0.00233	0.00288	0.00219	
20	---	0.00022	0.00029	0.00021	

conventional semiclassical approximation it is not (see Appendix A), one would expect that the disagreement at E_{lab} = 210 MeV be twice as large than for E_{lab} = 170 MeV since at E_{lab} = 210 MeV be twice as large than for E_{lab} = 170 MeV since at E_{lab} = 210 MeV the ratio $\bar{q}_2/\eta$ (which is a measure of how much the trajectory differs from a pure hyperbola) is twice as large as at E_{lab} = 170 MeV (see table III 3).

f) The sudden collision limit and the limit

We will now consider the sudden collision limit ($\xi_{02} = \xi = 0$). This limit corresponds to the case where the period of rotation of the target is much larger than the time during which the interaction takes place. In the conventional semiclassical approach one has that the backscattering excitation probability depends only on the parameters $\bar{q}_2$ and ξ_{02}. For $\xi_{02} = 0$, the excitation probability P(I) depends then only on the parameter $\bar{q}_2$, this $\xi_{02} = 0$ limit has been studied by Alder and Winther[17].

In the USCA approach one has that the excitation probabilities not only depend on $\bar{q}_2$ and ξ_{02}, but also on the ratio $\bar{q}_2/\eta$. As already mentioned, $\bar{q}_2/\eta$ is a measure of how much the trajectory differs from a pure hyperbola. If we take $\eta \to \infty$ in the USCA method, the trajectories will also be "pure hyperbolas". In the conventional semiclassical method, problems with fixed $\bar{q}_2$ and ξ_{02} but different η have all the same excitation probability (for backscattering); in the USCA the resulting excitation probability is not the same for all the different η. From all this set of different USCA results, the one that would correspond closest to the conventional semiclassical result is the one with $\eta \to \infty$.

A nice feature of the USCA method is that the $\xi_{02} = 0, \eta \to \infty$ limit

for backscattering can be solved analytically. The result for the quantum number function and the phase is

$$\hat{I}(\beta_o) = 2\bar{q}_2 \sin(2\beta_o) \tag{66}$$

$$\Phi(\beta_o) = 2\bar{q}_2 (\sin^2\beta_o - \beta_o \sin(2\beta_o)) \tag{67}$$

From eqs. (66) and (55) we find that in this limit $2\bar{q}_2 - \frac{1}{2}$ is the largest angular momentum that can be classically transferred. In the $\xi_{02} = 0$ limit, as expected, $\beta_{max} = \pi/2$.

From eqs. (66) and (67) the phase difference $\Delta\Phi$ and the $\bar{p}$'s can be found

$$\Delta\Phi = 2\bar{q}_2 \begin{cases} |\sqrt{1-f^2} - f \operatorname{Arccos} f| & f \leq 1 \\ |\sqrt{f^2-1} - f \operatorname{Log}(f+\sqrt{f^2-1})| & f \geq 1 \end{cases} \tag{68}$$

$$\left.\begin{matrix}\bar{P}_1 \\ \bar{P}_2\end{matrix}\right\} = \frac{(1-\frac{1}{4}\delta_{10})}{2\bar{q}_2\sqrt{1-f^2}} \begin{cases} \sin(\frac{1}{2}\operatorname{Arcsin} f) \\ \cos(\frac{1}{2}\operatorname{Arcsin} f) \end{cases} \qquad f < 1 \tag{69a}$$

$$\left.\begin{matrix}\bar{P}_1 \\ \bar{P}_2\end{matrix}\right\} = \frac{1}{4\bar{q}_2}\left[\frac{1}{\sqrt{f-1}} \pm \frac{i}{\sqrt{f+1}}\right] \qquad f > 1 \tag{69b}$$

where f is defined by

$$f = \frac{I+\frac{1}{2}}{2\bar{q}_2} \tag{70}$$

Substituting eqs. (69) and (68) back into eqs. (46) and (47) we find the excitation probabilities in the $\xi_{02} = 0, \eta \to \infty$ limit. Let's note that in this case we are using the "exact" expression (47) for the classically forbidden transitions (that is for $f > 1$) and not the approximate expression (49). For the special case $f = 1$ the excitation probability is:

$$P_{unif} = \frac{\pi}{\sqrt{2}} \left(\frac{2}{\bar{q}_2} \right)^{2/3} Ai^2(0) \qquad (71)$$

In Fig. III 13 the phase difference $\Delta\Phi$ vs. $\bar{q}_2$ for $f < 1$ is plotted for the $\xi_{02} = 0, \eta \to \infty$ limit. The regions of the constructive and destructive interference are also indicated. With this figure one readily understands the features of the excitation probability in this limit which, for some spins I, is tabulated in table III-5 and plotted in Fig. III-14. For comparison, the results obtained by Alder and Winther[27] are also shown. The agreement is excellent; this gives an indication that the systematic deviation one observed in Fig. III 12 is really due to the fact that the USCA method treats the dynamics of the problem exactly, while the conventional semi-classical approximation does not. Fig. III 15 shows the backscattering excitation amplitude for $\xi_{02} = 0$ and $\bar{q}_2 = 9.0$ versus $100/\eta$. In experimental situation (for which $\bar{q}_2 = 9.0$) $100/\eta$ will always be between 0.2 and 0.5, and in this interval the excitation probability doesn't differ very much from its value in the $\eta \to \infty$ limit. By varying η from 50 to 350 the phase difference $\Delta\Phi$ increases for the various states between 0.3 and 0.7 radians; with this fact and Fig. III 13 we can rationalize the variations of the excitation probability with η in Fig. III 15. For

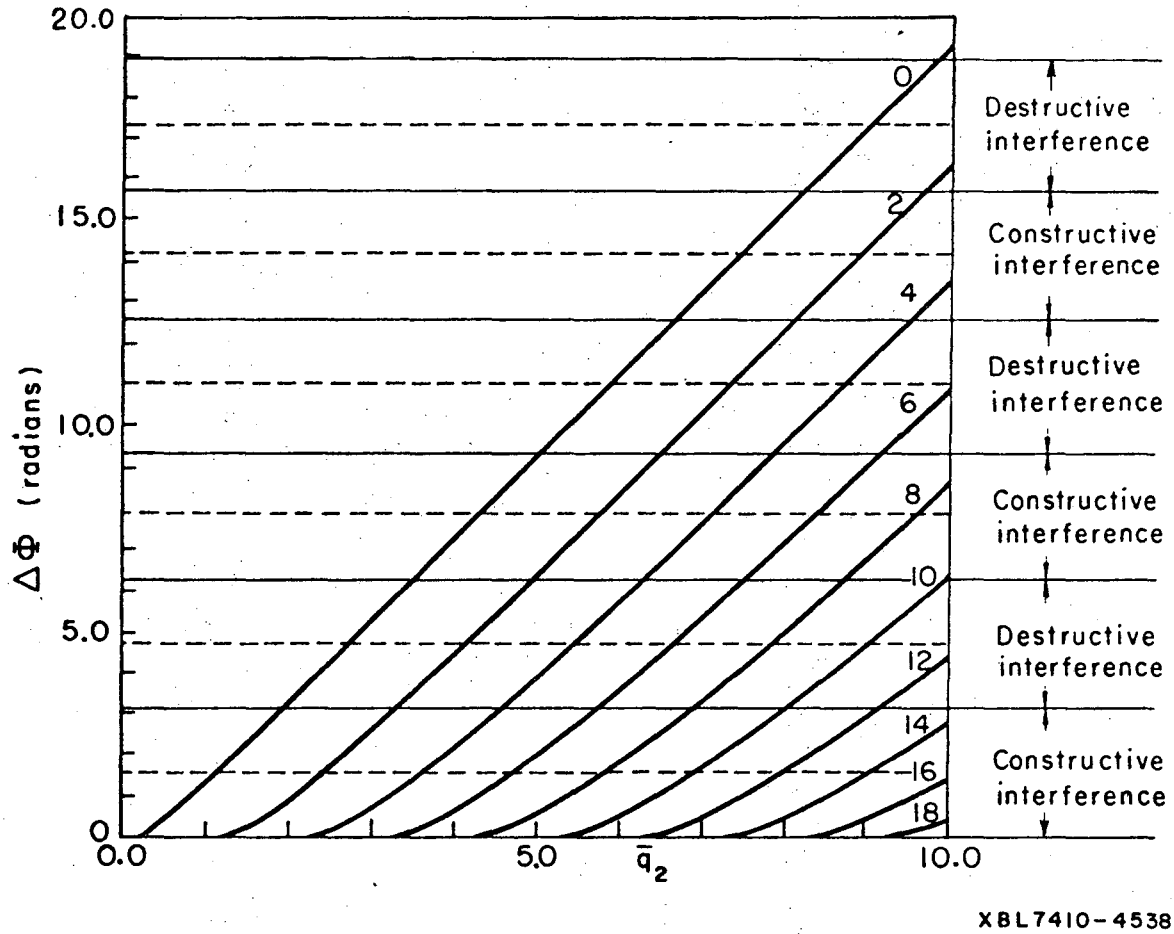

Fig. III-13 Graph of the phase difference $\Delta\Phi$ versus $\bar{q}_2$ for the $\xi_{02} = 0$, $\eta \to \infty$ limit. Shown are the results for all spins up to $I = 18$, but only for $f \leq 1$.

Table III-5 The probabilities for excitation of rotational states in an even-even nucleus in the limit $\frac{\pi}{\beta} = 0$ and $\eta = \infty$. Tabulated are the results of the USCA and the traditional semi-classical approximation (ref. 27).

$\bar{q}_2$	USCA P_0	A-W P_0	USCA P_2	A-W P_2	USCA P_4	A-W P_4	USCA P_{10}	A-W P_{10}	USCA P_{14}	A-W P_{14}	USCA P_{18}	A-W P_{18}
1.0	0.6339	0.6945	0.2518	0.2850	0.0003	0.0006						
1.5	0.3830	0.4300	0.4917	0.4812	0.0039	0.0057						
2.0	0.1940	0.2152	0.5733	0.5597	0.0203	0.0260	0.0000	0.0001				
2.5	0.0988	0.1021	0.4892	0.4842	0.0650	0.0750	0.0004	0.0006				
3.0	0.0842	0.0835	0.3084	0.3098	0.1485	0.1572	0.0022	0.0029				
3.5	0.1067	0.1108	0.1362	0.1389	0.2568	0.2563	0.0084	0.0104		0.0001		
4.0	0.1227	0.1317	0.0509	0.0514	0.3385	0.3354	0.0247	0.0286	0.0003	0.0004		
4.5	0.1115	0.1214	0.0622	0.0600	0.3571	0.3555	0.0581	0.0634	0.0011	0.0014		
5.0	0.0820	0.0881	0.1193	0.1158	0.2999	0.3006	0.1127	0.1171	0.0038	0.0046		
5.5	0.0553	0.0571	0.1569	0.1540	0.1911	0.1932	0.1829	0.1831	0.0107	0.0124		0.0002
6.0	0.0461	0.0463	0.1427	0.1412	0.0828	0.0848	0.2451	0.2436	0.0255	0.0283	0.0006	0.0007
6.5	0.0530	0.0547	0.0921	0.0917	0.0242	0.0250	0.2768	0.2757	0.0523	0.0558	0.0018	0.0022
7.0	0.0630	0.0671	0.0462	0.0459	0.0317	0.0312	0.2615	0.2616	0.0933	0.0961	0.0050	0.0058
7.5	0.0637	0.0687	0.0352	0.0343	0.0809	0.0798	0.2004	0.2014	0.1452	0.1455	0.0120	0.0134
8.0	0.0532	0.0570	0.0568	0.0552	0.1251	0.1242	0.1160	0.1174	0.1946	0.1938	0.0253	0.0274
8.5	0.0396	0.0413	0.0836	0.0819	0.1293	0.1292	0.0436	0.0446	0.2266	0.2258	0.0478	0.0503
9.0	0.0324	0.0329	0.0892	0.0879	0.0925	0.0930	0.0124	0.0128	0.2277	0.2275	0.0808	0.0828
9.5	0.0345	0.0355	0.0692	0.0685	0.0442	0.0447	0.0290	0.0286	0.1930	0.1935	0.1221	0.1225
10.0	0.0409	0.0432	0.0412	0.0408	0.0188	0.0189	0.0725	0.0719	0.1316	0.1326	0.1627	0.1622

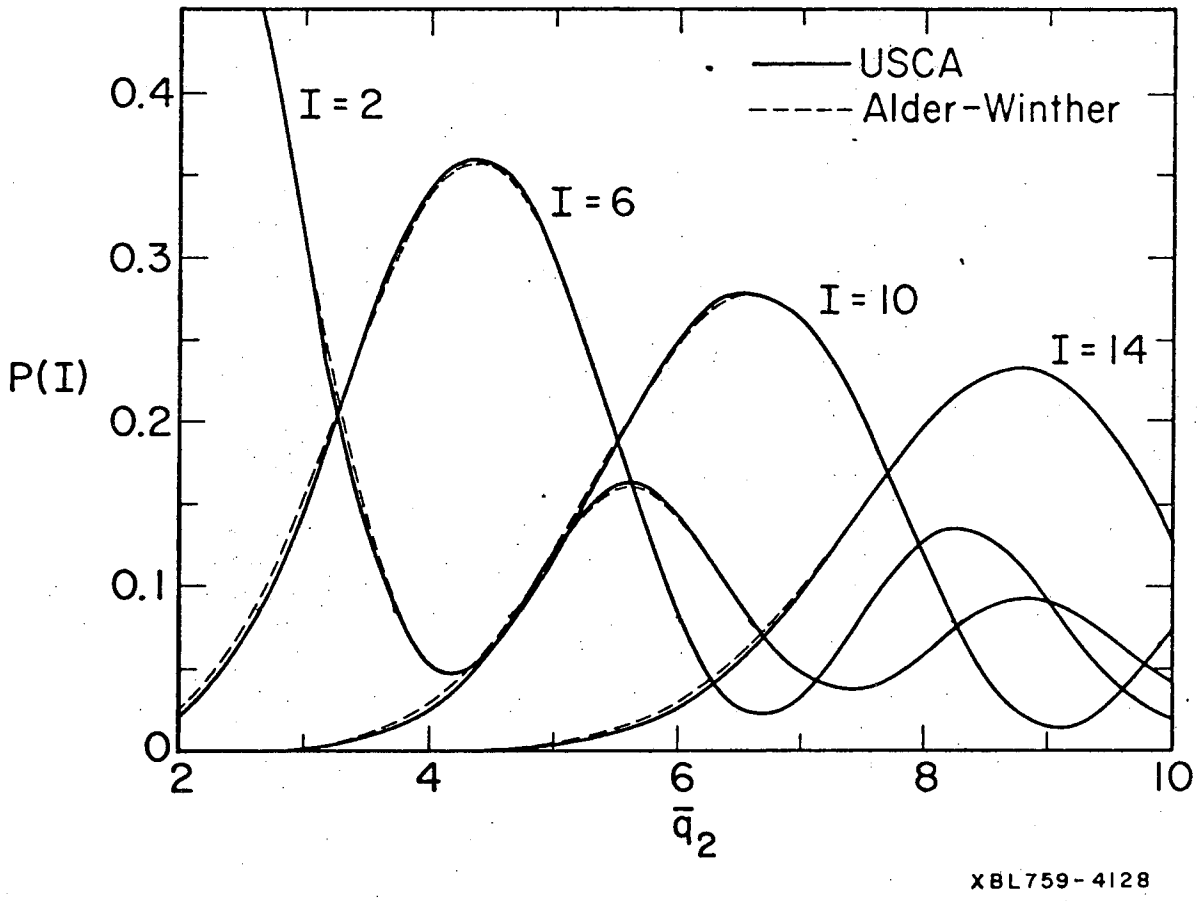

Fig. III-14 Graphs showing the excitation probability to excite selected rotational states in the collision of a spherical nucleus on a deformed nucleus in the limit $\xi_{02} = 0$, $\eta \to \infty$, versus the quadrupole strength parameter $\bar{q}_2$. The agreement between the USCA results and the results using the conventional semi-classical method (see ref. 27) is excellent. See also Table III-5.

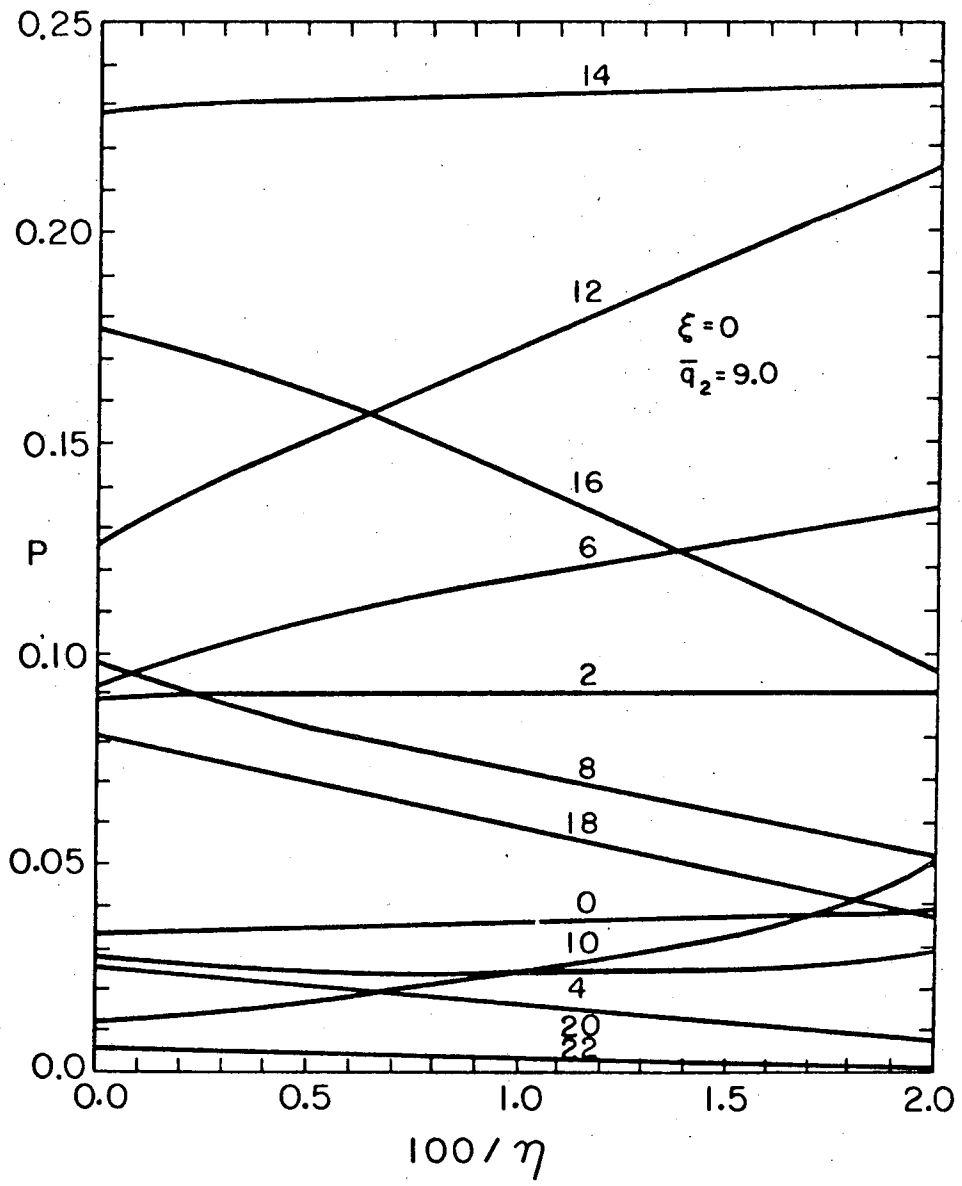

Fig. III-15 Backward scattering excitation probabilities to Coulomb excite members of a ground rotational band of a doubly even target. Results are shown versus η for $\xi_{02} = 0$ and $\bar{q}_2 = 9.0$. The $\eta \to \infty$ was evaluated using the analytical formulas derived in section III-1f.

example for I = 6, $\Delta\Phi$ moves away from the region of constructive interference with increasing η ; therefore the excitation probability decreases. For I = 8, $\Delta\Phi$ moves into a region of constructive interference; the excitation probability increases with η . The variation of $\Delta\Phi$ with η is the main contribution to the change in the excitation probability with η ; the $\bar{p}$'s also vary with η (the larger the spin I, the greater the variation). For I = 14, $\Delta\Phi$ moves deeper into the constructive interference region and the excitation probability should increase with η, but this is cancelled by the decrease of the $\bar{p}$'s with increasing η , so the excitation probability actually goes down a little.

g) Inclusion of the electric hexadecupole moment.

One of the advantages of the USCA method is the ease of including other terms in the interaction potential. Here we will consider the electric hexadecupole potential

$$V_{Hexa} = \frac{Z_p e^2 Q_o^{(4)}}{2r^5} P_4(\cos\chi) \qquad (72)$$

where the intrinsic hexadecupole moment $Q_o^{(4)}$ is defined by the equation (24). We will show here the effect the inclusion of a hexadecupole moment has for the example studied in section 3), that is, $^{40}Ar + ^{238}U$ at bombarding energy E_{lab} = 200. MeV. In Fig. III 16 the quantum number function is shown for this example for three cases which are $Q_o^{(4)} = 0$ and $Q_o^{(4)} = \pm$ 3.0 eb^2 (the true hexadecupole moment for ^{238}U is closer to the value $Q_o^{(4)}$ = 1.96 eb^2, but in order to show its effect more clearly the calculations were performed with a larger value and also with both signs). Fig. III 17

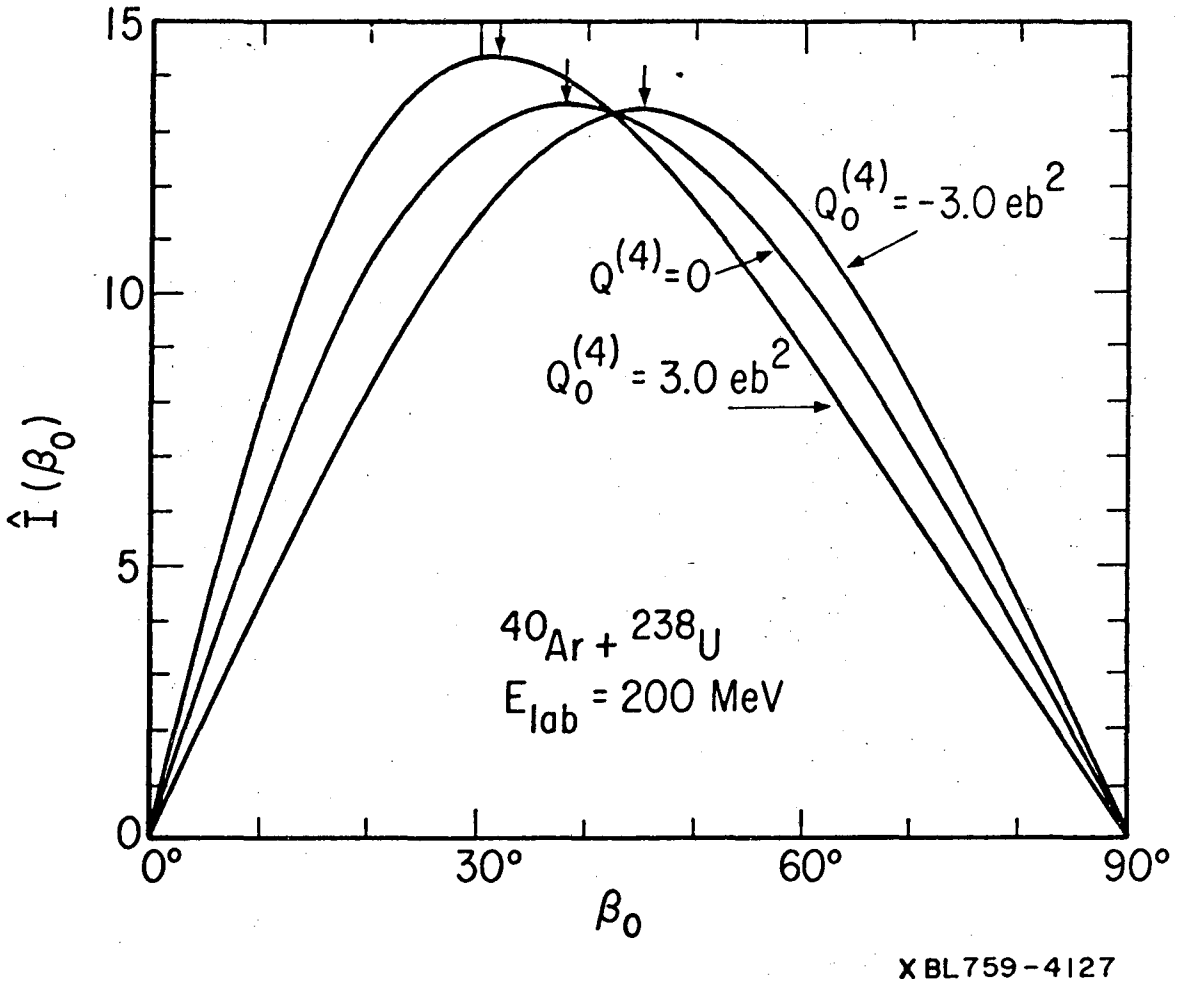

Fig. III-16 Graph of the quantum number function $\hat{I}(\beta_o)$ versus β_o for the backscattering of ^{40}Ar on ^{238}U at E_{lab} = 200 MeV with $Q_o^{(2)}$ = 11.12 eb. The three curves correspond three different values of the electric hexadecupole moment of the ^{238}U; $Q_o^{(4)}$ = 0.0 eb and $Q_o^{(4)}$ = 3.0 eb^2.

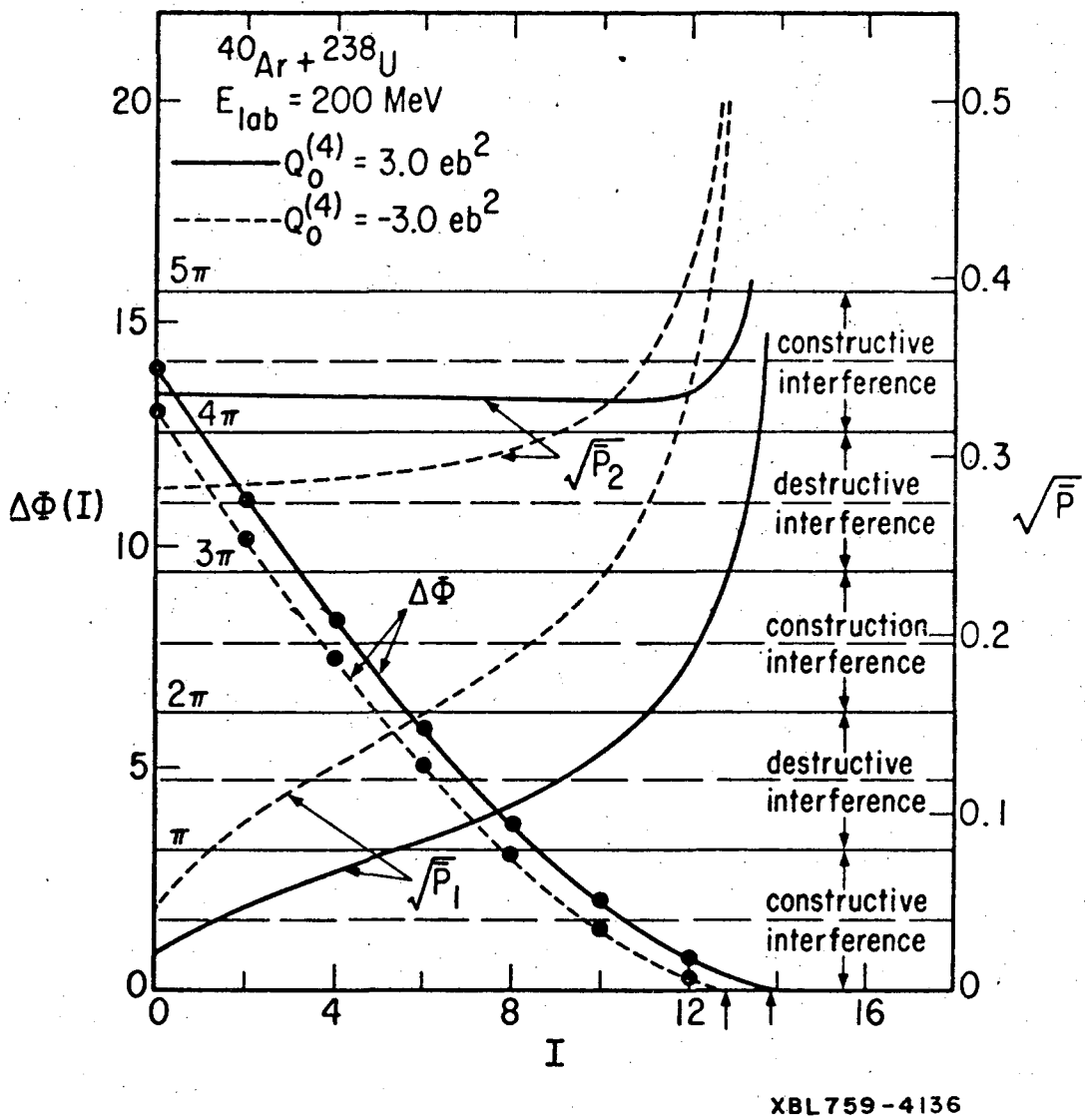

Fig. III-17 Graphs of $\Delta\Phi$, $\sqrt{\bar{p}_1}$ and $\sqrt{\bar{p}_2}$ versus I for the same example shown in Fig. III-16. (For the case $Q_o^{(4)} = 0$, see Fig. III-9).

shows a graph of the function $\bar{p}_1$, $\bar{p}_2$ and the phase difference $\Delta\Phi$ versus spin I. For a negative $Q_o^{(4)}$ the difference between $\bar{p}_1$ and $\bar{p}_2$ is smaller than for positive $Q_o^{(4)}$ (for $Q_o^{(4)} = 0$ the values of $\bar{p}_1$, $\bar{p}_2$ and $\Delta\Phi$ lie in between, see Fig. III 9). This has as a consequence that the interference pattern for negative $Q_o^{(4)}$ will be more pronounced than for positive $Q_o^{(4)}$. This can be observed in Fig. III 18, which shows a plot of the excitation probability vs. I for this example.

In Fig. III 19 the excitation probability for a few selected states (I = 4, 6 and 10) of the rotational band of ^{238}U in the backscattering of ^{40}Ar ions are shown for the bombarding energies between 150 and 210 MeV. One finds the same quantitative agreement with the conventional semiclassical approximation (de Boer-Winther) as for the case $Q_o^{(4)} = 0$ (Fig. III 12). Also one observes here more clearly that for negative $Q_o^{(4)}$ the interference pattern is larger than for positive $Q_o^{(4)}$.

The next step in the development of the backscattering problem of heavy ions will be the inclusion of an optical nuclear potential, to which we devote the next section.

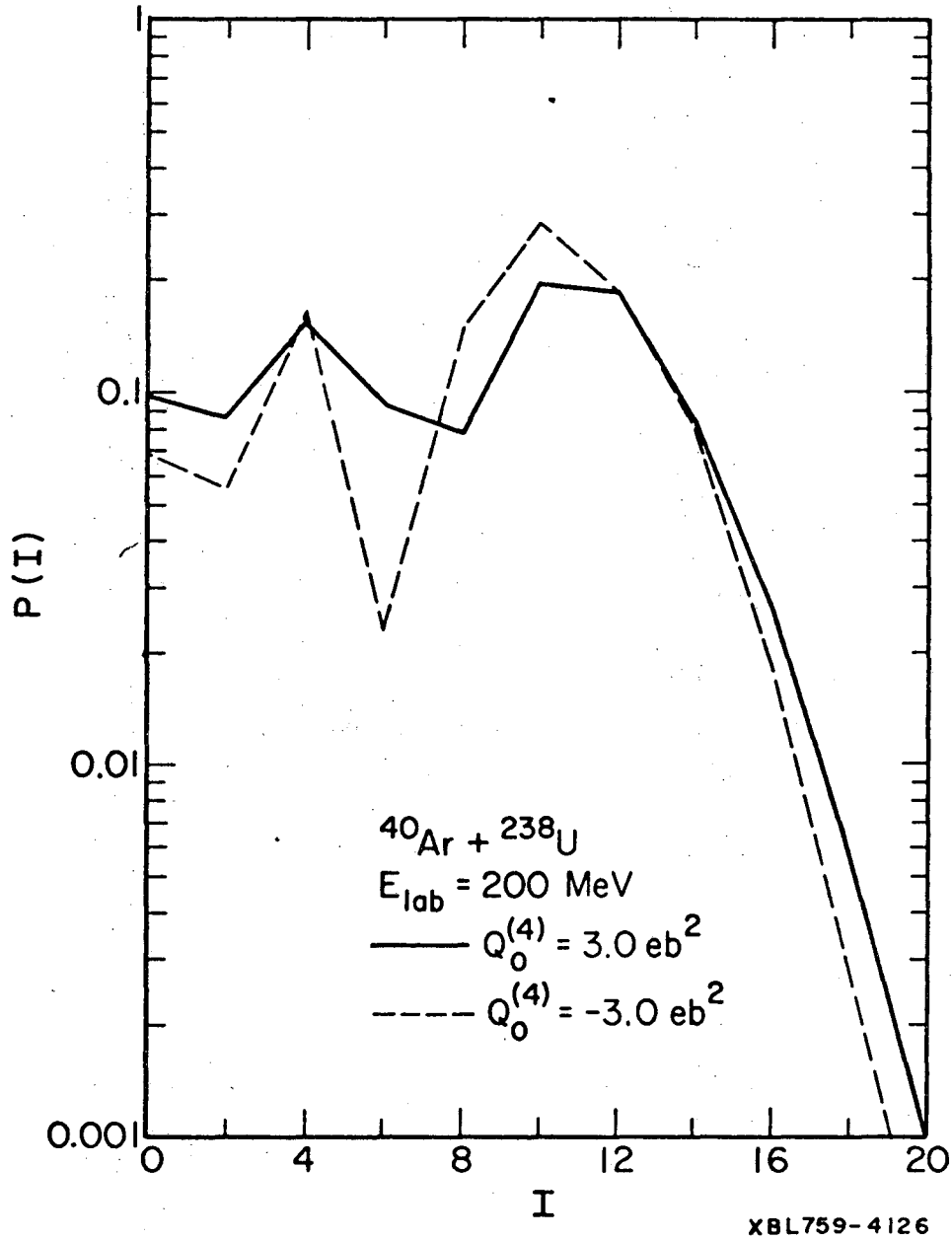

Fig. III-18 Excitation probabilities, using the USCA, of exciting rotational states in ^{238}U for the same example as Fig. III-17.

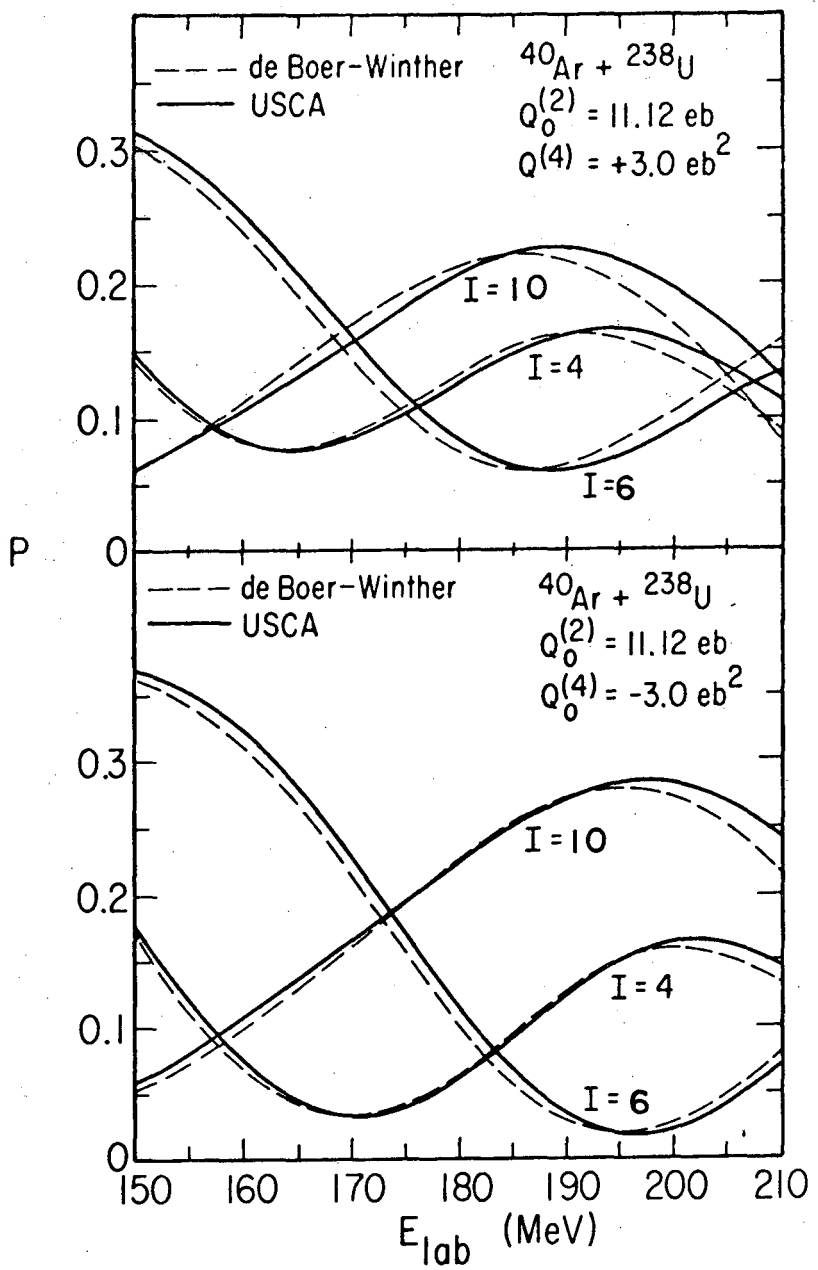

Fig. III-19 Same as Fig. III-12, but including the hexadecupole interaction with a) $Q_0^{(4)}$ = + 3.0 eb^2, b) $Q_0^{(4)}$ = -3.0 eb^2.

3) Nuclear Coulomb Interference with Heavy Ions.

a) The optical potential

In view of the success in applying the USCA method to backscattering Coulomb excitation, we will now go one step further and include the nuclear potential.[28] In the USCA method this implies changing somewhat the equation of motion the system has to follow. With this relatively minor change it is hoped that we will be able to say something about the Coulomb-nuclear interference effect in deformed nuclei with very heavy ions, a problem for which as yet no other method seems applicable. The nuclear force will be included by representing the interaction between target and projectile through a complex optical potential. As in the previous sections, the only phenomenon we will be studying here will be the excitation of rotational bands in the target (by means of the Coulomb and nuclear force) and therefore the bombarding energies considered will be not higher than the Coulomb barrier.

The optical potential will be assumed to have a Wood-Saxon type form factor, that is

$$Re\left[U(r,\beta)\right] = -V_o\left(1+\exp\left(\frac{r-R_R(\beta)}{a_R}\right)\right)^{-1} \qquad (73a)$$

$$Im\left[U(r,\beta)\right] = -W_o\left(1+\exp\left(\frac{r-R_R(\beta)}{a_R}\right)\right)^{-1} \qquad (73b)$$

where the nuclear radii are given by

$$R_\alpha(\beta) = r_{0\alpha} A_p^{1/3} + r_{0\alpha} A_T^{1/3} \left(1 + \beta_2 Y_{20}(\beta) + \beta_4 Y_{40}(\beta) - \frac{\beta_2^2 + \beta_4^2}{4\pi} \right) \qquad (74)$$

The parameters β_2 and β_4 are deformation parameters, specifying the shape dependence of mass distribution of the target (the angle β being measured from the symmetry axis of the target). The nuclear potential, according to eqs. (73) and (74), is therefore specified by 6 parameters: V_0, W_0, a_R, a_I, r_{0R} and r_{0I}. The imaginary part of the nuclear potential is necessary in order to account for the incoming flux which does not end up in the "quasielastic" channels. Two very different sets will be used in this section and are shown in Table III 6. Both sets of parameters have been used successfully to fit the elastic scattering of heavy ions, but at energies above the Coulomb barrier. The set A was used by Vandenbosh et al.[29] to fit the elastic scattering of ^{84}Kr on ^{208}Pb at E_{lab} = 494. MeV. while set B, the so-called RAMM potential[30], was used to fit the elastic scattering of ^{40}Ar on ^{238}U at E_{lab} = 284. and 340. MeV. Here we will apply both sets of parameters to the backscattering of ^{40}Ar on ^{238}U, even though the parameter set A was derived for another system and both sets were used to describe elastic scattering at much higher energies. But since there is no better knowledge of what the nuclear potential for heavy ion collisions is for energies around the Coulomb barrier, we use both sets of parameters and study how the results will differ in both cases.

The equations of motion, when including the nuclear potential, will be complex, and therefore even if the integration is started with real initial conditions, all variables will become complex as soon as the

Table III 6. Potential parameters for the calculations described in the text. The potentials are defined by eqs. (73) and (74).

Parameter	Set A	Set B
V_o (MeV)	50.0	73.0
W_o (MeV)	2.0	80.3
a_I (Fm)	0.950	0.624
a_R (Fm)	0.280	0.624
r_{oR} (Fm)	1.167	1.131
r_{oI} (Fm)	1.305	1.131

system moves into the region where the nuclear potential cannot be neglected. In particular, after the integration the quantum number function $\hat{I}(\beta_\infty)$ will be complex. The roots of the equation

$$\hat{I}(\beta_0) = I + 1/2 \tag{75}$$

will be complex; that is, in order to satisy the boundary conditions, the integration has to be started with complex initial orientations. As already mentioned in section III 3b, the initial orientation of the target is not an observable and therefore may be complex. The roots of equation (75) in the complex initial orientation plane are plotted in Fig. III 20 for the backscattering of 200 MeV ^{40}Ar ions on ^{238}U, using for the nuclear potential parameters the set A. For $I \leqslant 10$, the initial orientations are mainly real (in the pure Coulomb excitation case these would correspond to the classically allowed case) and for $I \geqslant 12$ the roots of eq. (75) are essentially complex conjugates of each other (in the pure Coulomb excitation case these would correspond to the classically inaccessible case). It is clear from Fig. III 20 that one cannot make generally a distinction between classically allowed and forbidden transitions since both limits go over into each other in a continuous manner, not as in the case of pure Coulomb excitation, where there existed a singular point. We therefore have to use a formalism in which the classically allowed and forbidden cases are treated on the same footing. This is fortunately possible by using the expression II-(52) for the S-matrix:

$$S_{I\leftarrow 0} = -\sqrt{\pi}\, e^{\frac{i}{2}(\Phi_1+\Phi_2)} \left\{ \left(\sqrt{\bar{P}_1} + \sqrt{-\bar{P}_2}\right) \xi^{1/4} Ai(-\xi) + \right.$$
$$\left. + (-i)\left(\sqrt{\bar{P}_1} - \sqrt{-\bar{P}_2}\right) \frac{1}{\xi^{1/4}} Ai'(-\xi) \right\} \tag{76}$$

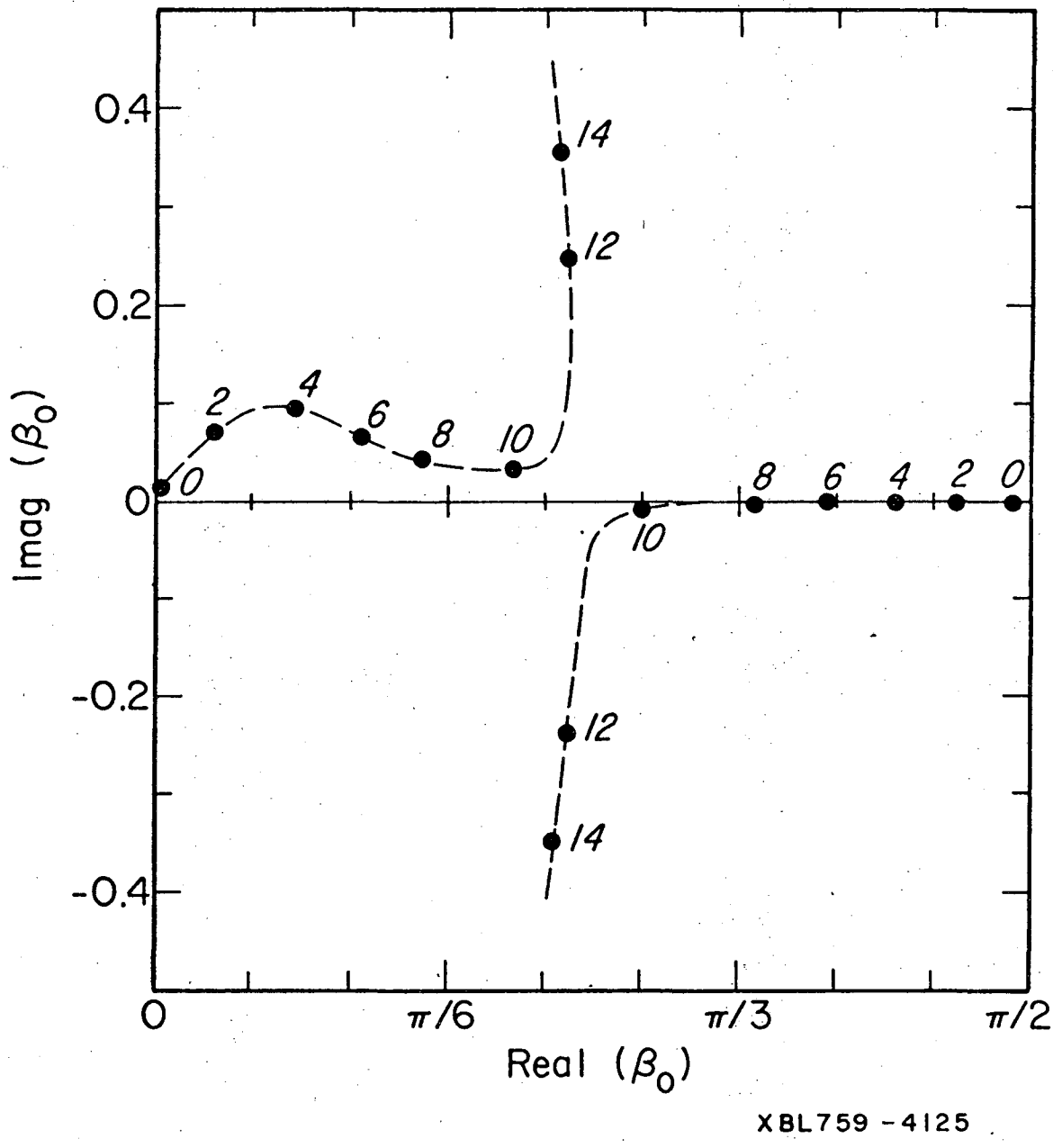

Fig. III-20 The complex roots of the equation $\hat{I}(\beta_0) = I + 1/2$; $\hat{I}(\beta_0)$ being the quantum number function for the backscattering of 200 MeV ^{40}Ar ions on ^{238}U.

with ξ and $\bar{p}_j$ given by

$$\xi^{1/2} = \left[\frac{3}{4}\left(\Phi_2 - \Phi_1\right)\right]^{1/3} \tag{77}$$

and

$$\bar{p}_j = \frac{2 \sin \bar{\beta}_j}{\left(\partial \hat{I}(\beta_0)/\partial \beta_0\right)_j} \qquad j = 1,2 \tag{78}$$

In eq. (78) $\bar{\beta}_{1,2}$ are the roots of eq. (75). The roots with the subindex 1 will be those belonging to the branch in Fig. III 20 for which, when $I = 0$, $\mathrm{Re}\left(\partial \hat{I}(\beta_0)/\partial \beta_0\right) > 0$. In applying eq. (74) one has to assure that one chooses the correct branch when taking the square root. For the pure Coulomb excitation case, the phase difference $\Delta\Phi$ is purely real for the allowed transitions and purely imaginary for the forbidden transitions. When the nuclear potential is included this is no longer true, since one cannot even make the distinction between allowed and forbidden transitions. The behavior of $\Delta\Phi$ for the same case considered in Fig. III 20 is shown in Fig. III 21. The phase of $\Delta\Phi$ changes between the mainly classically allowed transitions ($I \leqslant 8$) and the mainly classically forbidden ($I \geqslant 12$) in a continuous manner by approximately $3\pi/2$; therefore ξ (according to eq. (77)) describes a continuous path in the complex plane starting from mainly positive real values for the classically allowed transitions and ending up with mainly negative real values for the classically forbidden transitions.

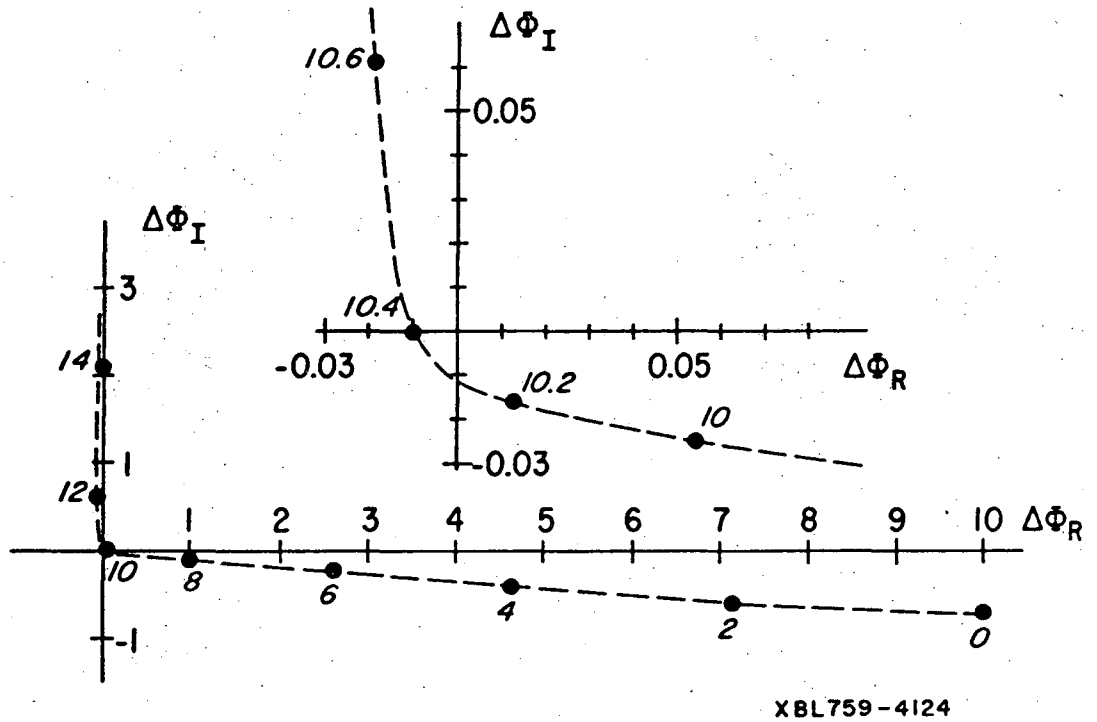

Fig. III-21 The phase difference $\Delta\Phi$ for various values of I. The case considered is the same as the one in the previous figure.

b) Examples

The effect of the nuclear force is two-fold; it modifies the quantum number function (see fig. III 22) and also shifts the phase difference $\Delta\Phi$ (see fig. III 23). Of course, both, $\hat{I}(\beta_\infty)$ and $\Delta\Phi$ will be complex, but if the bombarding energy is such that the nuclear force is only a small perturbation, then $\hat{I}(\beta_\infty)$ and $\Delta\Phi$ will be almost real. Figs. III 22 and III 23 correspond to such a case and only the real parts are plotted. Even though the nuclear interaction is very weak for the case shown in Figs. III 22 and III 23 (that is $^{40}Ar + ^{238}U$ at $E_{lab} = 180.0$ MeV and with the nuclear potential parameter set A) and reduces the quantum number function by only 5%, the effect on the excitation probability can be very large (see Fig. III 24). For I = 6 for example, the excitation probability P changes by more than 50%. The nuclear force introduces, for the example considered, an additional phase shift of approximately 0.5 radians (see Fig. III 23) which is enough to change the interference pattern. The changes in P(I) therefore come mainly from this additional phase shift.

In Fig. III 25 the summed probabilities $\sum_{I \geq I_o} P(I)$ (which is what is experimentally more accessible) are plotted for $I_o = 4, 6, 8, 10$ versus the laboratory bombarding energy. Shown are the results with no nuclear force (pure Coulomb excitation) and using the nuclear potential parameter sets A and B. The two sets of parameters give very different predictions for the excitation probabilities P(I). It is hoped therefore, that by measuring carefully the excitation probabilities one may be able to find a nuclear optical potential parameter set which reproduces the experimental data.

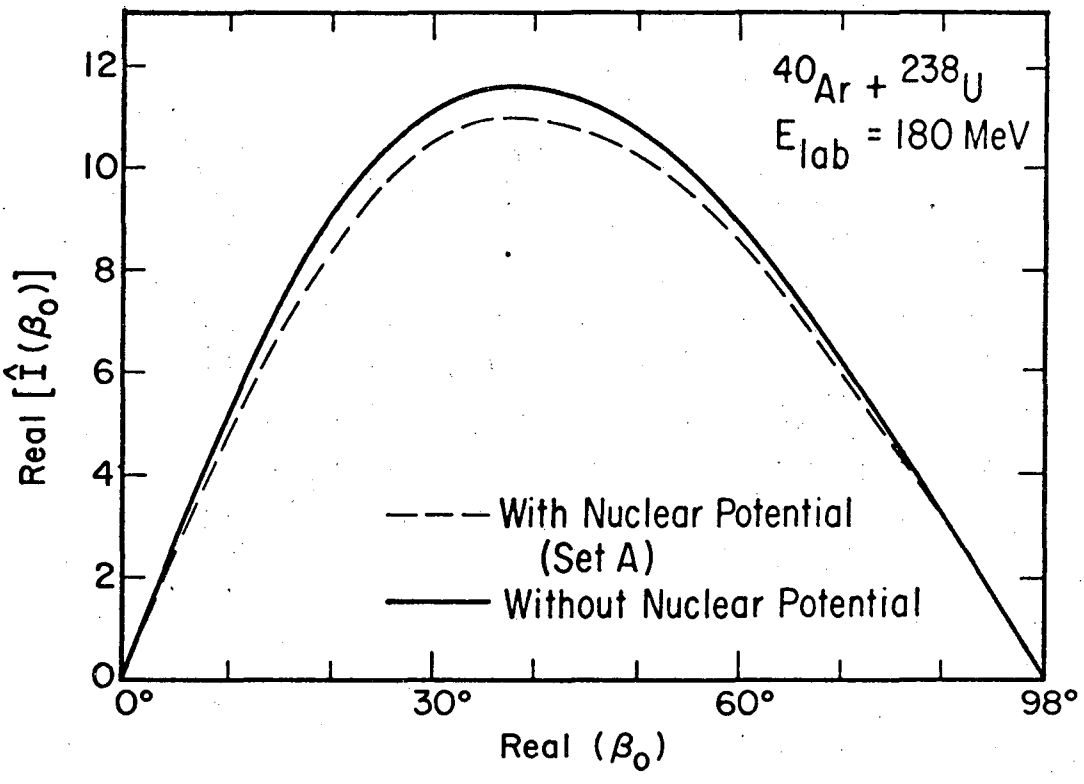

XBL 7510-8411

Fig. III-22 The real part of the quantum number function $\hat{I}(\beta_0)$ is plotted versus Real(β_0) for the backscattering of ^{40}Ar from ^{238}U at E_{lab} = 180 MeV. Shown are the cases of pure Coulomb excitation (full line) and the case where a nuclear potential (with parameter set A) is also included.

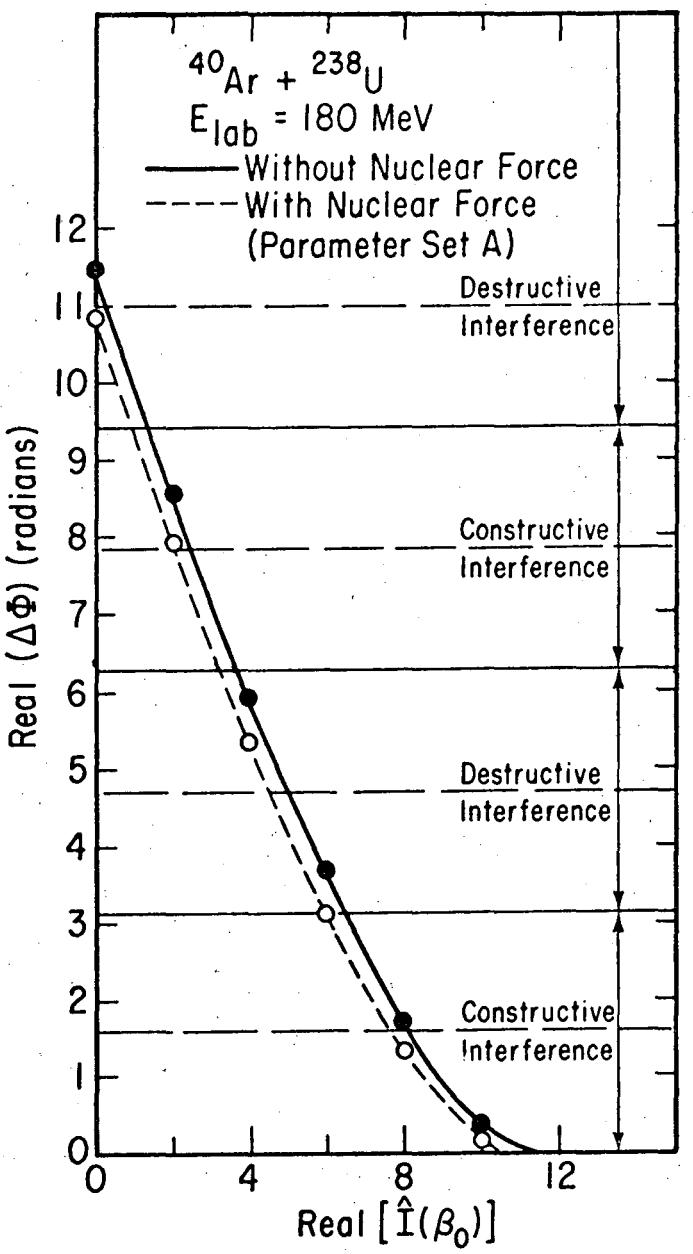

XBL 7510-8412

Fig. III-23 The real part of the phase difference $\Delta\Phi$ is plotted versus Real $(\hat{I}(\beta_0))$, for the same cases considered in the previous figure. The regions where the interference is constructive and destructive are also indicated.

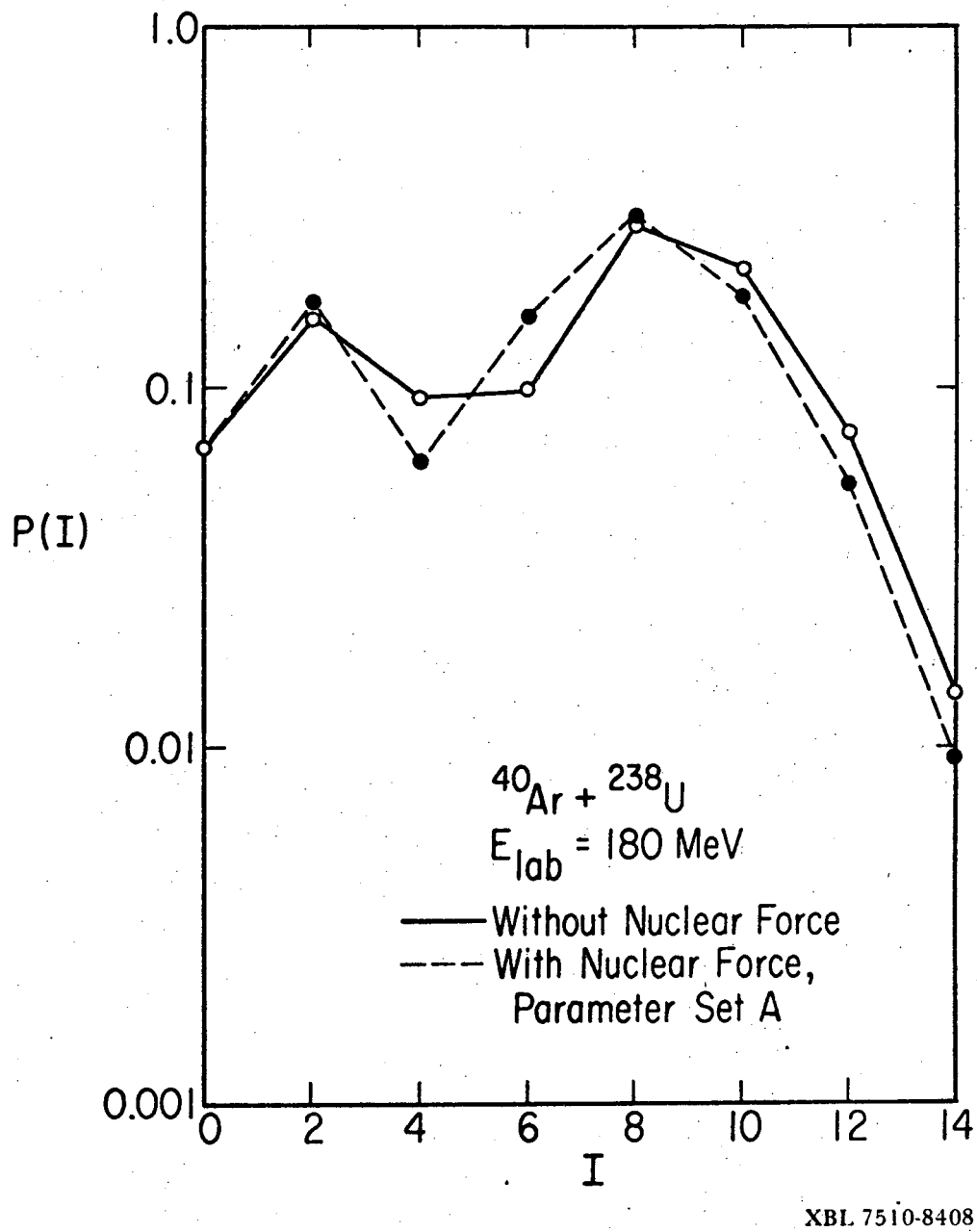

Fig. III-24 Plot of the excitation probability for exciting rotational states with even spin I for the cases considered in the previous figure.

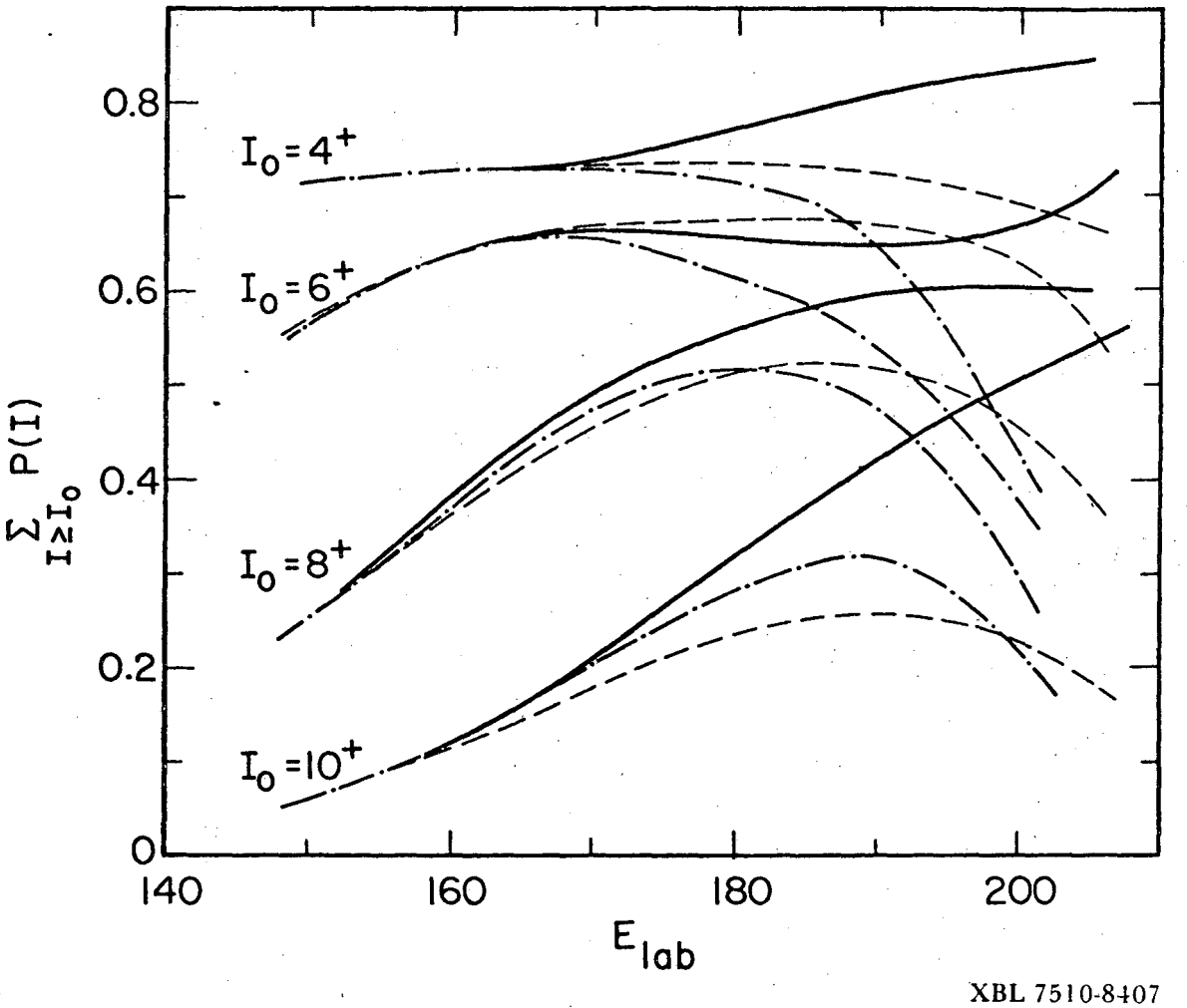

XBL 7510-8407

Fig. III-25 The summed probabilities ($\sum_{I \geq I_o} P(I)$) are plotted for I_o = 4,6,8 and 10 versus E_{lab}. The case considered is the backscattering of ^{40}Ar on ^{238}U. Shown are the result with no nuclear force and also including a nuclear potential with the parameter sets A and B.

In Fig. III-26 the backscattering of ^{40}Ar on ^{238}U at E_{lab}-195. MeV was considered. A purely real nuclear potential was used with parameters V=50 MeV, W=0, a=0.75 Fm and r_o was varied between 1.13 and 1.23 Fm. Fig. III-26 shows the strong dependence of P(I) on r_o. A similar strong dependence of P(I) is found when r_o is kept fixed and some other parameter is varied. By carefully fitting the theoretical to the experimental excitation probabilities to various rotational states I, it might be possible to choose one of the many nuclear optical potentials now being used for heavy ion collisions, all of which reproduce the elastic scattering data.

At higher bombarding energies, close to the barrier top, some additional features come in. In Fig. III-27 the potentials are shown for $^{40}Ar + ^{238}U$ using for the nuclear optical potential the parameter set B. For E_{lab}=205 MeV (~178 MeV in the center of mass frame) and for the case where the target nucleus points its tip toward the beam ($\beta_o=\infty$), one would expect, from looking at the real part of the potential, that they system should go over the barrier until Real(r) is approx. 9.5 Fm. For various time paths in the complex time plane (Fig. III-28) the complex trajectories that r traces are shown in Fig. III-29. The nuclear optical potential is singular for a certain set of values of r, some of these poles are shown in Fig. IV-29. To these singularities in the complex r plane correspond branch points in the complex time plane. Time trajectories which are topologically equivalent and have the same end points give always the same phase $\Delta\Phi$. Trajectories which go around different branch points correspond

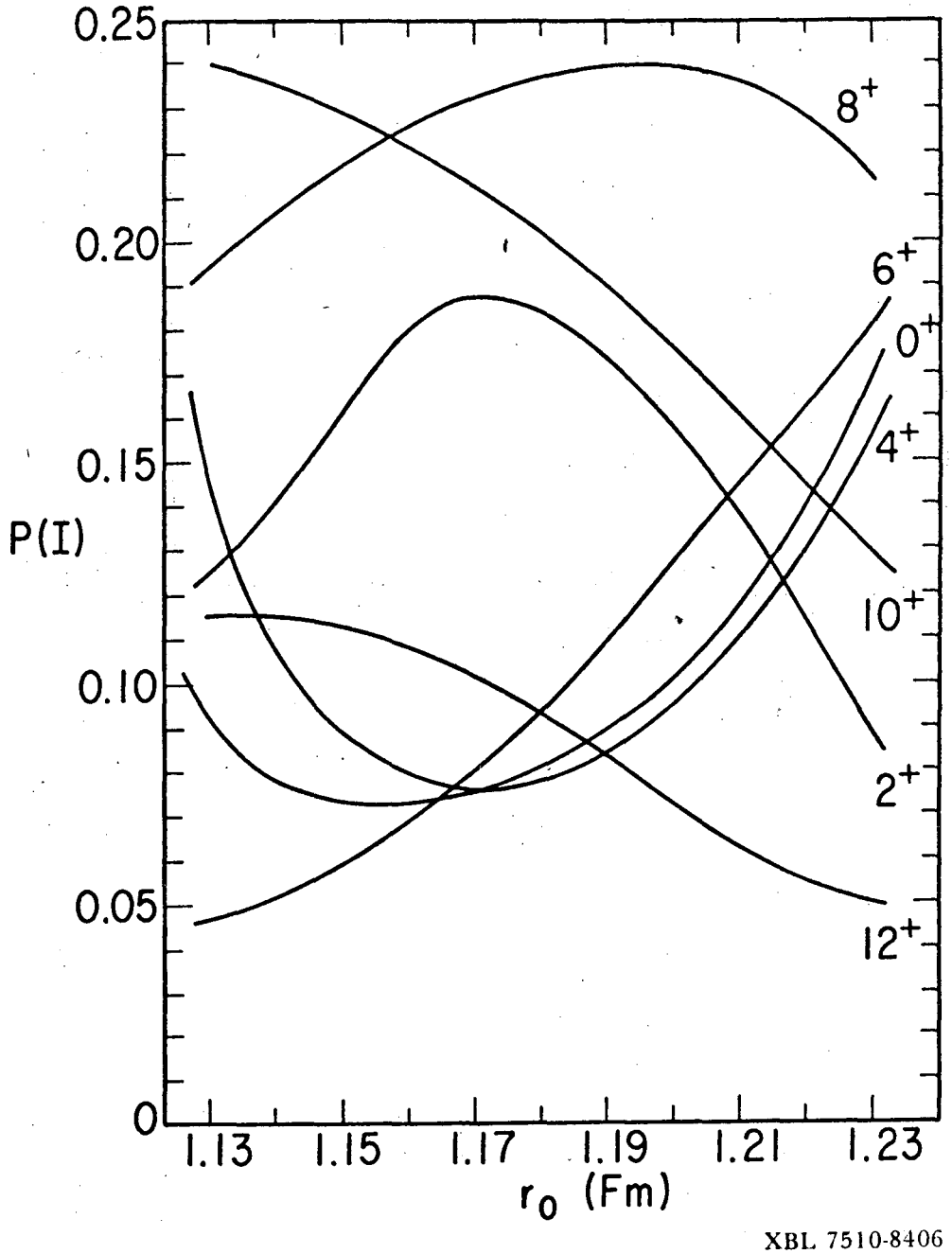

Fig. III-26 Figure showing the strong dependence of the excitation probability P(I) on the parameter r_o keeping all other parameters constant (see text).

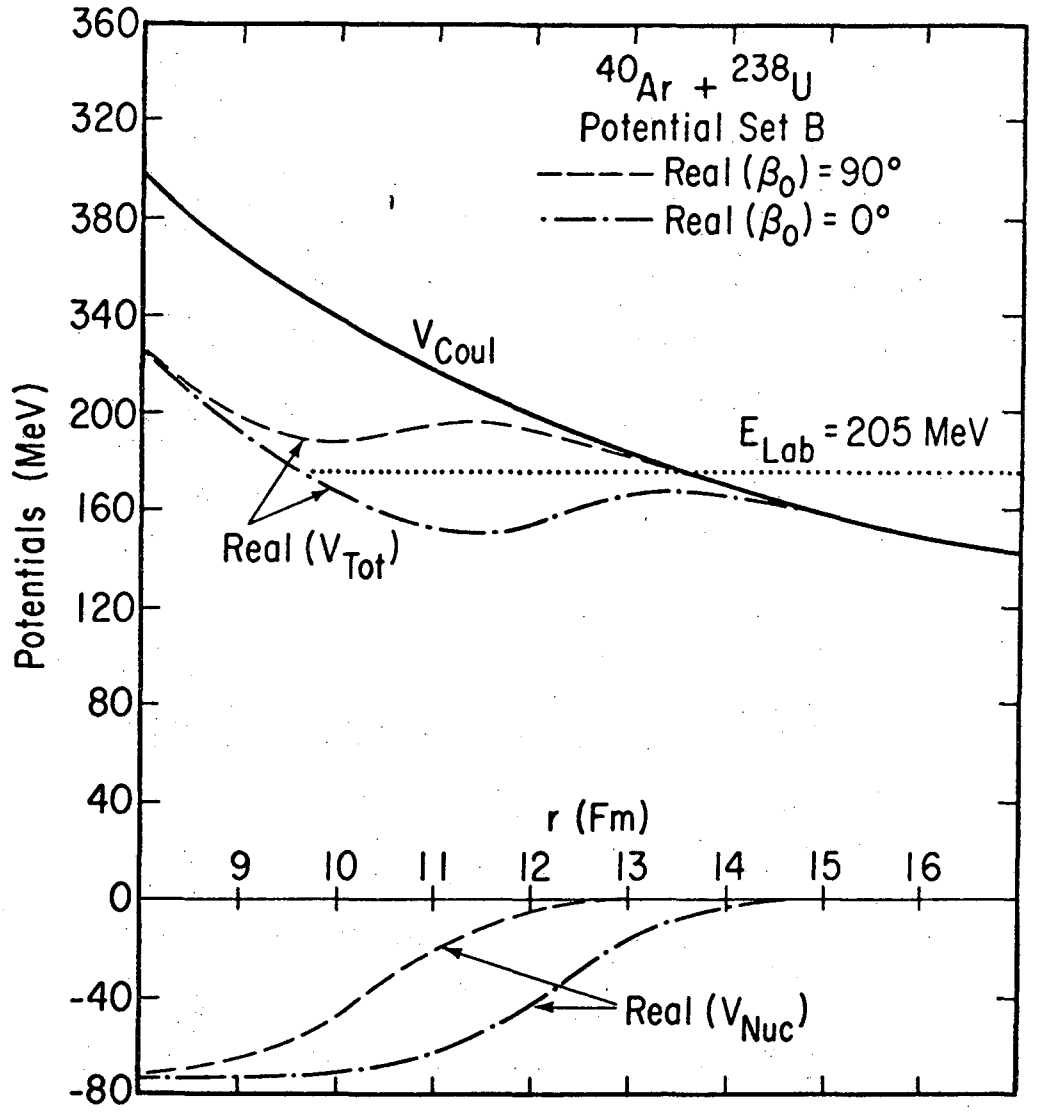

XBL 7510-8413

Fig. III-27 The total potential for the head-on collision of ^{40}Ar on ^{238}U using for the nuclear potential the parameter set B is shown for the initial orientations on the target $\beta_0 = 0°$ (dash-dotted line) and $\beta = 90°$ (dashed line). Also shown are the Coulomb potential (assuming point charges) and the pure nuclear potential.

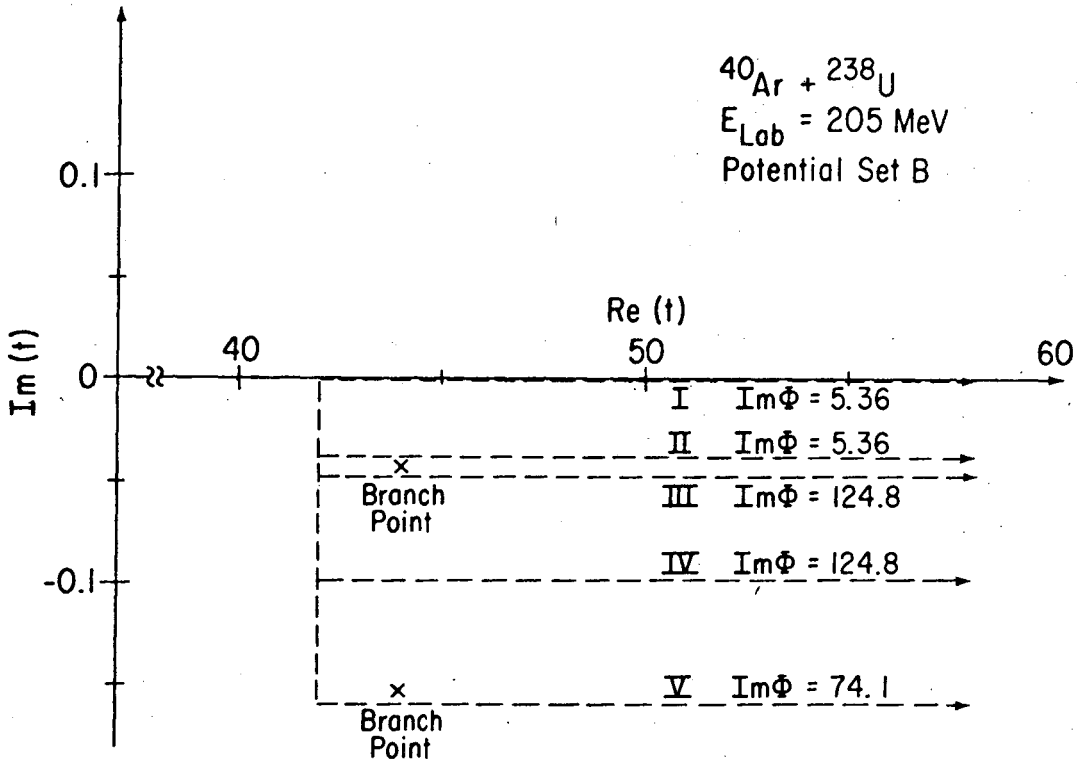

XBL 7510-8409

Fig. III-28 Several time paths in the complex time plane are shown. The case considered is the head-on-collision of ^{40}Ar on ^{238}U at E_{lab} = 205 MeV nuclear potential parameter set B and initial orientation of the target $\beta_o = 0$. For this case the branch points in the complex time plane are indicated.

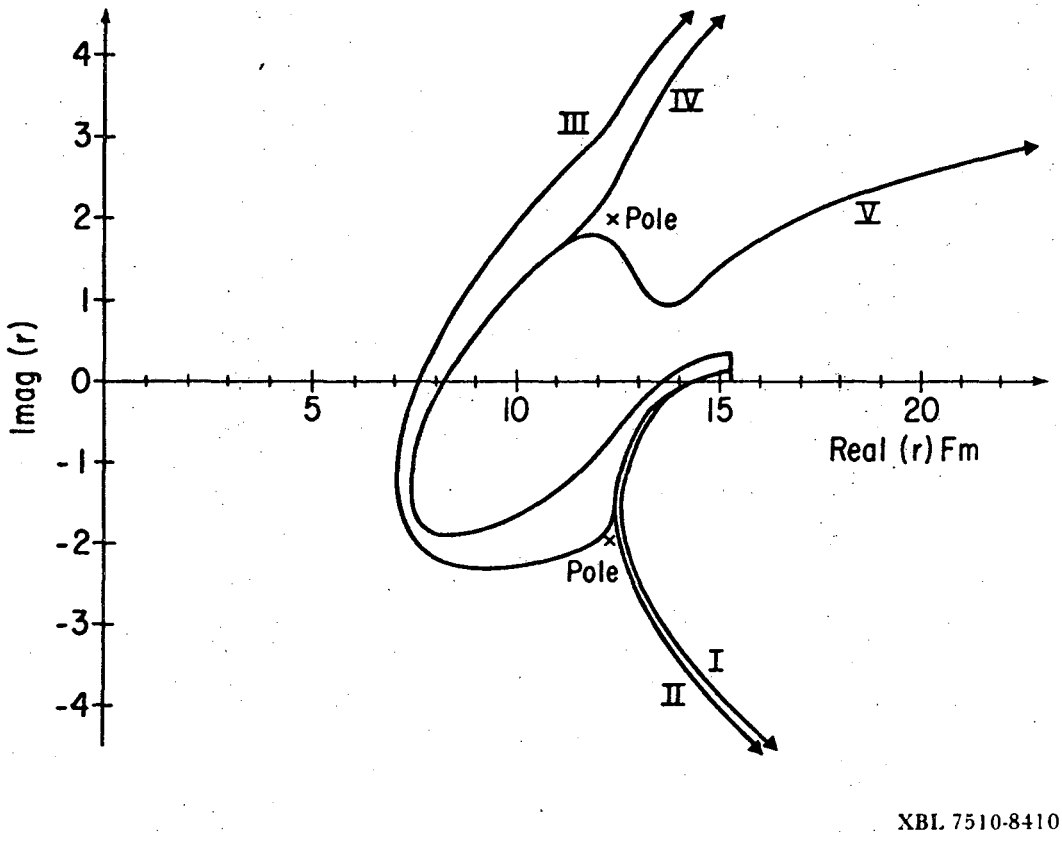

Fig. III-29 Shown are the trajectories in the complex r-plane for the various time paths shown in the previous figure. In the complex r-plane, the total potential has poles; these poles are also indicated.

to different processes and do not give the same phase $\Delta\Phi$. Fig. III-28 shows also the imaginary phase $Im(\Phi)$ (which is a measure of how much the particular trajectory is absorbed). The trajectories which penetrate into the nucleus (trajectories III, IV and V) are almost completely absorbed and therefore there contribution to the quasi-elastic scattering is negligible.

IV TWO DIMENSIONAL TUNNELING OF A FISSION BARRIER MODEL.

1) The problem and conventional approaches.

a) Introduction

The usual procedure in studying the nuclear fission process is to parametrize the shape of the fissioning nucleus by a set of coordinates and then study how the potential energy and the mass parameters for the various degrees of freedom change when the shape parameters are changed. Before fissioning the nucleus usually sits in a well in this potential energy surface and in order to fission, has to tunnel through a barrier to reach a region in the coordinate space where the coordinates describe two separate nuclei.

Presently, nearly all the fission barriers are calculated by the so-called macroscopic-microscopic method. In this method the smooth trends of the potential energy (with respect to particle numbers and deformation) are taken from a macroscopic model, the liquid drop model, and the local fluctuations, also called shell corrections, are taken from a microscopic model. Prior to the Strutinsky[31] method of applying the shell corrections to the liquid drop potential surfaces, the fission barrier heights and shapes were simply not at all understood, but since then much progress has been made in the determination of the collective Hamiltonian describing the fission process. Several groups[32-38] have made careful application of the Strutinsky method and now one has confidence that the main aspects of the potential landscape along the fission trajectories are well known. In all but the heaviest end of the region where spontaneous fission rates

are known there seems to be a two-humped barrier, with the notable fission isomer discovered by Polikanov et al.[39], being a shape-isomeric metastable state in the minimum between the two barriers. It also appears that the innermost saddle may often be unstable with respect to gamma deformation[40], i.e. deviations from cylindrical symmetry, while the outer saddle may be unstable with respect to the reflection symmetry[41]. It would appear that the asymmetry in the fission fragment mass distribution derives from this instability at the second barrier.

In order to describe the deformation energy surfaces for the fission process one needs at least two or three deformation parameters to define the nuclear shape. These generalized coordinates, which are usually strongly coupled, give the generalized forces acting on the fissioning nucleus. For a complete dynamical description of the fission process, however, it is not enough to have a good knowledge of the potential surface, but also a knowledge of the inertial tensor is needed in order to find out how the nucleus will react to the generalized forces. The inertial tensor, of such great importance to the barrier penetration calculations, is only poorly known.

R. Nix[42] has carried out extensive derivations and calculations of irrotational flow hydrodynamical inertial tensors for fission trajectories. The inertial tensor so obtained is, however, too small by a factor of approximately five, i.e. the flow during the barrier penetration is not irrotational. Now it is generally assumed that the first stage of the fission process, the penetration through the barrier, occurs adiabatically and that the cranking model can be used to evaluate the inertial tensor. The Pauli-Strutinsky group[32, 43] and others[44] have extensively been

exploring cranking calculations for the inertial tensor. These calculations show that the inertial tensor depends strongly on the generalized coordinates, i.e. also the inertial tensor couples the different degrees of freedom. In the one-dimensional case however, the coordinate dependence of the inertia introduces no new difficulty since it can be transformed away. H. Hofmann and K. Dietrich[46] have shown how to transform the Schrodinger equation with variable mass $m(q)$ into one with constant mass m_o by modifying the potential. The one-dimensional Schrödinger equation is*

$$H\Psi(q) = \left[-\frac{\hbar^2}{2} \frac{1}{\sqrt{m(q)}} \frac{d}{dq} \frac{1}{\sqrt{m(q)}} \frac{d}{dq} + V(q) \right] \Psi(q) = E\Psi(q) \qquad (1)$$

Performing the following transformation

$$x(q) = \int^{q} \sqrt{\frac{m(q')}{m_o}}\, dq' \qquad (2)$$

where m_o is an arbitrary constant mass, one obtains the Schrödinger equation:

$$\left\{ -\frac{\hbar^2}{2m_o} \frac{d^2}{dx^2} + \tilde{V}(x) \right\} \tilde{\Psi}(x) = E\tilde{\Psi}(x) \qquad (3)$$

where $\tilde{V}(x) = \tilde{V}(x(q)) = V(q)$ and $\tilde{\Psi}(x) = \tilde{\Psi}(x(q)) = \Psi(q)$. This transformation corresponds to a stretching of the potential in such a way that the mass becomes constant. For the more general case of several coupled degrees of freedom, however, it is not possible to find such a

---

* The general expression for the kinetic energy with variable inertia in curvilinear coordinates for many degrees of freedom has been described by Hofmann[46].

transformation.

Another aspect of the fission problem that has recently been stressed by L. Moretto and R. P. Babinet[47] is that besides the coordinates describing the surface configuration, one should also consider the pairing correlation parameters as dynamical variables.

To summarize, the fission process is a challenging multi-dimensional barrier penetration problem, a problem that has been tackled by many groups introducing more or less drastic approximations. Some of these approaches we will now describe briefly.

b) One-dimensional WKB method.

The first calculations of fission lifetimes[33] after the Strutinsky prescription was introduced, took into account as coordinates only ε_2 and ε_4 (that is, quadrupole and hexadecupole deformations) to define the nuclear shape. In order to calculate the penetrability the problem was simplified to a one-dimensional barrier penetration problem, constructing a path on the energy surface by minimizing the potential energy with respect to ε_4 for each ε_2 and then projecting this path into the ε_2 axis. The penetrability *) is then obtained by using the one-dimensional WKB approximation:

$$P_{WKB} = \exp\left\{-2\int_{\varepsilon'}^{\varepsilon''}\sqrt{\frac{2B}{\hbar^2}\left(W(\varepsilon)-E\right)}\,d\varepsilon\right\} \equiv e^{-2K} \qquad (4)$$

An improved expression which does not lose its validity when the penetrability P becomes small, was shown by P. Fröman and N. Fröman[48] to be:

---

*) The penetrability P is roughly related to the spontaneous fission half-life τ by $\tau = 10^{-28.04}/P$ (years)

$$P = \frac{1}{1+e^{2K}} \qquad (5)$$

In these early calculations the inertial mass B associated with fission was taken as a constant or in some cases parametrized as a function of ε in some simple manner. In eq. (4) E is the initial energy of the nucleus in the fission direction and $W(\varepsilon)$ represents the barrier as obtained from the potential energy surface just as described above. The points ε' and ε'' represent the entrance and exit points of the tunneling region, that is $W(\varepsilon') = W(\varepsilon'') = E$ and for ε between ε' and ε'' $W(\varepsilon) > E$. Later essentially the same type of calculations were performed by Randrup et al.[49] to predict the fission half-lives of heavy elements, including not only $P_2(\cos\theta)$ and $P_4(\cos\theta)$ distortions of the nucleus but also $P_3(\cos\theta)$, $P_5(\cos\theta)$ distortions and the gamma degree of freedom.

c) The stationary action path method.

The next refinement in the fission penetration problem was introduced by the Pauli-Strutinsky group (see Brack et. al 32). The two shape coordinates used in their calculations to describe the shape of the fissioning nucleus were a separation or elongation coordinate c and a necking-in coordinate h. The potential energy surface was found using the Strutinsky prescription; the inertial tensor was calculated using the cranking model. A strong shape dependence of the inertial tensor was found; in particular the component corresponding to the elongation coordinate generally exhibits

a large maximum at the saddle. It seems likely that the fission trajectory for barrier penetration might avoid the high-inertial region by avoiding the saddle, even at the cost of a higher potential barrier. As J. Griffin[50] pointed out, if the inertial tensor has nonzero off-diagonal components or if the components depend on the coordinates, then one's intuition of the fission trajectory based on the potential map may be completely wrong. In other words, to assume that the fission trajectory follows along the bottom of the valley may not be adequate. In order to find the path one resorts to classical mechanics by invoking the least action principle.

In classical mechanics the action is defined by:

$$S = \int_{t_1}^{t_2} \sum_i p_i \dot{q}_i \, dt = \int_{q_1}^{q_2} \sum_i p_i \, dq_i \tag{6}$$

Here $\{q_i\}$ are the coordinates describing the system and $\{p_i\}$ are the corresponding canonically conjugate momenta. The principle of least action states[51,17], that in a system for which the Hamiltonian H is conserved (i.e. if H (q,p) = E =const.) one has

$$\Delta S = 0 \tag{7}$$

where the variation Δ does not include all the virtual displacements of the system, but only those for which the energy is conserved along the varied path. One has:

$$p_i = \frac{\partial L}{\partial \dot{q}_i} = \frac{\partial}{\partial \dot{q}_i} \left(\sum_{ij} B_{ij}(q) \dot{q}_i \dot{q}_j - W(q) \right) \tag{8}$$

also

$$E = \frac{1}{2}\sum_{ij} B_{ij}(q)\,\frac{dq_i}{dt}\,\frac{dq_j}{dt} + W(q) \tag{9}$$

from which dt can be found:

$$dt = \sqrt{\sum_{ij} B_{ij}(q)\,dq_i\,dq_j}\Big/\Big(2(E-W(q))\Big) \tag{10}$$

Substituting (10) and (8) in eq. (6) we find:

$$S = \int_{\sigma_1}^{\sigma_2} \sqrt{2\big(E-W(\sigma)\big)\sum_{ij} B_{ij}(q)\frac{dq_i}{d\sigma}\,\frac{dq_j}{d\sigma}}\;d\sigma \tag{11}$$

where σ is some arbitrary parameter along the trajectory and B_{ij} is the inertial tensor which may also depend on σ. During the tunneling process $W > E$, and the integrand in eq. (11) is purely imaginary. The tunneling probability is given in the usual way by:

$$P = \left|e^{iS}\right|^2 = e^{-2|S|} \tag{12}$$

The way Brack et al.[32] proceeded to find the trajectory which makes $|S|$ smallest was by forcing the trajectory through several points between the endpoints σ_1 and σ_2. These intermediate points were then varied until the smallest action $|S|$ was obtained. The trajectory so obtained usually did not follow the steepest descent of the potential and did not lead through the extremal points of the deformation energy. It should still be noted that the entrance (σ_1) and exit (σ_2) points in eq. (11) should

be determined in such a way that the action integral is also stationary against variation of these endpoints. The entrance point σ_1 is usually chosen to lie 0.5 MeV (zero point energy) above the bottom of the well (which is a local minimum of the total deformation energy surface); σ_2 then has to lie on the energy contour with the same energy E.

T. Ledergerber and H. C. Pauli[44] using the same method (as the one described in ref. (32), have done calculations using three deformation parameters; an elongation coordinate, a constriction or necking-in coordinate and a parameter describing the left-right asymmetry. The lifetimes obtained from those calculations are in order-of-magnitude agreement with the experimental data; they also show that mass asymmetric fission is favored and that the most probable mass division (peak-to-peak ratio) agrees with the experimental data.

In this multidimensional approach[32,44], however, one still ignores the kinetic energy tied up in the motion orthogonal to the fission path (which may change along the path). The question of inclusion of zero-point energy for the fission degree of freedom depends on how the potential surface was derived. It has been customary in shell-corrected liquid drop model work (Strutinsky method) to ignore all zero-point vibrational energy corrections, since they would require assumptions about an inertial tensor. Thus, liquid drop model parameters are adjusted to fission barrier heights. With such a surface it is clearly incorrect simply to add zero-point energies. On the other hand is it impossible to do correct quantum mechanical dynamics in more than one dimension without taking into account zero-point corrections. A solution to this dilemma has been proposed by Maruhn and Greiner[52]: they readjust the three liquid drop

parameters a_1, a_2 and r_o appearing in the Myers-Swiatecki-formula[53] to lower the groundstate potential energy (and that of the final fragments) by the zero-point energy, which was obtained from the first 2^+ state experimentally observed. The third parameter is used to keep the barrier height at its experimentally determined value. By this procedure it is possible to get the right penetrabilities and to allow an inclusion of the zero-point motion, which is important for dynamical calculations. However, it is not clear if the change of the zero-point energies along the fission valley is reproduced by this fit in the right way. This point needs further investigation.

d) Tunneling and the inverted potential energy surface.

Consider a system which moves toward a potential barrier and let time be the parameter in the equations of motion parametrizing the evolution of the system. If the time increments are kept real, the system will move toward the barrier and then reflect at the barrier and move back. If, however, one takes purely imaginary time increments when the system is at the turning point, the system will start tunneling. In other words, during the tunneling process the system follows the classical equations of motion but with purely imaginary time increments (see also Fig. IV 3).

If at the classical turning point of the fission degree of freedom also all other degrees of freedom are at a turning point or, in other

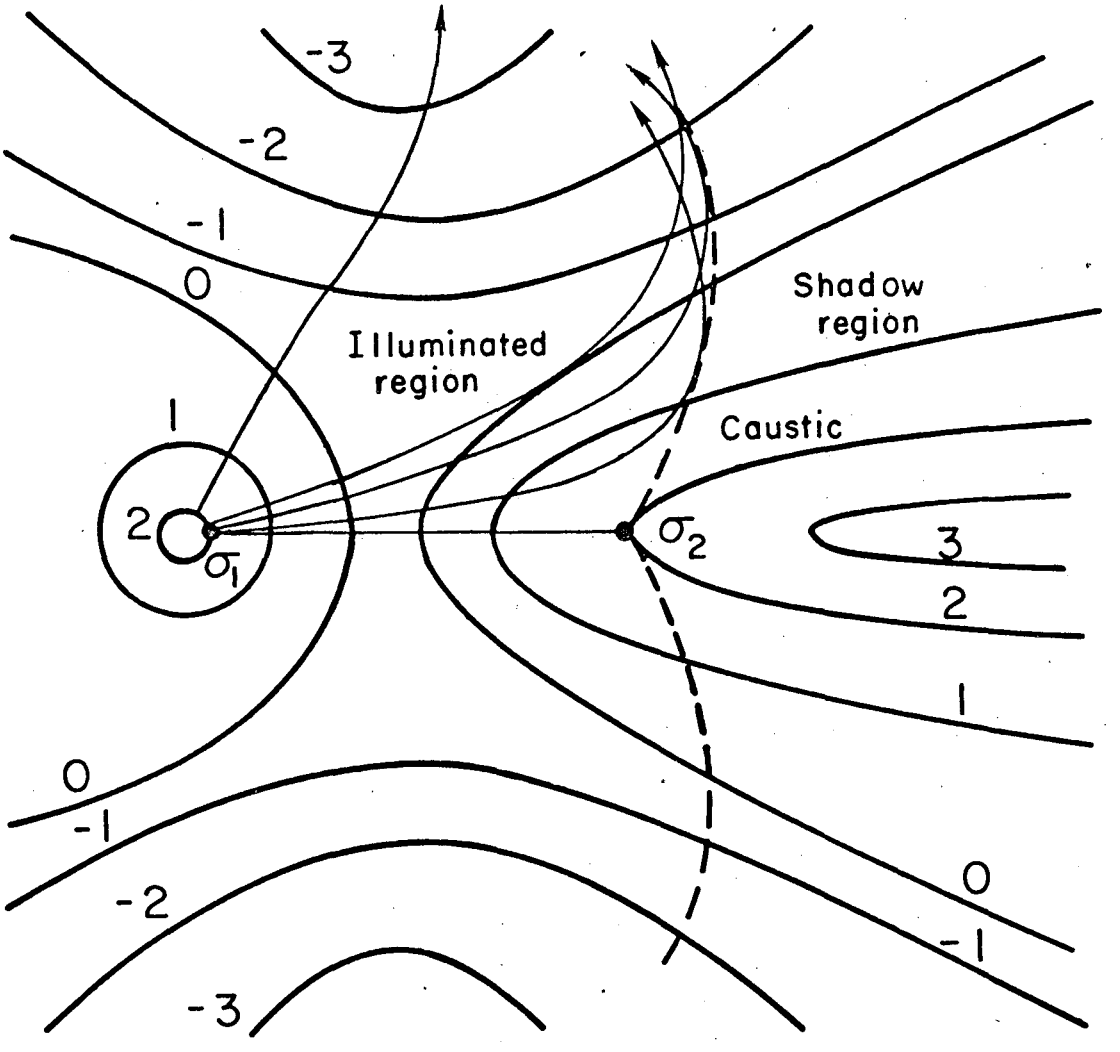

XBL759-3877

Fig. IV-1 Schematic representation of a contour map of a potential energy surface turned around to study the classical motion below the barrier. The entrance and exit points, σ_1 and σ_2, lie on the same equipotential. The bill at the left side corresponds to the potential well in which the nucleus sits before fissioning and the mountain range at the right represents the fission valley.

words, if the system when it reaches the barrier is at rest*, then the tunneling process can be visualized by a very simple picture. If the system is at rest at the turning point and if one uses purely imaginary time increments thereafter (until the tunneling is completed), all the coordinates will remain real, all quantities related to odd powers of the time (for example velocities, momenta, angular momenta, etc.) will be purely imaginary; quantities which depend on the square of momenta (for example the kinetic energy, centrifugal force, etc.) will change sign. It is now easy to see that the system can equivalently be described by using only real time increments and changing the sign of (V-E). That is, the tunneling trajectories can be obtained by finding how the system moves on the inverted potential surface[54]. For the fission example, the entrance point σ_1 will now be close to the top of a hill and the fission valley will be a mountain ridge starting somewhere close to the hill (see Fig. IV 1 for a simple illustration of this idea). The system now has to "roll" down the hill and up the mountain ridge (following the classical equations of motion) in such a way that it does not fall off the ridge to either side but reaches the exit point σ_2, where the velocity

---

* This is one of the basic hypotheses of the least action path method; one assumes there that at the entrance and exit points (σ_1 and σ_2) the system is at rest. This hypothesis will be considered later in some detail. In an actual multidimensional tunneling process this hypothesis is actually never fulfilled, since all the coordinates orthogonal to the coordinate along the fission trajectory are more or less harmonic and even all these "harmonic" degrees of freedom are in their "ground" state, there still remains the zero point energy, and so it becomes very unlikely that the system will find itself at rest on the potential surface at any time.

is zero again (at this point, if one wants to follow the system into the fission valley, one would switch to the ordinary potential surface again). If, after the system reaches σ_2, the time increments are kept purely imaginary (or equivalently, using real time one keeps the inverted potential surface), the system will move toward σ_1 again. Finding the tunneling trajectory then (in the least action sense, as described in the previous subsection) is equivalent to finding the periodic orbit on the inverted potential surface. In the example shown in Fig. IV 1 there is only one point (in the general case it can be one or more intervals) on the entrance and one point on the exit energy contour which are connected through classical equations of motion; therefore, when looking for the trajectory with the minimum action $|S|$ in the least action path method, one also has to vary the endpoints σ_1 and σ_2 until the minimum is achieved.

Another example of tunneling and motion on the inverted potential surface is given in appendix B.

It is clear that in the stationary path method, once the "tunneling" trajectory is found, that the tunneling probability depends only on the trajectory and not on the features adjacent to the fission path, that is, it does not include zero-point energy effects of the degrees of freedom orthogonal to the fission path. If, for example, the width of the "harmonic" potential of the orthogonal coordinates to the fission path narrows, the zero-point energy will become higher and as a consequence the energy available in the fission direction will diminish, reducing the tunneling probability. If the tunneling is viewed as the classical motion on the inverted potential surface, the narrowing of the harmonic potential reflects

itself by making the ridge steeper in Fig. IV 1, that is, it will be more difficult to reach the exit point σ_2 (easier to fall off to either side), and consequently the tunneling probability will be smaller.

It seems natural to assume that if one wants to know whether, during a tunneling process, the system behaves adiabatically or non-adiabatically, one looks at how fast the system would move on the inverted potential surface. Contrary to what is occasionally stated, during the tunneling stage of the fission process the system would be least adiabatic at the saddle point.

e) Quantum mechanical DWBA approach

The two-dimensional Schrödinger equation has the form:

$$H\Psi = \left\{ -\frac{\hbar^2}{2} \sum_{ij=1,2} \frac{1}{D} \frac{\partial}{\partial q_i} D g^{ij} \frac{\partial}{\partial q_j} + V(q^1, q^2) \right\} \Psi = E\Psi \qquad (13)$$

where g^{ij} are the contravariant components of the inertial tensor (g_{ij}) and $D = \sqrt{\det(g_{ij})}$; $V(q^1, q^2)$ is the potential energy, a function of the curvilinear coordinates q^1, q^2.

In Appendix A of ref. 55, H. Hofmann describes a method for finding a coordinate transformation $x = x(q^1, q^2)$, $y = y(q^1, q^2)$ which has the following properties: i) that the off-diagonal components of the inertial tensor expressed in the new coordinates vanish (i.e. if m_{ij} represent the convariant components of the inertial tensor in the new coordinate system, then $m_{xy} = m_{yx} = 0$), ii) that the trajectory $y = 0$ defines a path of minimal potential energy (i.e. $(\partial V(x,y)/\partial y)_{y=0} = 0$). After performing such a coordinate transformation the Hamiltonian eq. (13) becomes:

$$H = -\frac{\hbar^2}{2}\left[\frac{1}{\sqrt{B_x B_y}}\frac{\partial}{\partial x}\sqrt{\frac{B_y}{B_x}}\frac{\partial}{\partial x} + \frac{1}{\sqrt{B_x B_y}}\frac{\partial}{\partial y}\sqrt{\frac{B_x}{B_y}}\frac{\partial}{\partial y}\right] + V \qquad (14)$$

where the notation $B_x = m_{xx}$ and $B_y = m_{yy}$ was introduced.

Hofmann[55] also introduced a harmonic approximation for the potential perpendicular to the fission path and with the additional assumption that the mass tensor components do not depend on the coordinate y, reduced the Hamiltonian eq. (14) to:

$$H = -\frac{\hbar^2}{2}\left[\frac{1}{\sqrt{B_x B_y}}\frac{\partial}{\partial x}\sqrt{\frac{B_y}{B_x}}\frac{\partial}{\partial x} + \frac{1}{B_y}\frac{\partial^2}{\partial y^2}\right] + V(x,0) + \frac{B_y\omega^2}{2}y^2 \qquad (15)$$

and solved it approximately in what can be called the first truly two-dimensional quantum mechanical dynamical treatment of the fission process. In eq. (15) $\omega(x)$ is defined by

$$\omega^2(x) \equiv \frac{1}{B_y(x)}\left.\frac{\partial^2 V(x,y)}{\partial y^2}\right|_{y=0} \qquad (16)$$

The Hamiltonian is then separated into an adiabatic H^{ad} and a non-adiabatic H^{nad} part. If the system is initially in an oscillator state n, then $H^{nad} = H - H^{ad}$ can produce transitions to other oscillator states m. The probability amplitudes A_{mn} of finding the system after the barrier penetration in a state m satisfies an integral equation for which Hoffmann uses the Born approximation (DWBA) to get an approximate solution. This use of the DWBA however, as we see later, is probably only good

when considering transitions which start from the ground state before fission. When starting from an excited state, the transition probabilities to the ground state are usually higher by some orders of magnitude than the one to excited states (even in the case where the coupling between the two degrees of freedom is quite small). The reason is that the system can penetrate much easier within the ground state.

f) A two-dimensional fission barrier model.

In order to investigate the full two-dimensional dynamics and test various approximations it is of value to study a simple model system for which also a quantum mechanical solution can be given. In section IV 2 we will describe how to carry out such a fully quantum mechanical calculation by the method of coupled channels. In section IV 3 we will study an example where we take a Hamiltonian with a potential giving a Gaussian barrier in the x direction (x being the fission coordinate) and an harmonic potential in the y direction. The mass tensor is taken to be diagonal and constant; the width of the valley however is variable (it changes when going over the barrier) which introduces a coupling of the two degrees of freedom. This problem will be solved using the USCA and a comparison to the exact quantum mechanical solution and the other approximate methods described in this section will be made.

2) Quantum mechanical solution to the two-dimensional fission barrier penetration problem[56].

a) The Schrödinger equation.

We will consider a Hamiltonian of the form eq. (14), which can be written as:

$$H = -\frac{\hbar^2}{2}\left\{\frac{1}{B_x}\left[\frac{\partial^2}{\partial x^2}+\left(\frac{\partial}{\partial x}\,\mathrm{Log}\sqrt{\frac{B_y}{B_x}}\right)\frac{\partial}{\partial x}\right]+\right.$$

$$\left.+\frac{1}{B_y}\left[\frac{\partial^2}{\partial y^2}+\left(\frac{\partial}{\partial y}\,\mathrm{Log}\sqrt{\frac{B_x}{B_y}}\right)\frac{\partial}{\partial y}\right]\right\}+V(x,y) \qquad (17)$$

where (see section IV 1e) y = 0 defines the path of minimal potential energy; y therefore represents the coordinate which describes the motion in the direction perpendicular to the fission path. The potential along the fission valley has in a typical case a shape like the one shown in Fig. IV 2. Before fissioning the system sits in the local minimum at $x = x_o$; $x = x_{sc}$ shall be the scission point (that is, the place where the nucleus breaks up into two fragments). The system, in order to fission, has to penetrate the potential barrier from $x = x_o$ to x_1. Let's remember that Fig. IV 2 shows only one dimension of the barrier, the barrier along the fission valley.

In order to be able to solve the problem we will introduce the following simplification: That for $x < x_o$ and $x > x_{sc}$ the components of the mass tensor and the potential go asymptotically toward constant values. That is, we will assume the asymptotic behaviour:

$$B_x(x,y) \xrightarrow[x\to\pm\infty]{} B_x^{\pm} \quad \text{(independent of } x \text{ and } y\text{)}$$

$$B_y(x,y) \xrightarrow[x\to\pm\infty]{} B_y^{\pm}(y)$$

$$V(x,y) \xrightarrow[x\to\pm\infty]{} V^{\pm}(y) \qquad (18)$$

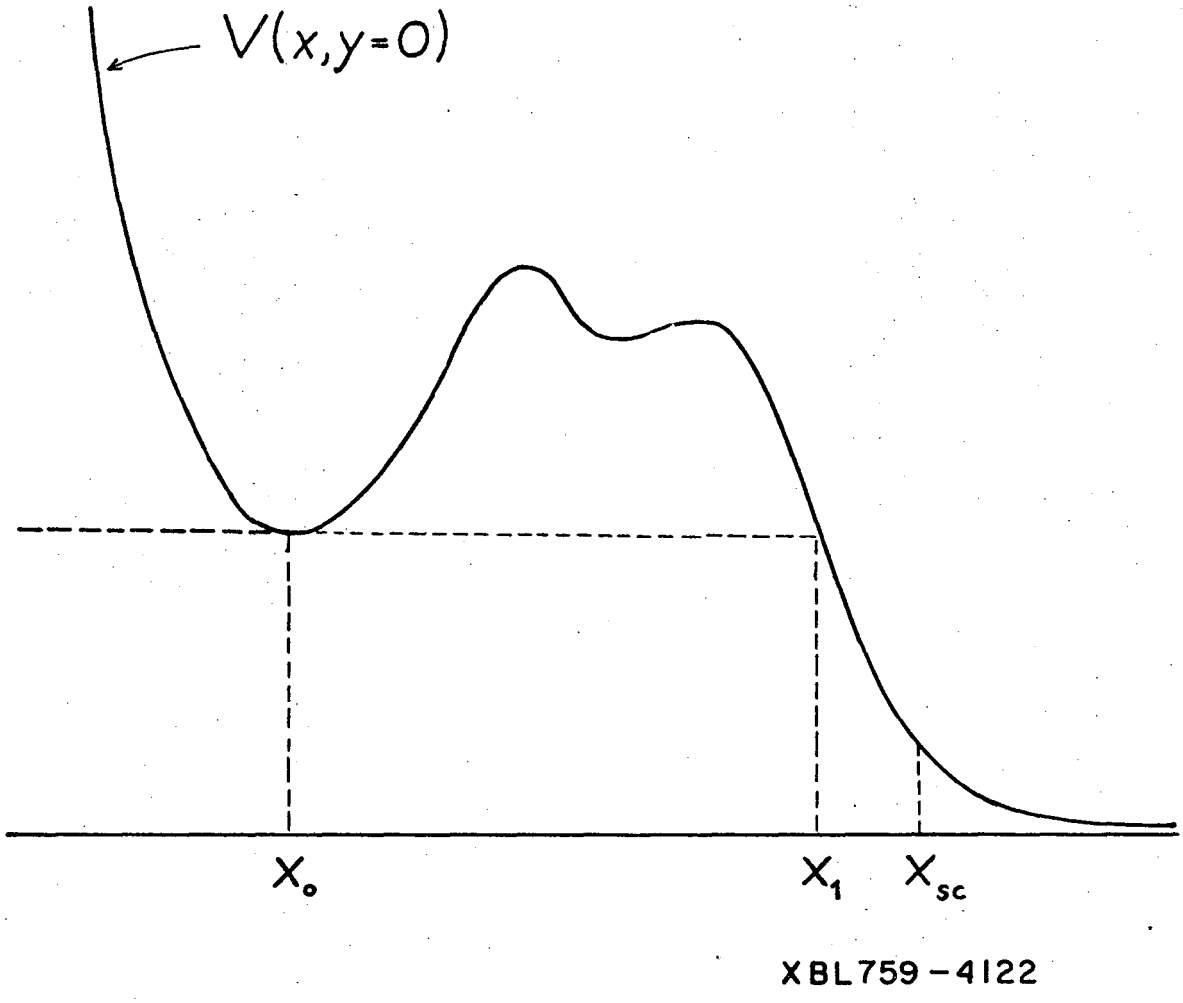

Fig. IV-2 Schematic representation of a fission barrier. Shown is the potential along the fission valley.

For the potential this condition means that for $x < x_o$ the potential will be more like the dashed line in Fig. IV 2.

The Schrodinger equation we wish to solve is (using the Hamiltonian eq. (17)):

$$\left\{\frac{\partial^2}{\partial x^2}+\left(\frac{\partial}{\partial x}\operatorname{Log}\sqrt{\frac{B_y}{B_x}}\right)\frac{\partial}{\partial x}+\frac{B_x}{B_y}\left[\frac{\partial^2}{\partial y^2}+\left(\frac{\partial}{\partial y}\operatorname{Log}\sqrt{\frac{B_x}{B_y}}\right)\frac{\partial}{\partial y}\right]+\right.$$

$$\left.+\frac{2B_x}{\hbar^2}\left(E-V(x,y)\right)\right\}\Psi=0 \tag{19}$$

Let's expand the wave function Ψ in terms of harmonic oscillator wave functions of oscillator length α :

$$\Psi(x,y)=\sum_n u_n(x)\,\varphi_n(y) \tag{20}$$

where $\varphi_n(y)$ are the harmonic oscillator wave functions

$$\varphi_n(y)=\frac{1}{\sqrt{\alpha}}\,h_n\!\left(\frac{y}{\alpha}\right)e^{-\frac{y^2}{2\alpha^2}} \tag{21}$$

where h_n satisfies the recursion relation

$$h_n(z)=\sqrt{\frac{2}{n}}\,z\,h_{n-1}(z)-\sqrt{\frac{n-1}{n}}\,h_{n-2}(z) \tag{22}$$

and is related to the Hermite polynomials by

$$h_n(z)=\frac{1}{\sqrt[4]{\pi}}\,\frac{H_n(z)}{\sqrt{2^n\,n!}} \tag{23}$$

Substituting the expansion for Ψ (eq. (20)) in (19) we get

$$\sum_{n'} \varphi_{n'}(y) \frac{\partial^2}{\partial x^2} U_n(x) = \sum_{n'} \left(-\frac{1}{2}\right)\left(\frac{\partial}{\partial x} \mathrm{Log} \frac{B_y}{B_x}\right) \varphi_{n'}(y) \frac{\partial}{\partial x} U_{n'}(x) +$$

$$+\sum_{n'} -\left[\frac{B_x}{B_y} \frac{\partial^2}{\partial y^2} + \frac{1}{2}\left(\frac{\partial}{\partial y} \frac{B_x}{B_y}\right) \frac{\partial}{\partial y} + \frac{2B_x}{\hbar^2}\left(V-E\right)\right] \varphi_{n'}(y) U_{n'}(x) = 0 \tag{24}$$

Multiplying eq. (24) from the left by $\varphi_n^*(y)$, integrating over y and using the orthonormality of the wave functions φ_n . $\left(\int \varphi_n^* \varphi_{n'} = \delta_{nn'}\right)$ one finds

$$\frac{\partial^2}{\partial x^2} U_n(x) = \sum_{n'} \left\{ A_{nn'}(x) \frac{\partial}{\partial x} + B_{nn'}(x) \right\} U_{n'}(x) \tag{25}$$

or with $V_n(x) \equiv \frac{\partial}{\partial x} U_n(x)$ one finds the system of coupled equations:

$$\frac{d}{dx} U_n(x) = V_n(x) \tag{26a}$$

$$\frac{d}{dx} V_n(x) = \sum_{n'} \left[A_{nn'}(x)\, V_{n'}(x) + B_{nn'} U_{n'}(x) \right] \tag{26b}$$

or in a more compact way

$$\frac{d}{dx}\begin{pmatrix} U \\ V \end{pmatrix} = \begin{pmatrix} 0 & 1 \\ B & A \end{pmatrix}\begin{pmatrix} U \\ V \end{pmatrix} \tag{27}$$

The matrices A and B are given by

$$A_{nn'}(x) \equiv -\frac{1}{2}\int_{-\infty}^{+\infty}\varphi_n^*(y)\left[\frac{\partial}{\partial x}\mathrm{Log}\left(\frac{B_y(x,y)}{B_x(x,y)}\right)\right]\varphi_{n'}(y)\,dy$$

$$= -\frac{1}{2}\left\langle n\left|\frac{\partial}{\partial x}\mathrm{Log}\,\frac{B_y}{B_x}\right|n'\right\rangle \qquad (28)$$

and

$$B_{nn'}(x) \equiv \int_{-\infty}^{+\infty}\varphi_n(y)\left\{-\frac{B_x(x,y)}{B_y(x,y)}\frac{\partial^2}{\partial y^2} - \frac{1}{2}\left(\frac{\partial}{\partial y}\frac{B_x(x,y)}{B_y(x,y)}\right)\frac{\partial}{\partial y} + \right.$$

$$\left. - \frac{2B_x(x,y)}{\hbar^2}\Big(V(x,y)-E\Big)\right\}\varphi_{n'}(y)\,dy$$

$$= \left\langle n\left|\left\{-\frac{B_x}{B_y}\frac{\partial^2}{\partial y^2} - \frac{1}{2}\left(\frac{\partial}{\partial y}\frac{B_x}{B_y}\right)\frac{\partial}{\partial y} + \frac{2B_x}{\hbar^2}\Big(V-E\Big)\right\}\right|n'\right\rangle \qquad (29)$$

b) Evaluation of the matrices A and B.

Let $\mathcal{F}(y)$ be an arbitrary function of y. There are three types of matrix elements needed for the evaluation of the matrices A and B, they are:

i) $$M_1 = \left\langle n\left|\mathcal{F}(y)\frac{\partial^2}{\partial y^2}\right|n'\right\rangle \qquad (30)$$

Using the relation

$$\left(-\frac{\partial^2}{\partial y^2}+\frac{1}{\alpha^4}y^2\right)|n\rangle=\frac{2}{\alpha^2}\left(n+\frac{1}{2}\right)|n\rangle \tag{31}$$

which the harmonic oscillator functions satisfy, one finds

$$M_1=\langle n|\,\mathcal{F}(y)\left(\frac{y^2}{\alpha^4}-\frac{2}{\alpha^2}\left(n+\frac{1}{2}\right)\right)|n'\rangle \tag{32}$$

For the evaluation of matrix elements of this type see iii)

ii) $$M_2=\langle n|\,\mathcal{F}(y)\frac{\partial}{\partial y}|n'\rangle \tag{33}$$

Using the relation

$$\frac{\partial}{\partial y}|n\rangle=\frac{y}{\alpha^2}|n\rangle-\frac{\sqrt{2(n+1)}}{\alpha}|n+1\rangle \tag{34}$$

one finds

$$M_2=\frac{1}{\alpha^2}\langle n|\,\mathcal{F}(y)y|n'\rangle-\frac{\sqrt{2(n'+1)}}{\alpha}\langle n|\,\mathcal{F}(y)|n'+1\rangle \tag{35}$$

For the evaluation of the matrix elements of this type see iii)

iii) $$M_3=\langle n|\,\mathcal{F}(y)|n'\rangle \tag{36}$$

Using eq. (21) this can be written as

$$M_3 = \frac{1}{\alpha}\int_{-\infty}^{+\infty} h_n\left(\frac{y}{\alpha}\right) e^{-\frac{y^2}{2\alpha^2}} \mathcal{F}(y)\, h_{n'}\left(\frac{y}{\alpha}\right) e^{-\frac{y^2}{2\alpha^2}}\, dy$$

$$= \int_0^{+\infty} h_n(z) h_{n'}(z) e^{-z^2} \left(\mathcal{F}(\alpha z) + (-1)^{n+n'} \mathcal{F}(-\alpha z)\right) dz \qquad (37)$$

Integrals of this type must be evaluated numerically (unless the function $\mathcal{F}(\alpha z)$ is of a particularly simple form). The numerical integration of integrals of the type eq. (37) is most conveniently carried out using the so-called Hermite integration method, the results being

$$M_3 \simeq \sum_{i=1}^{N} w_i\, h_n(z_i) h_{n'}(z_i) \left(\mathcal{F}(\alpha z_i) + (-1)^{n+n'} \mathcal{F}(-\alpha z_i)\right) \qquad (38)$$

where the value of the abscissas z_i and the weight factors w_i for the Hermite integration are tabulated in reference 23.

c) The boundary conditions

Usually the more difficult part in solving the Schrödinger equation numerically is not to find a solution but rather to find the solution which satisfied the correct boundary conditions.

In the asymptotic region the x-motion decouples from the y motion and the Hamiltonian can be written as

$$H^{\pm} = H_x^{\pm} + H_y^{\pm} \qquad (39)$$

where

$$H_x^{\pm} = -\frac{\hbar^2}{2B_x^{\pm}} \frac{\partial^2}{\partial x^2} \qquad (40a)$$

$$H_y^{\pm} = -\frac{\hbar^2}{2B_y^{\pm}(y)} \left[\frac{\partial^2}{\partial y^2} - \frac{1}{B_y^{\pm}(y)} \left(\frac{\partial}{\partial y} B_y^{\pm}(y)\right) \frac{\partial}{\partial y}\right] + V^{\pm}(y) \qquad (40b)$$

The eigenstates of $H_y^{\pm}$, $\varphi^{\pm}(y)$ define the ingoing and outgoing channels

$$H_y^- \varphi_\nu^-(y) = \varepsilon_\nu \varphi_\nu^-(y) \tag{41a}$$

$$H_y^+ \varphi_\mu^+(y) = \varepsilon_\mu \varphi_\mu^+(y) \tag{41b}$$

One can express the asymptotic eigenstates φ_ν^-, φ_μ^+ in the oscillator basis $\{\varphi_n\}$; the same basis used to expand Ψ (eq. (20))

$$\varphi_\nu^- = \sum_n d_{n\nu}^- \varphi_n \tag{42a}$$

$$\varphi_\mu^+ = \sum_n d_{n\mu}^+ \varphi_n \tag{42b}$$

The matrices $d_{n\mu}^{\pm}$ are unitary matrices, i.e.

$$\sum_n d_{n\mu}^{\pm *} d_{n\mu'}^{\pm} = \delta_{\mu\mu'} \tag{43}$$

Using (42) and (43) one finds for the wave function

$$\Psi = \sum_n u_n(x) \varphi_n(x) = \begin{cases} \sum_{\mu n} d_{n\mu}^{+*} u_n(x) \varphi_\mu^+(y) & (44a) \\ \sum_{\nu n} d_{n\nu}^{-*} u_n(x) \varphi_\nu^-(y) & (44b) \end{cases}$$

We want a wave function Ψ which fulfills the following boundary conditions:

i) for $x \to -\infty$ has in all open channels only outgoing waves, except in the channel ν where one also has an incoming wave with amplitude 1 (for the closed channels only exponentially decreasing waves ($x \to -\infty$)).

ii) for $x \to +\infty$ has in the open channels only outgoing waves and in the closed channels only exponentially decreasing waves.

To assure that one has only outgoing waves for $x \to +\infty$, one integrates the coupled equations starting from $x = +\infty$ with an outgoing wave in some channel μ in the asymptotic region $+\infty$. If the channel is closed, one starts with an exponentially decreasing wave (instead of the outgoing wave).

Let $\Psi_\mu(x, y)$ be a wave function which has the boundary condition that for $x \to +\infty$, there are no components in the channels $\mu' \neq \mu$, and in the channel μ there is an outgoing wave with amplitude 1. In the region $x \to +\infty$, $\Psi_\mu(x, y)$ is therefore given by:

$$\Psi_\mu(x,y) \xrightarrow{(x \to +\infty)} \begin{cases} e^{i k_\mu x}\, \varphi_\mu^+(y) & \text{for } \varepsilon_\mu \leq E \\ e^{-\chi_\mu x}\, \varphi_\mu^+(y) & \text{for } \varepsilon_\mu > E \end{cases} \tag{45}$$

where k_μ and χ_μ are given by

$$k_\mu = \sqrt{\frac{2B_x^+}{\hbar^2}\left(E - \varepsilon_\mu\right)} \tag{46a}$$

$$\chi_\mu = \sqrt{\frac{2B_x^+}{\hbar^2}\left(\varepsilon_\mu - E\right)} \tag{46b}$$

The integration is therefore performed by solving the coupled differential equations (26) for $u_n^{(\mu)}(x)$ starting at $x = +\infty$ with

$$\begin{cases} U_n^{(\mu)}(+\infty) = d_{n\mu}^{+} e^{i\kappa_\mu x} \\ V_n^{(\mu)}(+\infty) = i\kappa_\mu d_{n\mu}^{+} e^{-i\kappa_\mu x} \end{cases} \quad \text{if } \varepsilon_\mu \leq E \text{ (open channels)} \tag{47}$$

$$\begin{cases} U_n^{(\mu)}(+\infty) = d_{n\mu}^{+} e^{-\chi_\mu x} \\ V_n^{(\mu)}(+\infty) = -\chi_\mu d_{n\mu}^{+} e^{-\chi_\mu x} \end{cases} \quad \text{if } \varepsilon_\mu > E \text{ (closed channels)} \tag{48}$$

After the integration, at $x = -\infty$, the wave function Ψ_μ has the form

$$\Psi_\mu(x,y) \underset{x\to-\infty}{=} \sum_{\nu\,(\text{open})} \left(a_{\nu\mu} e^{i\kappa_\nu x} + b_{\nu\mu} e^{-i\kappa_\nu x} \right) \varphi_\nu^{-}(y) + \sum_{\nu\,(\text{closed})} \left(a_{\nu\mu} e^{-\chi_\nu x} + b_{\nu\mu} e^{\chi_\nu x} \right) \varphi_\nu^{-}(y) \tag{49}$$

The numerical integration of the differential equations yields then $U_n^{(\mu)}(x)$ and $V_n^{(\mu)}(x) = U_n'^{(\mu)}(x)$ for $x \to -\infty$. Using eq. (40) one can write

$$U_n^{(\mu)}(x) \underset{x\to-\infty}{=} \sum_{\nu'\,(\text{open})} \left(a_{\nu'\mu} e^{i\kappa_{\nu'} x} + b_{\nu'\mu} e^{-i\kappa_{\nu'} x} \right) d_{n\nu'}^{-} + \sum_{\nu'\,(\text{closed})} \left(a_{\nu'\mu} e^{-\chi_{\nu'} x} + b_{\nu'\mu} e^{\chi_{\nu'} x} \right) d_{n\nu'}^{-} \tag{50a}$$

and

$$V_n^{(\mu)}(x) \underset{x\to-\infty}{=} \sum_{(\text{open})} \left(i\kappa_{\nu'} a_{\nu'\mu} e^{i\kappa_{\nu'} x} - i\kappa_{\nu'} b_{\nu'\mu} e^{-i\kappa_{\nu'} x} \right) d_{n\nu'}^{-} + \sum_{\nu'\,(\text{closed})} \left(-\chi_{\nu'} a_{\nu'\mu} e^{-\chi_{\nu'} x} + \chi_{\nu'} b_{\nu'\mu} e^{\chi_{\nu'} x} \right) d_{n\nu'}^{-} \tag{50b}$$

Multiplying these eqs. by $\bar{d}^{-*}_{n\nu}$ and summing over n one finds

$$S^{(\mu)}_{\nu}(x) \equiv \sum_n \bar{d}^{-*}_{n\nu}\, U^{(\mu)}_n(x)$$

$$= \begin{cases} a_{\nu\mu} e^{i\kappa_\nu x} + b_{\nu\mu} e^{-i\kappa_\nu x} & \text{if } \nu \text{ is open} \\ a_{\nu\mu} e^{-\chi_\nu x} + b_{\nu\mu} e^{\chi_\nu x} & \text{if } \nu \text{ is closed} \end{cases} \tag{51}$$

and

$$S'^{(\mu)}_{\nu}(x) \equiv \sum_n \bar{d}^{-*}_{n\nu}\, U'^{(\mu)}_n(x) = \sum_n \bar{d}^{-*}_{n\nu}\, V^{(\mu)}_n(x)$$

$$= \begin{cases} i\kappa_\nu a_{\nu\mu} e^{i\kappa_\nu x} - i\kappa_\nu b_{\nu\mu} e^{-i\kappa_\nu x} & \text{if } \nu \text{ is open} \\ -\chi_\nu a_{\nu\mu} e^{-\chi_\nu x} + \chi_\nu b_{\nu\mu} e^{\chi_\nu x} & \text{if } \nu \text{ is closed} \end{cases} \tag{52}$$

From eqs. (51) and (52) one can solve for the complex coefficients $a_{\nu\mu}$, $b_{\nu\mu}$. One finds for the case that ν is an open channel

$$\begin{cases} a_{\nu\mu} = \frac{1}{2} e^{-i\kappa_\nu x}\left(S^{(\mu)}_{\nu}(x) + \frac{1}{i\kappa_\nu} S'^{(\mu)}_{\nu}(x) \right) \\ b_{\nu\mu} = \frac{1}{2} e^{i\kappa_\nu x}\left(S^{(\mu)}_{\nu}(x) - \frac{1}{i\kappa_\nu} S'^{(\mu)}_{\nu}(x) \right) \end{cases} \tag{53a}$$

If ν corresponds to a close channel, then

$$\begin{cases} a_{\nu\mu} = \frac{1}{2} e^{\chi_\nu x}\left(S^{(\mu)}_{\nu}(x) - \frac{1}{\chi_\nu} S'^{(\mu)}_{\nu}(x) \right) \\ b_{\nu\mu} = \frac{1}{2} e^{-\chi_\nu x}\left(S^{(\mu)}_{\nu}(x) + \frac{1}{\chi_\nu} S'^{(\mu)}_{\nu}(x) \right) \end{cases} \tag{53b}$$

d) The final solution.

The final solution of the Schrödinger equation we are looking for is a linear superposition of the Ψ_μ

$$\Psi^{(\nu_0)} = \sum_\mu c_{\mu\nu_0} \Psi_\mu \tag{54}$$

where the coefficients $c_{\mu\nu_0}$ are determined by the conditions

i) $\Psi^{(\nu_0)}(x \longrightarrow +\infty)$ = outgoing waves

ii) $\Psi^{(\nu_0)}(x \longrightarrow -\infty) = e^{i(k_{\nu_0}x+\alpha)}\varphi_{\nu_0}(y)$ + outgoing waves

The condition i) is fulfilled (by construction), since all the Ψ_μ contain only outgoing parts for $x \to +\infty$. At $x \to -\infty$ one has (using 49)):

$$\Psi^{(\nu_0)}(x \longrightarrow -\infty) = \sum_{\substack{\mu \\ \nu\,(open)}} c_{\mu\nu_0}\left(a_{\nu\mu}e^{ik_\nu x} + b_{\nu\mu}e^{-ik_\nu x}\right)\varphi_\nu^-(x) +$$

$$+ \sum_{\substack{\mu \\ \nu\,(closed)}} c_{\mu\nu_0}\left(a_{\nu\mu}e^{-\chi_\nu x} + b_{\nu\mu}e^{\chi_\nu x}\right)\varphi_\nu^-(x) \tag{55}$$

In order to fulfill condition ii) one has to have:

$$\sum_\mu a_{\nu\mu}\, c_{\mu\nu_0} = \delta_{\nu\nu_0} \tag{56}$$

that is, one has to solve the complex linear system eq. (56).

This is equivalent to a matrix inversion:

$$c_{\mu\nu_0} = \left(a_{\nu_0\mu} \right)^{-1} \tag{57}$$

Once the final solution $\psi^{(\nu_0)}$ is known, one can evaluate the transmission and reflection probabilities T and R. For $x \to +\infty$ (eqs. (54) and (45)) one has:

$$\psi^{(\nu_0)} \xrightarrow[x\to+\infty]{} \sum_{\substack{\mu \\ (open)}} c_{\mu\nu_0} e^{iK_\mu x} \varphi_\mu^+(y) + \sum_{\substack{\mu \\ (closed)}} c_{\mu\nu_0} e^{-\chi_\mu x} \varphi_\mu^+(y)$$

and the transmission probability $T_{\mu\leftarrow\nu_0}$ is then given by

$$T_{\mu\leftarrow\nu_0} = |c_{\mu\nu_0}|^2 = |(a_{\nu_0\mu})^{-1}|^2 \tag{58}$$

For $x \to -\infty$ (from eq. (55) and (58))

$$\psi^{(\nu_0)} \longrightarrow \sum_{\substack{\nu \\ (open)}} c_{\mu\nu_0} b_{\nu\mu} e^{-iK_\nu x} \varphi_\nu^-(x) + \sum_{\substack{\nu \\ (closed)}} c_{\mu\nu_0} b_{\nu\mu} \cdot e^{\chi_\nu x} \varphi_\nu^-(x) + e^{iK_{\nu_0} x} \varphi_{\nu_0}^-(x)$$

One finds for the reflection probability $R_{\nu\leftarrow\nu_0}$

$$R_{\nu\leftarrow\nu_0} = |(bc)_{\nu\nu_0}|^2 = |(ba^{-1})_{\nu\nu_0}|^2 \tag{59}$$

e) Summary

Here we summarize the steps one has to follow in order to solve the two-dimensional barrier penetration within the coupled channel method just

described.

i) Diagonalize the asymptotic Hamiltonians $H_y^{\pm}(y)$ within the basis φ_n, that is, solve the following system of linear equations

$$\begin{cases} \sum_{n'} H^{-}_{nn'}(y)\, d^{-}_{n'\mu} = \varepsilon_\mu\, d^{-}_{n\mu} \\ \sum_{n'} H^{+}_{nn'}(y)\, d^{+}_{n'\nu} = \varepsilon_\nu\, d^{+}_{n\nu} \end{cases}$$

where $$H^{\pm}_{nn'}(y) = \langle n | H_y^{\pm} | n' \rangle$$

ii) Solve the coupled differential equations (26) for u and v starting at $x = x_+$ $(\to +\infty)$ with

$$U_n^{(\mu)}(x_+) = d^{+}_{n\mu} e^{i\kappa_\mu x_+} \qquad \left(\text{or } d^{+}_{n\mu} e^{-\chi_\mu x}\right)$$

$$V_n^{(\mu)}(x_+) = i\kappa_\mu d^{+}_{n\mu} e^{i\kappa_\mu x_+} \qquad \left(\text{or } -\chi_\mu d^{+}_{n\mu} e^{-\chi_\mu x_+}\right)$$

This has to be repeated for all μ's.

iii) After the integration, at $x = x_-(\to -\infty)$ one evaluates

$$S^{(\mu)}_\nu = \sum_n d^{-*}_{n\nu}\, U_n^{(\mu)}(x_-)$$

and

$$S'^{(\mu)}_\nu = \sum_n d^{-*}_{n\nu}\, V_n^{(\mu)}(x_-)$$

iv) Evaluate the matrices $a_{\nu\mu}$ and $b_{\nu\mu}$ using eqs. (53) and (54). Using the matrix b and the inverse matrix of a, find the transmission and reflection probabilities using eqs. (58) and (59).

A computer code was developed which follows the steps just outlined. An application to a simple example will be shown in the next section.

3) USCA solution of the two-dimensional barrier penetration problem.

a) Tunneling and complex time.

The way of describing a tunneling process within the framework of the USCA S-matrix theory is by an analytical continuation of classical mechanics. The first question that comes to mind is how can tunneling be achieved with classical trajectories. In order to find out how one has to proceed, it is convenient to study a simple, analytically solvable, one-dimensional example: the barrier penetration through a symmetrical Eckard potential barrier [2]. The symmetrical Eckard potential is given by

$$V(x) = \frac{V_o}{\cosh^2\left(\frac{x}{a}\right)} \tag{60}$$

The classical trajectory of a particle with mass m and energy E moving on this potential is given by (for $E < V_o$)

$$x(t) = -a \ \mathrm{Arcsinh}\left(\lambda \cosh\left(\frac{vt}{a}\right)\right) \tag{61}$$

where v is the velocity in the asymptotic region (i.e. $v = \sqrt{2mE}$) and λ is given by

$$\lambda = \sqrt{\frac{V_o}{E} - 1} \tag{62}$$

Initially the particle is to the left of the barrier (i.e. $x(t = -\infty) = -\infty$); the time origin $t = 0$ occurs when the particle reaches the classical turning point on the barrier. For $t > 0$ the particle has reflected from the barrier and is moving back toward $x = -\infty$. If however, starting from $t = 0$ we take imaginary time increments, that is, we take

$$t = -i\tau \qquad (\tau \text{ real} \geq 0) \tag{63}$$

and analytically continue $x(t)$ into the complex t plane, we find

$$x(t) = -a \operatorname{Arcsinh}\left(\lambda \cos\left(\frac{V\tau}{a}\right)\right) \tag{64}$$

The particle will now move into the barrier and reach the turning point on the other side for $\tau = +\frac{\pi a}{V}$. If at that time we switch again to real time increments, the particle will emerge on the right side of the barrier; tunneling has been achieved. It is clear that the behaviour of the solution $x(t)$ will be related to the analytic properties of the multivalued function $\operatorname{Arcsinh}(z)$ which has branch points at $z = \pm i$ (joined by a cut between them). In the complex time plane one will therefore find branch points when

$$\lambda \cos\left(\frac{V\tau}{a}\right) = \lambda \cos\left(\frac{iVt}{a}\right) = \pm i \tag{65}$$

From eq. (65) one finds that the branch points in the complex t-plane are at

$$t = \pm \frac{a}{V} \operatorname{Arctanh} \sqrt{\frac{E}{V_0}} + i\left(n + \frac{1}{2}\right)\frac{\pi a}{V} \qquad (E < V_0) \tag{66}$$

with n an integer.

Fig. IV 3 shows the complex time plane with its branch points and cuts. Also illustrated is what happens to the particle trajectory if one takes various different time paths in the complex time plane. Because of the analyticity, the results do not depend on the path in the t-plane as long as one does not go around different branch points.

Let's remember here that (see section IV 1d) solving the classical equations of motion with purely imaginary time increments is equivalent to using real time increments, but on the "inverted" potential surface.

Now let's consider the phase Φ which, in the USCA, one evaluates along the classical trajectories. Since this example here is a one-dimensional problem (there is no internal degree of freedom), the USCA equations simplify and the probability to find the particle on the right side is simply given by

$$P = \left| e^{i\Phi} \right|^2 \tag{66}$$

where Φ is given by

$$\Phi = \frac{1}{\hbar} \int_{t_0}^{t} p(t') \dot{x}(t') dt'$$

$$= \frac{1}{\hbar} \int_{x_-}^{x_+} \sqrt{2m\left(E - V(x)\right)}\, dx \tag{67}$$

where x_- and x_+ are some large distances away from the barrier on either side. It is clear from eq. (66) that only the imaginary part of Φ is

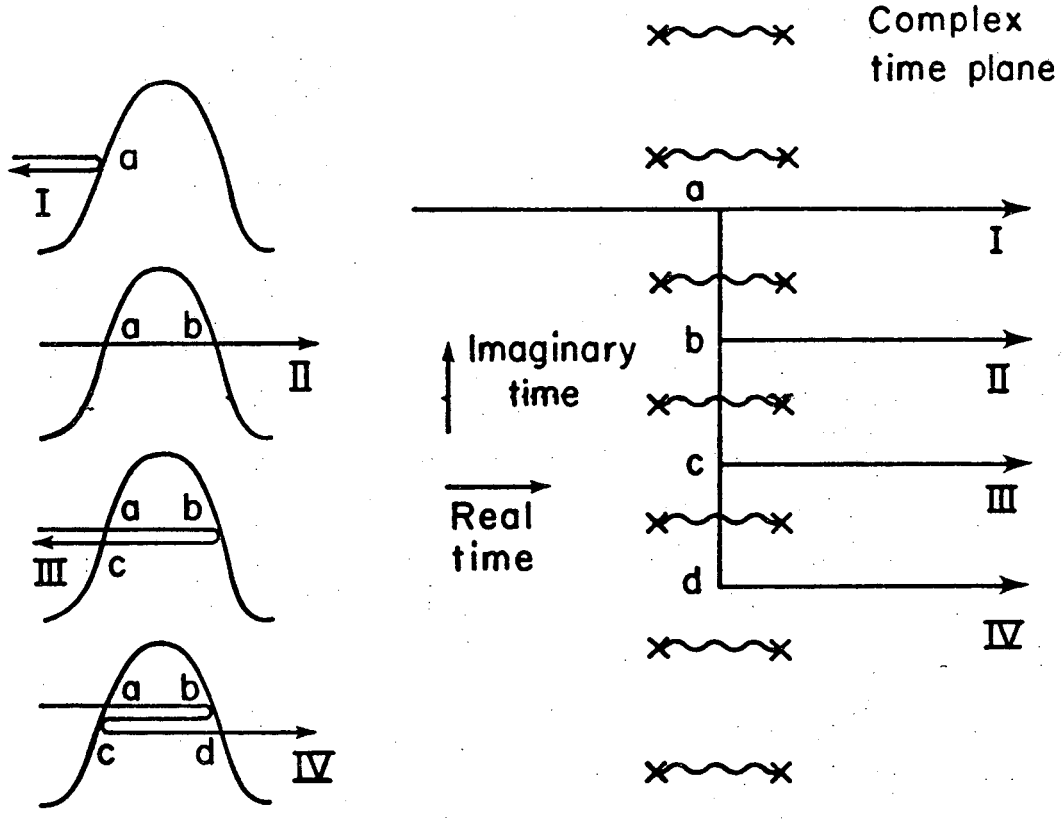

XBL755-2885

Fig. IV-3 Diagram showing on the right hand side the different time paths one has to follow in order to obtain the trajectories shown on the left hand side. The crosses represent the branch points and the wiggly line corresponds to the cuts joining them.

interesting. The phase Φ acquires an imaginary component only while the particle tunnels and we have

$$\mathrm{Im}\,\Phi = \frac{1}{\hbar}\int_{-x_0}^{x_0}\sqrt{2m\left(V(x)-E\right)}\,dx \tag{68}$$

where $\pm x_0$ are the two classical turning points on either side of the barrier. For the tunneling probability we therefore find

$$P = \exp\left\{-2\int_{-x_0}^{x_0}\sqrt{2m\left(V(x)-E\right)}\,dx\right\} \tag{69}$$

which is exactly the one-dimensional WKB approximation for the tunneling probability already mentioned in section IV-1b. In the one-dimensional case we find then that the USCA tunneling probability reduces exactly to the WKB limit.

Additional results concerning the symmetrical Eckard potential eq. (60) are given in Appendix B.

b) An unsolved problem.

Let's compare the penetration probability adding coherently together all the possible trajectories as shown in Fig. IV 3. One has

$$S = e^{-K} - e^{-3K} + e^{-5K} - e^{-7K} + \ldots = \frac{e^{-K}}{1+e^{-2K}} \tag{70}$$

with

$$K = \frac{1}{\hbar}\int_{x_1}^{x_2}\sqrt{2m\left(V(x)-E\right)}\,dx \tag{71}$$

where x_1 and x_2 are the classical turning points. The first term in eq. (70) corresponds to the trajectory which reaches the first turning point, then penetrates the barrier and reaches the second turning point and then leaves the barrier on the right side. This term, unless the incident energy is close to the barrier top, is the only important term in the series and is identical to the WKB result (see previous subsection). The second term in eq. (70) corresponds to a trajectory which is reflected twice inside the barrier (see trajectory IV in Fig. IV 3). Remembering that a reflection introduces a phase change of $\pi/2$ (19), (see also section II 2), the alternating signs in eq. (70) are explained. From eq. (70) one finds for the penetration probability

$$P = |S|^2 = \frac{e^{-2K}}{(1+e^{-2K})^2} \qquad (71)$$

This expression differs from the expression given by Fröman and Fröman [48] eq. (5), which has been shown to be correct for various limiting cases. For the particular case that the energy is equal to the barrier top (i.e. K= 0), equation (71) gives for the penetrability P = ¼ while the correct result is P = ½.

Even though much effort has been done to solve this difficulty, it still remains at this stage an unsolved problem.

If the fission probability is low, let's say less than 0.1, which is the case for many practical applications, then only the lowest order term in the series eq. (70) for the S-matrix contributes, and to this lowest order the expression for the penetration probability P (eqs. (71) and (5)) do coincide.

c) A simple fission barrier model system[56].

As already announced in section IV-f, we will now study the penetration through a simple two-dimensional fission barrier using the USCA method and then compare the results one obtains with other methods. The simple model we will study has a Hamiltonian with potential giving a Gaussian barrier in the x direction (x being the fission coordinates) and an harmonic potential in the y direction. The mass tensor will be taken to be diagonal and constant; the width of the valley, however, will be variable. The Hamiltonian is:

$$H = \frac{p_x^2}{2m_x} + \frac{p_y^2}{2m_y} + V_o e^{-\left(\frac{x}{a}\right)^2} + \frac{1}{2} C \left(1 + \alpha e^{-\left(\frac{x}{a}\right)^2}\right) y^2 \qquad (72)$$

A non-zero value of the "coupling constant" α allows the width of the valley to vary over the saddle, and by doing so couples the two degrees of freedom. The numerical values were chosen so as to correspond to a typical fission case: $m_x = 500\ \text{MeV}^{-1}$, $V_o = 7$ MeV, $m_y = 4.7\ \text{MeV}^{-1}$, $a = 0.185$, $C = 5.1$ MeV, $E_{tot} = 6.0$ MeV. This choice of C and m_y gives a frequency of about 1 MeV, typical of say a gamma vibrational mode. The coordinates x and y are dimensionless and correspond, for instance, to the deformation parameters ε_2 and ε_4.

In the asymptotic region (that is, for $|x| \to \infty$) the two degrees of freedom are uncoupled and the system will find itself in a definite quantum state in the transverse harmonic degree of freedom. If initially (i.e. for $x \to -\infty$) the system is in a state in the transverse degree of freedom specified by the oscillator quantum number n_μ, let us determine what the probability $P_{\nu \leftarrow \mu}$ is to find the system after the tunneling

(i.e. for $x \to +\infty$) in a quantum state n_y. Let's introduce for the model problem in the asymptotic regions, that is for $|x| \to \infty$, the action angle bariables (J, q) for the transverse collective degree of freedom; since it is J which is related by the correspondence principle to the "quantum number" of the harmonic oscillator through

$$J = 2\pi\hbar\left(n + \frac{1}{2}\right) \tag{73}$$

The angle variable q is related to the phase ϕ of the oscillator through

$$q = \frac{\phi}{2\pi} \tag{74}$$

The transformation between the action angle variables and the cartesian coordinates is given by:

$$\begin{cases} y = \sqrt{\dfrac{\omega_0 J}{\pi C}}\cos(2\pi q) & (75a) \\ P_y = -m_y\omega_0\sqrt{\dfrac{\omega_0 J}{\pi C}}\sin(2\pi q) & (75b) \end{cases}$$

and

$$\begin{cases} q = -\text{Arctan}\left(\dfrac{P_y}{m_y\omega_0 y}\right) = -\dfrac{i}{4\pi}\text{Log}\left(\dfrac{m_y\omega_0 y - iP_y}{m_y\omega_0 y + iP_y}\right) & (76a) \\ J = \dfrac{\pi}{\omega_0}\left(Cy^2 + \dfrac{P_y^2}{m_y}\right) & (76b) \end{cases}$$

where

$$\omega_0 \equiv \sqrt{\frac{C}{m_y}} \tag{77}$$

The transformation to action angle variables is only of practical use in the asymptotic region where the width of the transverse valley does not change. It is possible to transform all the classical equations of motion into action angle variables (J, q) using the transformation equation (76), and then integrate these equations in the action angle coordinates; however, this introduces some problems as soon as the valley changes width, because of the multivaluedness of the transformation. It is much more convenient to integrate the equations of motion using the cartesian coordinates.

If $F_4(p_y, J)$ is one of the generating functions[17] of the canonical transformation relating the coordinates (p_y, y) and (J, q) then the phase

$$\Phi(J_\nu, J_\mu) \equiv -\frac{1}{\hbar}\int_{t_\mu}^{t_\nu} (x\dot{p}_x + q\dot{J})\,dt \tag{78}$$

which is the phase along the classical trajectories needed in the USCA expression for the S-matrix can be obtained from the phase

$$\Phi(P_{y_\nu}, P_{y_\mu}) \equiv -\frac{1}{\hbar}\int_{t_\mu}^{t_\nu} (x\dot{p}_x + y\dot{p}_y)\,dt \tag{79}$$

using the relation[3, 17]

$$\Phi(J_\nu, J_\mu) = \Phi(P_{y_\nu}, P_{y_\mu}) - \frac{1}{\hbar} F_4(p_y, J)\Big|_{t_\mu}^{t_\nu} \tag{80}$$

The generating function $F_4(p_y, J)$ of the transformation relating (p_y, y) and (J, q) is for the harmonic oscillator (see Appendix D)

$$F_4(P_y, y) = J(P_y, y)\, q(P_y, y) - \frac{1}{2} y P_y \tag{81}$$

and so we find for the phase $\phi(J_\nu, J_\mu)$ which we will denote by $\Phi(n_\nu, n_\mu)$

$$\Phi(n_\nu, n_\mu) = -\frac{1}{\hbar}\left(Jq - \frac{1}{2} y P_y\right)\Big|_{t_\mu}^{t_\nu} - \frac{1}{\hbar}\int_{t_\mu}^{t_\nu} (x\dot{P}_x + y\dot{P}_y)\, dt \tag{82}$$

The next step in applying the USCA method is to find the quantum number function $\hat{n}_\mu(q_0)$. To find it, one specifies the initial conditions for the integration, that is, starting at $t \to -\infty$ with the transverse oscillator on a quantum state n_μ and with some "phase" q_0. Then one chooses a time path in the complex time plane such that the system tunnels once (for the example considered here, multiple tunneling trajectories are completely negligible). After the integration, (that is for $t \to +\infty$), the degrees of freedom are uncoupled and from the energy in the transverse degree of freedom, $\hat{n}_\mu(q_0)$ can be found using the relation

$$E_{trans} \equiv \hbar\omega_0\left(\hat{n}_\mu(q_0) + \frac{1}{2}\right) = \frac{1}{2} C y^2 + \frac{P_y^2}{2m_y} \tag{83}$$

In order to find the classical trajectories with the correct boundary conditions, one has to solve for the roots of the equation

$$\hat{n}_\mu(q_0) = n_\nu \tag{84}$$

that is, to find the initial orientations q_o, for which after the tunneling the system is found in a quantum state, specified by the (non-negative integer) quantum number n_ν. In Fig. IV 4 the quantum number function $\hat{n}_\mu(q_o)$ is shown for $\mu = 3$ versus Real (q_o) for several values of Imag (q_o).

Due to the symmetries of the problem, only transitions for which $\Delta n = n_\mu - n_\nu$ is an even integer are possible (conservation of parity).

For $\Delta n = 0$, in the case of Fig. IV 4, that is, for $\mu = \nu = 3$, the roots of equation (84) are found for values of $\mathrm{Im}(q_o) \simeq 17 \pm 0.6$ and for these cases the quantum number function $\hat{n}_\mu(q_o)$ vs. Real (q_o) is rather flat (it does not even reach to the adjacent states n = 5 or n = 1). If the quantum number function is flat, the Airy uniform semiclassical approximation to the S-matrix, as used in the Coulomb excitation example, does not give accurate results. The integral expression for the S-matrix (eq. II 25) is of the type

$$I = \frac{1}{2\pi} \int_{-\pi}^{+\pi} g(u) e^{if(u)} du \qquad (85)$$

In section II 4c the phase f was mapped onto a cubic in such a way that the stationary phase points of f and the cubic correspons. Another possibility is to map the phase f into the following function[57]

$$f(u) = -\left\{ \cos(2y) - ky + A \right. \qquad (86)$$

If the quantum number function is flat, the phase f(u) can be approximated well by a function of the type $-\left\{ \cos(2u) - ku + A \right.$ and therefore the error

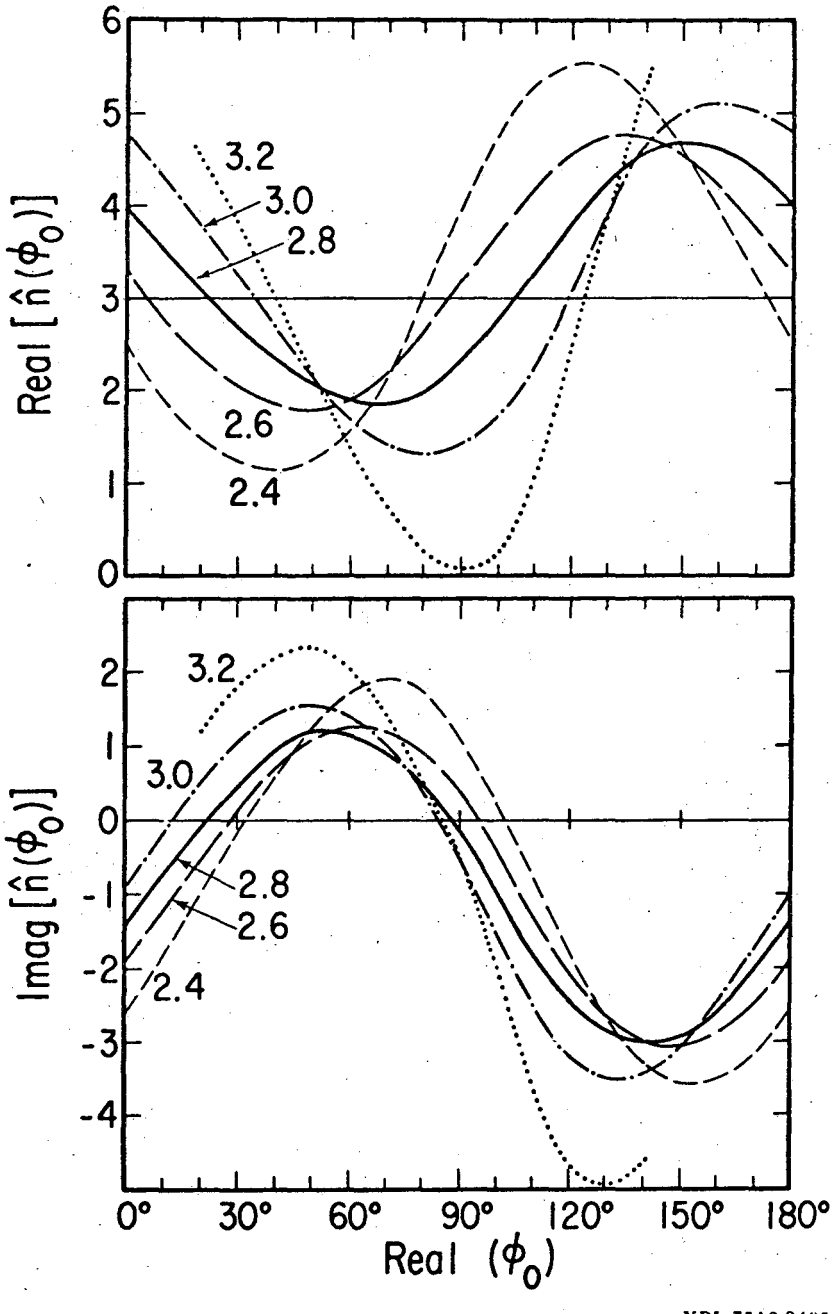

Fig. IV-4 Plot of the real and imaginary part of the quantum number function $\hat{n}_{\mu}(q_\phi)$ versus Real (ϕ_ϕ) = Real ($2\pi q_\phi$). The various curves are labelled by the value of Im(ϕ_ϕ).

introduced by the mapping eq. (86) is small. Using the mapping eq. (86) instead of mapping f onto a cubic, one finds for the S-matrix (see Appendix E) the so-called Bessel uniform semiclassical approximation:

$$S_{\nu\leftarrow\mu} = \frac{1+(-1)^K}{2}\sqrt{\frac{2\pi\xi}{\sqrt{1-\left(\frac{K}{2\xi}\right)^2}}}\, e^{\frac{i}{2}\left(\Phi_+(n_\nu,n_\mu)+\Phi_-(n_\nu,n_\mu)\right)} \cdot \left\{\sqrt{1-\left(\frac{K}{2\xi}\right)^2}\left(\frac{1}{\sqrt{\left(\frac{d\hat{n}_\mu(q_0)}{dq_0}\right)_+}}+\frac{1}{\sqrt{-\left(\frac{d\hat{n}_\mu(q_0)}{dq_0}\right)_-}}\right)J_{\frac{K}{2}}(\xi)+ i\left(\frac{1}{\sqrt{\left(\frac{d\hat{n}_\mu(q_0)}{dq_0}\right)_+}}-\frac{1}{\sqrt{-\left(\frac{d\hat{n}_\mu(q_0)}{dq_0}\right)_-}}\right)J'_{\frac{K}{2}}(\xi)\right\} \tag{87}$$

where ξ and K are given by

$$\frac{1}{2}\left(\Phi_- - \Phi_+\right) = \xi\sqrt{1-\left(\frac{K}{2\xi}\right)^2} - \frac{K}{2}\,\mathrm{Arccos}\left(\frac{K}{2\xi}\right) \tag{88}$$

$$K = |n_\mu - n_\nu| \tag{89}$$

The expression for the S-matrix (eq. (87)) shows explicitly the selection rule that, for a transition to be possible, $|n_\mu - n_\nu|$ has to be an even integer.

Once the S-matrix is known, the transition probabilities $P_{\nu\leftarrow\mu} = |S_{\nu\leftarrow\mu}|^2$ follow directly.

4) Results and Comparison.

We will now present the results for the tunneling problem with the Hamiltonian given by eq. (72), using the different methods discussed in this chapter.

Fig. IV 5 shows in its upper part the shape of the Gaussian barrier, together with the adiabatic translational energies in the x direction for the three y-vibrational channels $n = 0$, $n = 2$ and $n = 4$. Let's remember that the problem we are solving is typical of sub-barrier fission, with $\sim$ 4.5 MeV of excitation and $\sim$ 1.5 MeV below the classical barrier threshold. Higher n channels are obviously closed, and odd n channels are not coupled for parity reasons.

The lower part of Fig. IV-5 shows the square of the wavefunction for an incident wave from the left in channel $\mu = 2$ (i.e. $|U_{2\nu}(x)|^2$). These are results one obtains using the exact coupled-channel quantum mechanical code developed for this problem and described in section IV 2. In the coupled-channel code, three open channels and one closed channel were included. Taking along the fourth (closed) channel changed the results only in the fourth significant figure. We note the standing wave in the channel $\mu = 2$ on the left side of the barrier, as most of the flux is elastically reflected. About 10^{-5} is inelastically reflected in channel $\mu = 4$ and 10^{-8} in channel $\mu = 0$. To the right of the barrier $\nu = 0$, 2 and 4 waves are transmitted at the 10^{-10}, 10^{-15} and 10^{-24} probability levels, respectively. In Fig. IV 6 the lines show the penetrabilities $P_{\mu\nu}$ for different values of the coupling constant α between 0 and 0.15. These values of α correspond to a small coupling between the two degrees of freedom. Larger values for the coupling constant α were not considered

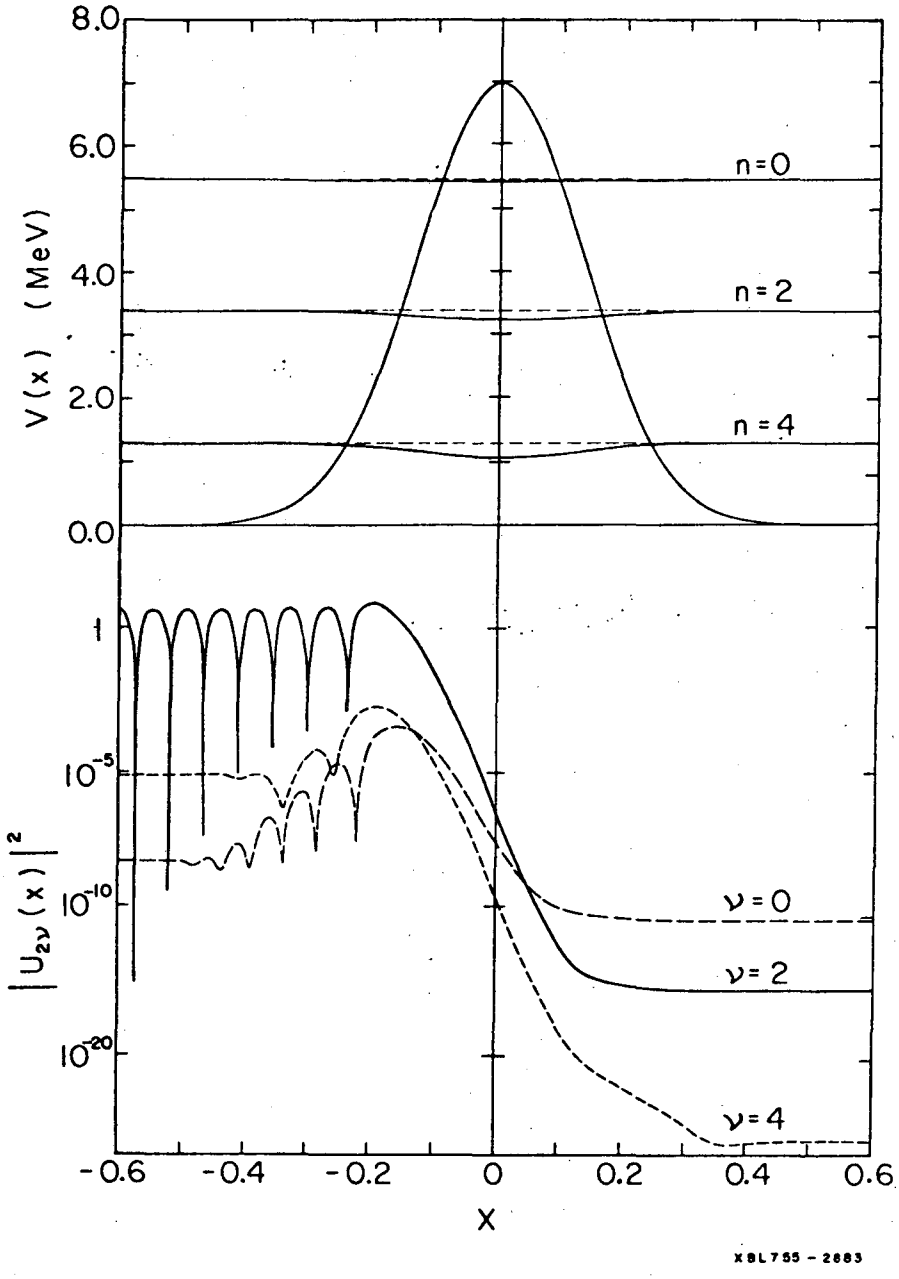

Fig. IV-5 Fission barrier and the square of the quantum mechanical channel function $u_{2\nu}(x)$ for an incoming wave in the channel $\mu = 2$.

(even though in realistic surfaces the coupling is probably much larger), since in order to expand the wavefunction eq. (20), many more channels have to be included. This not only involves more computer time, but also closed channels with higher energy require a special handling. From Fig. IV 6 we find that there is a vibrational "cooling" effect on the passage through the barrier, with $\nu = 0$ transmitted waves dominating regardless of the vibrational state incident on the barrier. Only in the case of α very close to zero, a constant valley width, will the "cooling" feature not appear.

An obvious approximation to be tested by the coupled-channel solution is the so-called vibrationally adiabatic approximation (QM_{VA}), where one assumes that during the fission process the system always stays in the same oscillator state μ, that is, consider the approximation in which the y-direction wave function adiabatically adjusts its width as the valley changes along the path. In this case the coupled-channel calculation reduces to a one-dimensional calculation, taking into account only the change of the oscillator energy. Table IV 1 shows the diagonal transition probabilities for no coupling ($\alpha = 0$), obtained with the exact quantum mechanical program (QM) and for a coupling $\alpha = 0.1$, obtained with the quantum mechanical code (QM) and for the vibrationally adiabatic approximation (QM_{VA}). Let's note that since for the model studied here the inertial tensor is coordinate-independent and diagonal, one has that the one-dimensional WKB approximation and the least action path method (described in section IV-1b and c respectively) give the same result (also shown in Table IV 1) and are independent of α.

For $\alpha = 0.1$ (let's remember that $\alpha = 0.1$ represents a small coupling),

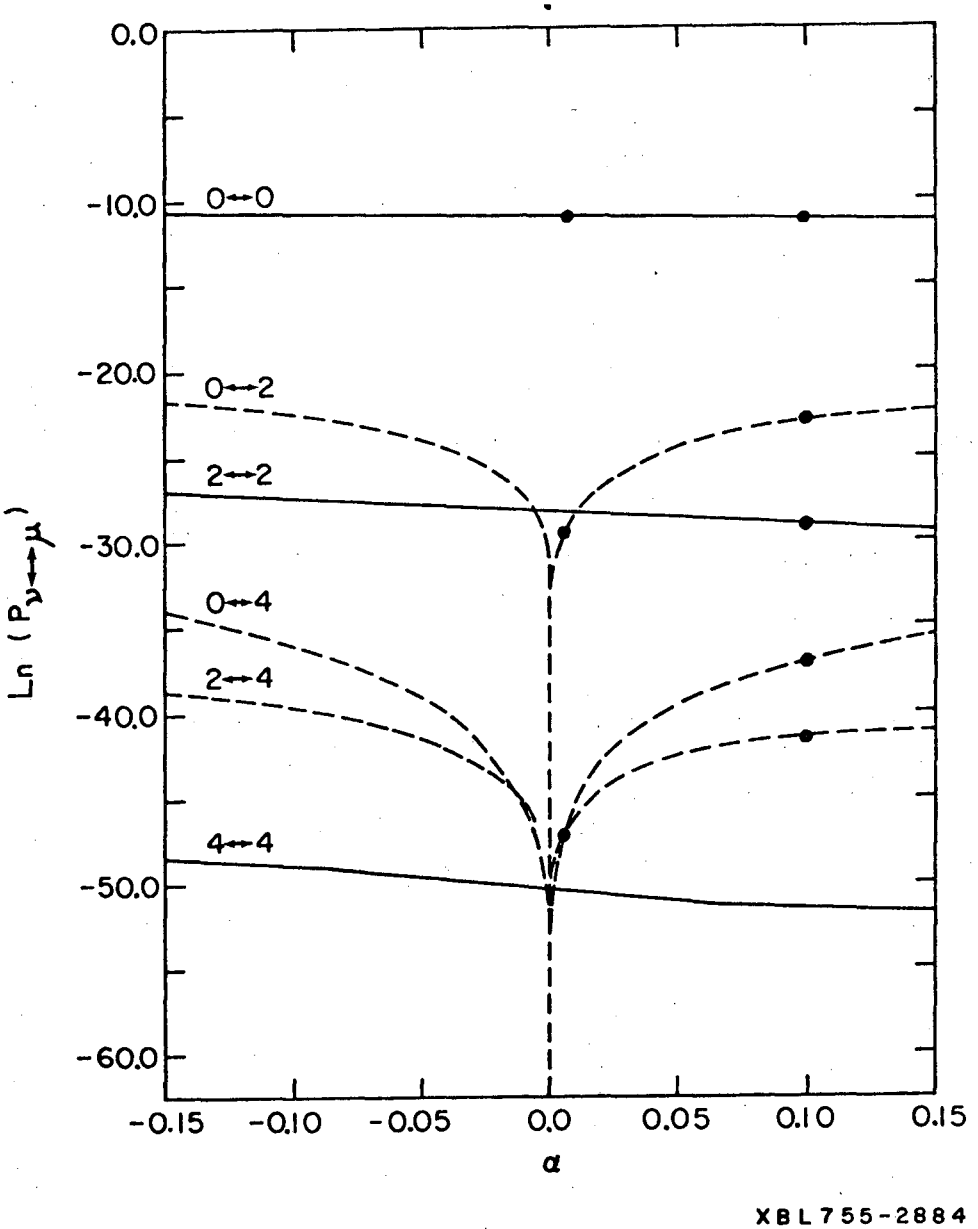

Fig. IV-6 Penetrabilities $P_{\mu\nu}$ for different values of the coupling constant α. The lines correspond to the QM coupled channel calculations (solid line for the diagonal and broken lines for the off-diagonal penetrabilities) and the dots correspond to the USCA calculations.

Table IV 1. Comparison between the QM, QM_{ad} and WKB calculations of the diagonal transitions.

	$\alpha = 0$	$\alpha = 0.1$		
	QM	QM	QM_{ad}	WKB
$0 \rightarrow 0$	$1.67\ 10^{-5}$	$1.40\ 10^{-5}$	$1.40\ 10^{-5}$	$1.60\ 10^{-5}$
$2 \rightarrow 2$	$5.48\ 10^{-13}$	$2.67\ 10^{-13}$	$2.42\ 10^{-13}$	$5.21\ 10^{-13}$
$4 \rightarrow 4$	$1.44\ 10^{-22}$	$4.66\ 10^{-23}$	$3.62\ 10^{-23}$	$1.34\ 10^{-22}$

one finds that the QM_{VA} calculation is quite good; considerably better than the one-dimensional WKB result. In other words, the main reason why the WKB and least action path method gives larger penetrability probabilities is because they neglect the increase of the zero point energy in the y-motion, which increases around the barrier (for positive α the valley becomes narrower on the top of the barrier), leaving less energy available in the fission degree of freedom to penetrate the barrier.

Neither the WKB nor the least action path method permit the evaluation of off-diagonal transitions (that is, cases for which the final quantum number is different than the initial quantum number). This, however, is no difficulty in the USCA method and Table IV 2 shows a comparison between USCA and the exact QM calculations. For $\alpha = 0$, the USCA results are identical to the WKB results and are shown in Table IV 1 (only the diagonal transitions are non-vanishing for $\alpha = 0$). In Fig. IV 6 the USCA results are shown by dots. The agreement between these USCA calculations and the exact quantum mechanical coupled-channel calculations is very good, even though the model here considered is highly non-classical.

Table IV 2. Comparison between the QM and USCA transition probabilities.

	$\alpha = 0.1$					$\alpha = 0.01$		
	$0 \leftrightarrow 0$	$0 \leftrightarrow 2$	$0 \leftrightarrow 4$	$2 \leftrightarrow 2$	$2 \leftrightarrow 4$	$0 \leftrightarrow 0$	$0 \leftrightarrow 2$	$0 \leftrightarrow 4$
QM	$1.40\ 10^{-5}$	$9.30\ 10^{-11}$	$1.03\ 10^{-16}$	$2.67\ 10^{-13}$	$9.86\ 10^{-19}$	$1.64\ 10^{-5}$	$1.22\ 10^{-12}$	$1.49\ 10^{-20}$
USCA	$1.44\ 10^{-5}$	$9.49\ 10^{-11}$	$0.97\ 10^{-16}$	$2.52\ 10^{-13}$	$9.15\ 10^{-19}$	$1.56\ 10^{-5}$	$1.30\ 10^{-12}$	$1.42\ 10^{-20}$

V CONCLUSIONS AND OUTLOOK

In this thesis we have applied a new semiclassical method (USCA) to some nuclear physics problems. This semicalssical method incorporates into classical dynamics the quantum mechanical principle of superposition. Many typical quantum effects like the quantization, interference, resonances, tunneling, selection rules are naturally contained in this semiclassical prescription. The USCA method, besides simplifying the calculations (as compared to a full quantum mechanical calculations), also gives, at least in some instances, considerable insight into the nature of the quantum effects in the problems. For example, in the case of backscattering Coulomb excitation one understands now the reason for the interference maxima and minima, their dependence on the bombarding energy and other parameters. One should not give up trying to find simple methods and models just because complicated computer codes can fit the data well. To really understand a subject, simple methods and models are of great importance. The USCA does not only satisfy this criterion, but also gives often a quantitative description of the problem.

There are several other problems, outgrowth of the problems considered in this thesis, where the USCA might be applied or at least give a qualitative description of the problem.

One of these problems is the sub-barrier nucleon transfer on a deformed nucleus. The orbitals most involved in transfer will be high-lying Nilsson levels, which have a certain spatial distribution within the target nucleus. In very simple terms, transfer would only occur when the nucleus is oriented in such a way as to place a major lobe of the involved Nilsson wave functions on the beam axis, see Fig. V 1. Thus transfer will be

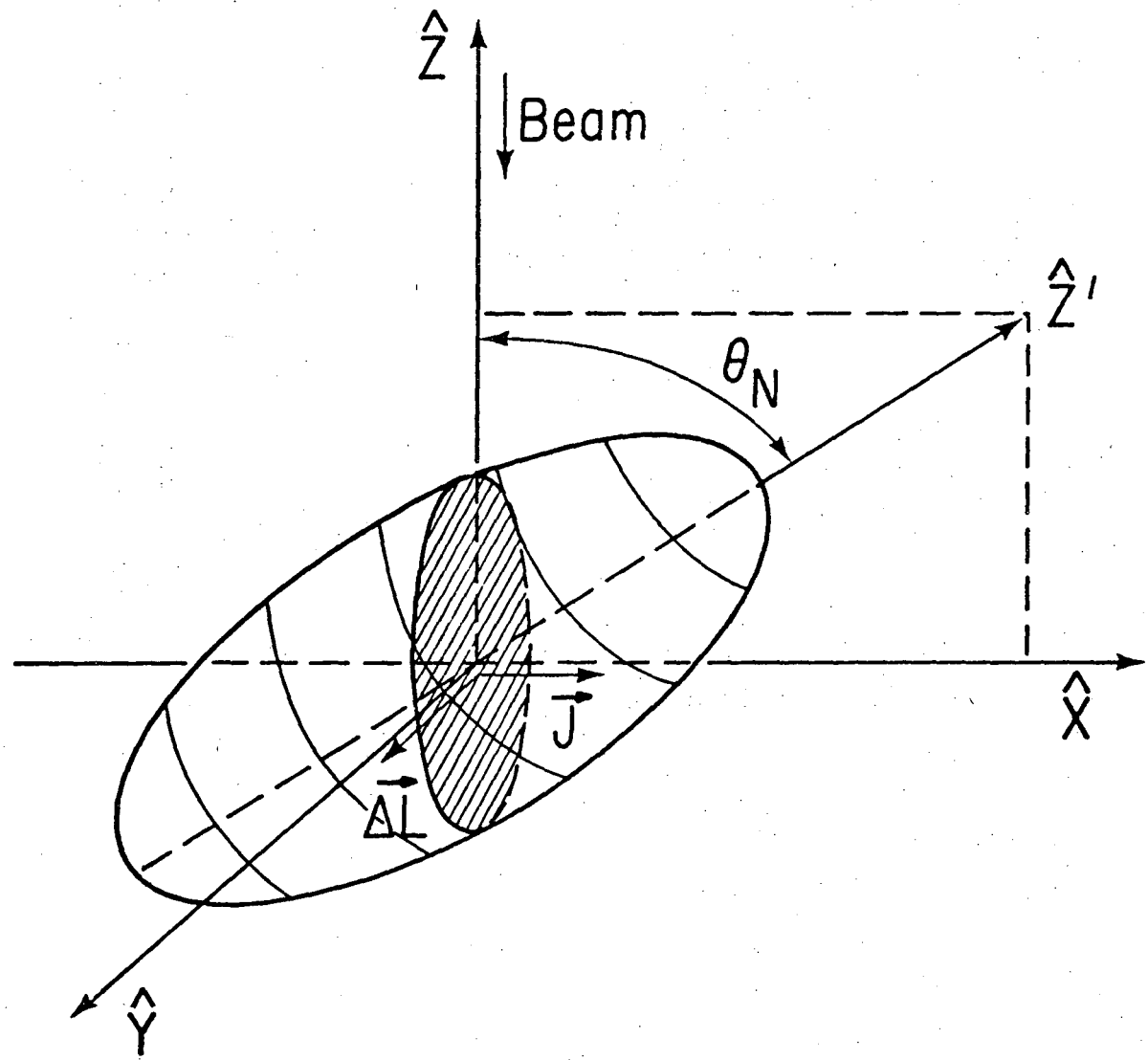

XBL 759-3879

Fig. V-1 Schematic view of a deformed even-even target before a neutron transfer. $\vec{j}$ represents the angular momentum of the Nilsson orbital, involved in the transfer $\Delta\vec{L}$ is the rotational angular momentum transferred to the target and the shaded area represents the position of the major lobe of the Nilsson wave function.

correlated with particular orientations of the deformed nucleus relative to the incoming beam and hence with the excitation of particular rotational states of the product nucleus. This is, of course, an oversimplification of the problem, the actual situation being slightly more complicated.

In a quite analogous way to that of the transfer reactions, one could investigate the excitation of rotational states built on the K = 0 octupole vibrational mode in the backscattering from a heavy deformed nucleus. Here one also expects that certain orientations of the deformed target (relative to the beam axis) to be more susceptible to octupole excitation than others. The octupole vibration has nodes at certain places (see Fig. V 2). If those nodes were presented to the incoming projectile, little octupole excitation is expected. Thus, just as in the transfer case, there is an orientation-dependent form factor associated with this excitation. In this model, therefore, one expects a selective population of certain states in the K = 0 octupole band. Both of these problems, the subbarrier nucleon transfer and the excitation of the K = 0 octupole band in deformed nuclei, are currently being investigated.

Now a few words about the experimental prospects. Using γ-ray spectroscopy in coincidence with the backscattered heavy-ion projectiles, one could gain experimental insight into these areas, that is, investigation of the Coulomb-nuclear interference effect with heavy ions and the study of the selective excitation of particular high-spin rotational states in correlation with heavy ion one- and two-nucleon transfer and excitation of the octupole vibration[58]. Setting energy gates on the back-scattered ion spectrum, one can gain information about all the processes mentioned as a function of energy in a single experiment[59].

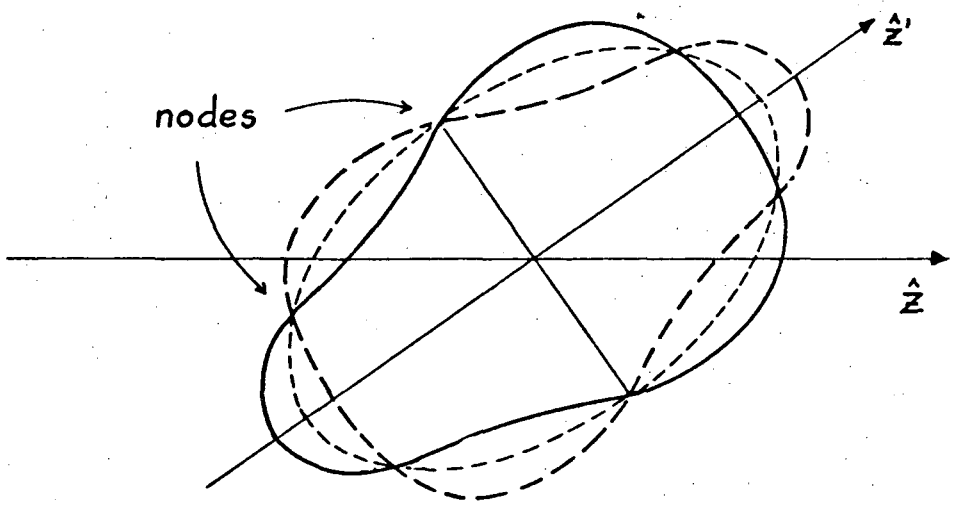

XBL759-4123

Fig. V-2 Schematic representation of an octupole vibration on a prolate deformed target.

Another problem which can be studied with the USCA and is a generalization of a problem studied in this thesis, is to consider the full three-dimensional Coulomb excitation (not only backscattering) problem. This problem is also currently being considered[60]. A full three-dimensional calculation for Coulomb excitation is considerably more complicated than the backscattering case considered in Chapter III. In the three-dimensional case, the system is specified by two quantum numbers, and two coordinates are necessary in order to specify the orientation of the target. After finding the two quantum number functions, a two-dimensional root search has to be performed in order to find the initial orientations leading to a given final state. In general there will be four roots and more general uniform expressions for the S-matrix have to be considered[21].

In Chapter IV the penetration through a two-dimensional fission barrier model was considered. The very good agreement of the USCA with the exact quantum mechanical results gives confidence that the semiclassical method may also be applied to more realistic cases with stronger coupling, where the numerical effort does not change very much and where a quantum mechanical calculation would be unfeasible. Since coordinate-dependent inertial parameters introduce no additional difficulty, the USCA could be a useful tool to investigate the full dynamics of the coupling between the fission coordinate and other degrees of freedom, such as hexadecupole deformations, mass asymmetries and degree of pairing correlations. There are other problems of similar nature, to which barrier penetration within the USCA might be possible to apply. There is the penetrability problem of anisotropic barriers in alpha decay. It was also recently suggested[61] that the USCA might be used to study the inverse to the fission problem,

that is, the zero impact parameter heavy-ion collision forming a compound nucleus and splitting up again. The two degrees of freedom would be r, the distance between the two heavy ions and η, a coordinate measuring the mass asymmetry. The potential surface and the inertial tensor components as a function of the coordinates r and η are available for a few systems. It should still be noted that in applying this semicalssical method one needs the analytical continuation of the equations of motion into the complex plane. For this to be possible one has to have an analytical function in the region of interest.

APPENDIX

A. Conventional semiclassical treatment of multiple Coulomb excitation.

In the conventional semiclassical picture[15, 27], the Coulomb excitation is caused by a well defined time-dependent electromagnetic field acting on the nucleus as the projectile moves along the classical hyperbola one obtains by considering only the monopole-monopole part of the interaction potential. The intrinsic wave function satisfies the Schrodinger equation:

$$i\hbar \frac{\partial}{\partial t}\Psi = \left(H_o + V(t)\right)\Psi \tag{1}$$

where H_o is the Hamiltonian of the free target and V(t) is the time-dependent electromagnetic interaction:

$$V(t) = \sum_{\lambda=1}^{\infty}\sum_{\mu=-\lambda}^{+\lambda} \frac{4\pi Z_p e}{2\lambda+1}\mathcal{M}^{*}(E\lambda,\mu)\frac{Y_{\lambda\mu}(\theta(t),\phi(t))}{r(t)^{\lambda+1}} \tag{2}$$

with

$$\mathcal{M}(E\lambda,\mu) \equiv \int r^{\lambda} Y_{\lambda\mu}(\theta\phi)\rho(\vec{r})d^3r \tag{3}$$

$\rho(\vec{r})$ being the nuclear charge density operator. The kinetic energy of the center-of-mass, as well as the monopole-monopole interaction, was included in the determination of the classical motion of the projectile and therefore does not appear in the Hamiltonian of eq. (1). Let $\{\psi_n\}$ be the complete set of eigen-states of H_o:

$$H_0 \psi_n = E_n \psi_n \tag{4}$$

We can expand Ψ in terms of ψ_n :

$$\Psi = \sum_m a_m(t)\, \psi_m\, e^{-\frac{i}{\hbar} E_m t} \tag{5}$$

The coefficients $a_m(t)$ are the time-dependent excitation amplitudes. At $t = -\infty$ the target nucleus is in its ground state and therefore:

$$a_m(t=-\infty) = \delta_{om} \tag{6}$$

At $t = +\infty$ the values of a_m are the excitation amplitudes after the collision, and the excitation probabilities are thus given by:

$$P_m = |a_m(t)|^2 \tag{7}$$

Substituting the wave function (5) into the Schrödinger equation (1) one finds, after multiplying both sides by ψ_n^* and integrating over the intrinsic variables (using $\langle \psi_n | \psi_m \rangle = \delta_{nm}$), the system of first-order coupled equations:

$$i\hbar \frac{da_n(t)}{dt} = \sum_m \langle \psi_n | V(t) | \psi_m \rangle e^{\frac{i}{\hbar}(E_n - E_m)t}\, a_m(t) \tag{8}$$

For the matrix element $\langle \psi_n | V(t) | \psi_m \rangle$ one has:

$$\langle \psi_n | V(t) | \psi_m \rangle = \sum_{\substack{\lambda,\mu \\ \lambda \geq 1}} \frac{4\pi Z_p e}{2\lambda+1} \frac{Y_{\lambda\mu}(\theta_p, \phi_p)}{r_p^{\lambda+1}} \langle \psi_m | \mathcal{M}(E\lambda,\mu) | \psi_n \rangle \tag{9}$$

The nuclear states are specified by the spin quantum numbers I and M:

$$\langle \psi_m | \mathcal{M}(E\lambda,\mu) | \psi_n \rangle = \langle I_m M_m | \mathcal{M}(E\lambda,\mu) | I_n M_n \rangle$$

$$= (-1)^{I_m - M_m} \begin{pmatrix} I_m & \lambda & I_n \\ -M_m & \mu & M_n \end{pmatrix} \langle I_m \| \mathcal{M}(E\lambda) \| I_n \rangle \qquad (10)$$

Substituting eqs. (10) and (9) into eq. (8) one finds:

$$i\hbar \frac{d}{dt} a_{I_n M_n}(t) = 4\pi Z_p e \sum_{\substack{\lambda,\mu \\ \lambda \geq 1}} \sum_{I_m M_m} \frac{(-1)^{I_m - M_m}}{2\lambda+1} \begin{pmatrix} I_m & \lambda & I_n \\ -M_m & \mu & M_n \end{pmatrix} \cdot$$

$$\cdot \langle I_m \| \mathcal{M}(E\lambda) \| I_n \rangle \frac{Y_{\lambda\mu}(\theta_p, \phi_p)}{r_p^{\lambda+1}} e^{\frac{i}{\hbar}(E_n - E_m)t} a_{I_m M_m}(t) \qquad (11)$$

A convenient parametric representation of the hyperbolic orbit is, in the focal system of the hyperbolic orbit, given by[62]:

$$x_p = a(\cosh w + \varepsilon) \qquad (12a)$$

$$y_p = a\sqrt{\varepsilon^2 - 1}\, \sinh w \qquad (12b)$$

$$z_p = 0 \qquad (12c)$$

$$r_p = a(\varepsilon \cosh w + 1) \qquad (12d)$$

$$t = \frac{a}{v}(\varepsilon \sinh w + w) \qquad (12e)$$

The focal coordinate system here considered is the coordinate system in which the $\hat{z}$ axis is perpendicular to the hyperbola and the $\hat{x}$ axis is the bisector of the hyperbola. In Eq. (12), $\mathcal{E}$ is the eccentricity of the hyperbola, v is the velocity of the projectile in the asymptotic region and a represents half the distance of closest approach. The values of $\mathcal{E}$, v and a one takes are the ones obtained by symmetrizing the hyperbolic orbit, that is, they are some average of the initial and final values. We will denote them with a bar on top. The eccentricity $\mathcal{E}$ of the hyperbolic orbit is related to the final scattering angle by:

$$\mathcal{E} = \frac{1}{\sin\left(\frac{\Theta}{2}\right)} \tag{13}$$

Using Eq. (12) one finds:

$$\frac{Y_{\lambda\mu}(\theta_p,\phi_p)}{r_p^{\lambda+1}} = Y_{\lambda\mu}\left(\frac{\pi}{2},0\right)\frac{\left(\cosh w+\bar{\mathcal{E}}+i\sqrt{\bar{\mathcal{E}}^2-1}\,\sinh w\right)^{\mu}}{r_p\left(\bar{\mathcal{E}}\cosh w+1\right)^{\lambda+\mu}} \tag{14}$$

$$\frac{i}{\hbar}(E_n-E_m)t \simeq i(\eta_m-\eta_n)\left(\bar{\mathcal{E}}\sinh w+w\right) \equiv i\bar{\xi}\left(\bar{\mathcal{E}}\sinh w+w\right) \tag{15}$$

Substituting (14) and (15) into (11) and using the definitions:

$$\chi^{(\lambda)}_{I_n I_m} \equiv \frac{4\pi Z_p e}{2\lambda+1}\langle I_m\|\mathcal{M}(E\lambda)\|I_n\rangle\frac{m}{\hbar^2 K\sqrt{\pi}}\frac{(\lambda-1)!}{(2\lambda-1)!!}\frac{1}{\bar{a}^{\lambda}\hat{I}_m} \tag{16}$$

$$W^{(\lambda,\mu)}_{I_n M_n, I_m M_m} = \sqrt{\pi}\,\hat{I}_m \frac{(2\lambda-1)!!}{(\lambda-1)!}(-1)^{I_m - M_m}\begin{pmatrix} I_m & \lambda & I_n \\ -M_m & \mu & M_n \end{pmatrix} Y_{\lambda\mu}\left(\frac{\pi}{2}, 0\right) \quad (17)$$

where the notation $\hat{I} \equiv \sqrt{2I+1}$ was used, the coupled differential equations become:

$$\frac{d}{dw} a_{I_n M_n}(w) = -i \sum_{\substack{I_m M_m \\ \lambda \geq 1}} \chi^{(\lambda)}_{I_n I_m} W^{(\lambda,\mu)}_{I_n M_n, I_m M_m} e^{i\bar{\xi}(\bar{\varepsilon}\sinh w + w)} \cdot$$

$$\cdot \frac{(\cosh w + \bar{\varepsilon} + i\sqrt{\bar{\varepsilon}^2 - 1}\sinh w)^{\mu}}{(\bar{\varepsilon}\cosh w + 1)^{\lambda+\mu}} a_{I_m M_m}(w) \quad (18)$$

In reference 14 the so-called Winther-de Boer code for multiple Coulomb excitation is described; this code numerically integrates the coupled first order differential equations (20).

For a perfect quantum mechanical rotor, the matrix elements are given by the rotational formula

$$\langle I_m \| \mathcal{M}(E\lambda) \| I_n \rangle = e Q_o^{(2)} \sqrt{\frac{2\lambda+1}{16\pi}}\,\hat{I}_n \hat{I}_m \begin{pmatrix} I_n & \lambda & I_m \\ 0 & 0 & 0 \end{pmatrix} \quad (19)$$

where $Q_o^{(2)}$ is the intrinsic quadrupole moment of the target.

Let's note that in first order the transfer of energy between target and projectile is included by using the average quantities $\bar{v}$, $\bar{a}$, $\bar{\varepsilon}$, $\bar{\eta}$, etc. This is sometimes referred to as symmetrization with respect to energy transfer. During the collision however the projectile also transfers angular momentum to the target. A procedure to account at least

approximately for the transfer of energy and angular momentum has been developed in reference[63]. Unfortunately, the improvements of the semi-classical calculations, expected to occur when the transfer of angular momentum is approximately accounted for, have not been convincingly achieved.

Once the final amplitudes $a_{IM}(t = +\infty)$ of the states with spin I and quantum number M are known, the quantities which are important for the experiments may easily be obtained. The total excitation probability of a level of spin I is given by

$$P_{I\leftarrow 0} = \frac{1}{2I+1} \sum_{M} |a_{IM}|^2 \tag{20}$$

The differential cross-section is obtained by multiplying $P_{I\leftarrow 0}$ with the Rutherford cross section, i.e.

$$\frac{d\sigma_{I\leftarrow 0}}{d\Omega} = P_{I\leftarrow 0} \left(\frac{d\sigma}{d\Omega}\right)_{\text{Rutherford}}$$

$$= P_{I\leftarrow 0} \left(\frac{\bar{a}}{2\sin^2\frac{\Theta}{2}}\right)^2 \tag{21}$$

B. Tunneling along a circular valley[64].

Let's consider a particle of mas μ, moving in a circular valley given by: (see Fig. A-1a)

$$V(r) = \frac{\hbar^2}{2\mu}\frac{A}{r^2} + \frac{1}{2}Cr^2 \tag{1}$$

with $\sqrt{A} \gg 1$. The minimum of the valley occurs for

$$r_o = \sqrt{\frac{\hbar}{\mu\omega}}\, A^{1/4} = a\, A^{1/4} \tag{2}$$

where $C = \mu\omega^2$ and $a = \sqrt{\frac{\hbar}{\mu\omega}}$. One also has $V(r_o) = \sqrt{A}\,\hbar\omega$. The Schrödinger equation we have to solve is:

$$\left\{-\frac{\hbar^2}{2\mu}\left(\frac{1}{r}\frac{\partial}{\partial r}\left(r\frac{\partial}{\partial r}\right) + \frac{1}{r^2}\frac{\partial^2}{\partial\phi^2}\right) + \frac{\hbar^2 A}{2\mu r^2} + \frac{C}{2}r^2 - E\right\}\Psi(r,\phi) = 0 \tag{3}$$

The solution to this equation is:

$$\Psi(r,\phi) = \frac{1}{\sqrt{2\pi}}R_{n\ell}\left(\frac{r}{a}\right)e^{i\ell\phi} \tag{4}$$

where $R_{n\ell}$ is solution of the radial equation:

$$\left\{\frac{d^2}{d\rho^2} + \frac{1}{\rho}\frac{d}{d\rho} + \left(\frac{2E_{n\ell}}{\hbar\omega} - \rho^2 - \frac{\ell^2 + A}{\rho^2}\right)\right\}R(\rho) = 0$$

The solution of this equation has acceptable boundary conditions only when $E_{n\ell}$ is given by:

$$E_{n\ell} = \hbar\omega\left(2n + 1 + \sqrt{A + \ell^2}\right)$$

$$= E_{oo} + E_{rad} + E_{ang}$$

$$= \hbar\omega\sqrt{A} + \hbar\omega(2n+1) + \hbar\omega\left(\sqrt{A+\ell^2} - \sqrt{A}\right) \qquad (6)$$

where n is an integer. The solution to eq. (5) can be expressed as :

$$R_{n\ell}(\rho) = N_{n\ell}\, e^{-\frac{\rho^2}{2}}\, \rho^{\sqrt{A+\ell^2}}\, L_n^{(\sqrt{A+\ell^2})}(\rho^2) \qquad (7)$$

where the Laguerre functions are defined by :

$$L_n^{(\alpha)}(z) \equiv \frac{e^z z^{-\alpha}}{n!} \frac{d^n}{dz^n}\left(e^{-z} z^{n+\alpha}\right)$$

A quantity measuring the average radial distance of a particle which moves around along the valley with angular momentum ℓ and whose energy is $E_{n\ell}$ is given by

$$r_1 \equiv \sqrt{\langle r^2 \rangle} = \left\{ \int_0^\infty R_{n\ell}^2 \left(\frac{r}{a}\right) r^3 dr \right\}^{1/2}$$

$$= a\left(2n+1+\sqrt{A+\ell^2}\right)^{1/2} \qquad (8)$$

We want to study a tunneling process, that is, a case where the energy in the angular direction is negative. This is obtained when one takes imaginary ℓ values (see eq. (6))

$$\ell = i\ell_o \qquad (\ell_o \text{ real} > 0)$$

Let us also consider the n = 0 case (for n ≠ 0 the reasoning is similar). From eq. (4) one sees that the wave function for imaginary ℓ is not a wave function corresponding to a stationary state, but to a state which is exponentially damped out when the system tunnels around (the angular part of the wave function is exp $(-\ell_0 \phi)$). For r_1 we have then (assuming $\sqrt{A} \gg \ell_0$)

$$r_1 = a\left\{1+\sqrt{A-\ell_0^2}\right\}^{1/2} \simeq a\sqrt[4]{A-\ell_0^2} \simeq r_0\left(1-\frac{\ell_0^2}{A}\right) \tag{9}$$

We find that the particle moves more on the inner side with respect to the bottom of the valley; that is, in this "tunneling process: the system "cuts the corner".

The same result can also be understood from a more classical point of view, by finding the minimum $\bar{r}_1$ of the effective potential:

$$V_{eff} \equiv V(r) + V_{cent}(r) \tag{10}$$
$$= \frac{\hbar^2}{2\mu}\frac{A}{r^2} + \frac{1}{2}Cr^2 + \frac{\hbar^2}{2\mu}\frac{(i\ell_0)^2}{r^2}$$

$$\bar{r}_1 = a\sqrt[4]{A-\ell_0^2} \tag{11}$$

$\bar{r}_1$ essentially agrees with r_1; that is, the minimum of the effective potential is further inside than the minimum of V(r).

This ties in with the idea that the tunneling process can be understood by using classical equations of motion on the inverted potential. The problem becomes now to find the stable orbit of a system moving on a

circular hill (with angular momentum ℓ_0), see Fig. 8-1b. The faster it moves, the more inside it must be. Equating the centrifugal force to the force acting on the system by the potential (hill) we find:

$$\vec{f}_{pot} = -\frac{\partial V}{\partial r}\hat{r} = \left(Cr - \frac{\hbar^2}{\mu}\frac{A}{r^3}\right)\hat{r}$$

$$\vec{f}_{cent} = \mu\frac{v^2}{r}\hat{r} = \frac{\ell_0^2}{\mu r^3}\hat{r}$$

$$\vec{f}_{cent} + \vec{f}_{pot} = \left(Cr - \frac{\hbar^2}{\mu}\frac{A}{r^3} + \frac{\ell_0^2}{\mu r^3}\right)\hat{r} = 0$$

$$\therefore \bar{r}_1 = a\sqrt[4]{A - \ell_0^2}$$

To summarize, for a system moving along a valley which turns a corner, for positive kinetic energies the centrifugal force pushes the system outwards (bobsled effect), for negative energies the centrifugal force is negative and during this tunneling process the system cuts the corner.

A quantity measuring the amount of corner cutting is $f = (r_o - r_1)/r_o$. Let us now express f in terms of C' (the "spring" constant of the circular valley), r_o (the curvature of the valley turning a corner) and E_{ang} (the energy in the tunneling direction). We find

$$f = \frac{8|E_{ang}|}{C' r_o^2} \tag{12}$$

with C' given by

$$C' = \frac{4\hbar^2 A}{a r^2} \tag{13}$$

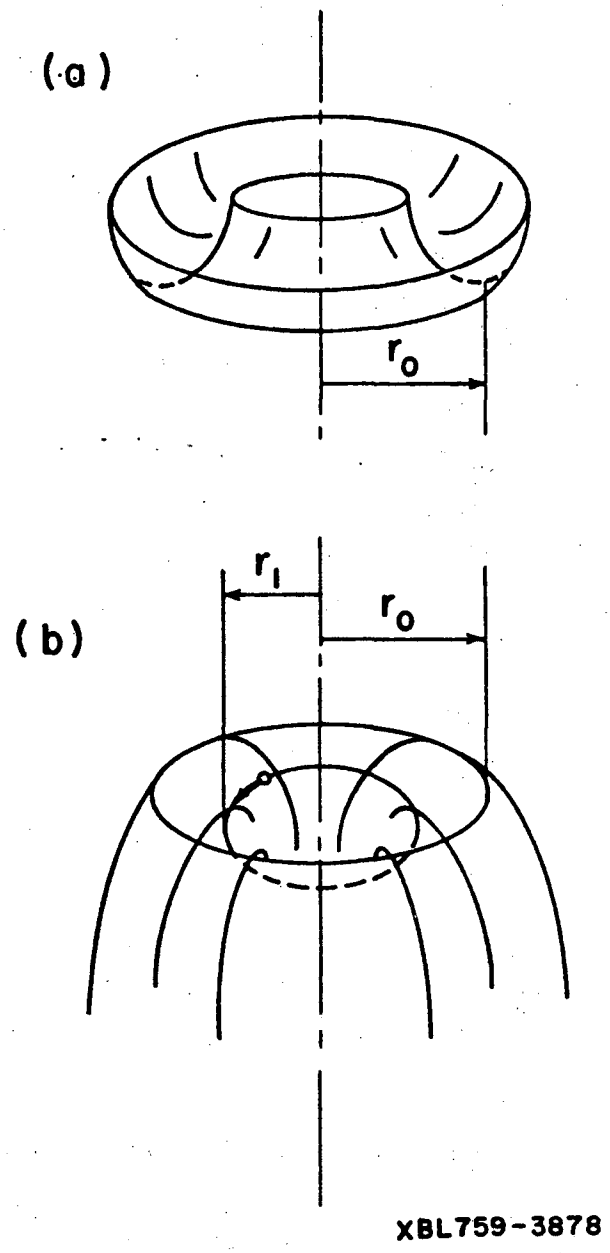

Fig. B-1 A circular valley with the valley floor at r_o is shown in a); if the potential shown in a) is inverted, one gets a circular hill as shown in b).

C. The symmetrical Eckard potential

Let's consider a particle of mass m and energy E moving in a symmetrical Eckard potential. The Hamiltonian for the system is then

$$H = \frac{p^2}{2m} + \frac{V_o}{\cosh^2(\frac{x}{a})} \tag{1}$$

If $E < V_o$ and the particle is initially on the left side of the barrier, in order for the particle to be found on the right side it has to tunnel through the barrier.

The WKB transmission probability T_{WKB} is given by

$$T_{WKB} = e^{-2K} \tag{2}$$

where

$$K = \int_{-x_o}^{+x_o} \frac{1}{\hbar} \left\{ 2m \left(\frac{V_o}{\cosh^2(\frac{x}{a})} - E \right) \right\}^{1/2} dx$$

$$= \frac{2}{\hbar} \sqrt{2mV_o} \int_o^{x_o} \left\{ 1 - \frac{E}{V_o} \cosh^2(\frac{x}{a}) \right\}^{1/2} \frac{dx}{\cosh(\frac{x}{a})} \tag{3}$$

x_o is the coordinate of the classical turning point:

$$\frac{V_o}{\cosh^2(\frac{x_o}{a})} = E \tag{4}$$

Equation (3) can be written as

$$K = \frac{2a}{\hbar} \sqrt{2mV_o}\, f\left(\sqrt{\frac{E}{V_o}}\right) \tag{5}$$

where f is

$$f(\alpha) \equiv \int_0^{\mathrm{Arccosh}\left(\frac{1}{\alpha}\right)} \left\{1-\alpha^2\cosh^2\left(\frac{x}{a}\right)\right\} \frac{dx}{\cosh\left(\frac{x}{a}\right)} \tag{6}$$

one has

$$\frac{df(\alpha)}{d\alpha} = \int_0^{\mathrm{Arccosh}\left(\frac{1}{\alpha}\right)} \frac{-\alpha\cosh(x/a)}{\sqrt{1-\alpha^2\cosh^2\left(\frac{x}{a}\right)}}\,dx = -\int_0^{\sqrt{1-\alpha^2}} \frac{du}{\sqrt{1-\alpha^2-u^2}} = -\frac{\pi}{2}$$

therefore

$$f(\alpha) = \frac{\pi}{2}(1-\alpha) \tag{7}$$

from eqs. (2), (5) and (7) we finally find

$$T_{WKB} = \exp\left(-\frac{2\pi a}{\hbar}\sqrt{2mV_0}\left(1-\sqrt{\frac{E}{V_0}}\right)\right) \tag{8}$$

For the symmetrical Eckard potential it is also possible to evaluate the exact quantum mechanical transmission probability which is given by[65]

$$T_{QM} = \frac{\sinh^2\left(\frac{\pi}{\hbar}\sqrt{2mE}\,a\right)}{\sinh^2\left(\frac{\pi}{\hbar}\sqrt{2mE}\,a\right)+\cosh^2\left(\frac{\pi}{\hbar}\sqrt{2mV_0-\frac{\hbar^2}{4a^2}}\,a\right)} \tag{9}$$

Expanding eq. (9) in terms of $\hbar$ and keeping only the lowest order term one has

$$\sinh^2\left(\frac{\pi}{\hbar}\sqrt{2mE}\,a\right) \underset{\hbar\to 0}{\simeq} \frac{1}{4}\exp\left(\frac{2\pi}{\hbar}\sqrt{2mE}\,a\right) \tag{10a}$$

$$\cosh^2\left(\frac{\pi}{\hbar}\sqrt{2mV_0 - \frac{\hbar^2}{4a^2}}\,a\right) \underset{\hbar\to 0}{\simeq} \frac{1}{4}\exp\left(\frac{2\pi}{\hbar}\sqrt{2mV_0}\,a\right) \qquad (10b)$$

and therefore one finds for the transmission probability

$$T_{QM} \simeq \frac{1}{1+\exp\left\{\frac{2\pi a}{\hbar}\sqrt{2mV_0}\left(1-\sqrt{\frac{E}{V_0}}\right)\right\}} \qquad (11)$$

Note that eq. (11) is the "improved" WKB result according to the rule given by Fröman and Fröman[48] (see also eqs.(IV 4) and IV-5)).

The equations of motion of a particle moving in the symmetrical Eckard potential can be integrated exactly, the result being:

$$x(t) = a\ \mathrm{Arcsinh}\left(\lambda\cosh\left(\frac{v_0}{a}(t-t_0)\right)\right) \quad \text{for } E<V_0 \qquad (12a)$$

$$x(t) = a\ \mathrm{Arcsinh}\left(\tilde{\lambda}\sinh\left(\frac{v_0}{a}(t-t_0)\right)\right) \quad \text{for } E>V_0 \qquad (12b)$$

where $\lambda = \sqrt{\frac{V_0}{E}-1}$ and $\tilde{\lambda} = \sqrt{1-\frac{V_0}{E}}$

The potential energy has poles when $\cosh\left(\frac{x}{a}\right)=0$, this occurs for

$$\frac{x}{a} = \pm i(2n+1)\frac{\pi}{2} \qquad (13)$$

This value of $\frac{x}{a}$ is obtained (see eq. 12)) if t is such that

$$\lambda\cosh\left(\frac{v_0}{a}(t-t_0)\right) = \pm i \quad \text{for } E<V_0 \qquad (14a)$$

or

$$\tilde{\lambda}\,\sinh\left(\frac{v_o}{a}(t-t_o)\right) = \pm i \qquad \text{for} \quad E > V_o \tag{14b}$$

The function $\mathrm{Arcsin}\, z$ has branch points at $z = \pm i$

Let's consider a complex Eckard potential

$$V = \frac{V_o e^{i\alpha}}{\cosh^2\left(\frac{x}{a}\right)} \tag{15}$$

one finds that the branch points in the complex time plane for $E < V_o$ are given by

$$t = \pm\frac{a}{2v_o}\left\{\frac{1}{2}\mathrm{Log}\left[\left(1-\frac{E}{V_o}\right)^2 + 4\frac{E}{V_o}\sin^2\frac{\alpha}{2}\right] - \mathrm{Log}\left[1-\frac{E}{V_o}-2\sqrt{\frac{E}{V_o}}\cos\frac{\alpha}{2}\right]\right.$$

$$\left. +(-i)\,\mathrm{Arctan}\left[\frac{2\sqrt{\frac{E}{V_o}}\sin\frac{\alpha}{2}}{1-\frac{E}{V_o}}\right]\right\} + \frac{a}{2v_o}\,i\pi(2n+1) \tag{16}$$

When $\alpha = 0$, that is the potential is purely real, then the branch points form two parallel columns of points with cuts parallel to the real time axis joining pairs of them (see Fig. IV 3). When $\alpha \neq 0$, that is the potential has an imaginary component, then the branch points are shifted; they still form two columns of points but the cuts are not aprallel to the real time axis. It should be noted, however, that for this potential the branch points on the time plane will never shift in such a way that a cut crosses the real time axis.

It is generally true, and it can be verified for the Eckard potential,

that branch points in the time plane correspond to coordinates for which the potential or some of its partial derivatives are divergent. For a potential having a Gaussian shape $V_o e^{-x^2}$ one has that the only place where it is divergent is for $x \to \pm i\infty$. In the complex time plane however, the Gaussian potential has branch points at finite values of t.

D. The $F_4(p_y, J)$ generating function.

It will be shown in this Appendix that the generating function for the canonical transformation between the cartesian coordinates (p_y, y) and the action-angle variables (J,q) for an harmonic oscillator is

$$F_4(P_y, J) = J\,q(P_y, J) - \frac{1}{2}\,y(P_y, J)\,P_y \tag{1}$$

The generator of the F_4 type is related to the generator of the F_2 type by [17]

$$F_4(P_y, J) = F_2(y, J) - yP_y \tag{2}$$

We will now show that $F_2(y,J)$ is given by

$$F_2(y, J) = Jq + \frac{1}{2}yP_y \tag{3}$$

Using the transformation equations (eq. IV 75)) one can write eq. (3) as:

$$F_2(y, J) = \frac{J}{2\pi}\,\mathrm{Arccos}\left(y\sqrt{\frac{\pi C}{\omega_0 J}}\right) - \frac{m_y \omega_0 y}{2}\sqrt{\frac{\omega_0 J}{\pi C} - y^2} \tag{4}$$

from which one can easily prove that

$$\frac{\partial F_2(y, J)}{\partial y} = P_y \tag{5a}$$

and

$$\frac{\partial F_2(q,J)}{\partial J} = q \qquad (5b)$$

but eqs. (5a) and (5b) are the necessary and sufficient conditions the generating function of type F_2 has to satisfy[17], thereby proving that F_2 is given by eq. (3).

E. Bessel Uniform Approximation.

Let's consider the integral expression for the S-matrix (see eqs. II-25) and (II-26)):

$$S_{\nu\leftarrow\mu} = \int_0^1 \frac{e^{i\Delta}}{\sqrt{\left(\frac{d\hat{q}(q_0)}{dq_0}\right)}}\, d\hat{q} \qquad (1)$$

with

$$\Delta = -\int_{t_i}^{t_f} (r\dot{p} + q\dot{J})dt + (J_f - J_\nu)q_f + (P_f - P_\nu)r_f + \frac{\pi}{2} \qquad (2)$$

Let's consider now the specific case of the fission barrier penetration model considered in section IV-3c. That example has the following symmetry: if initially the phase $\phi = 2\pi q$ of the harmonic oscillator is changed by π, then y and p change sign, but since the Hamiltonian depends only on the square of those quantities (eq. IV 72)) one obtains the same physical situation back. In other words, if ϕ_0 is a root, then also $\phi_0 + \pi$ is a root. Even though the problem is the same if the phase of the oscillator is changed by π, the phase Δ is not periodic. Analogous to equation (II 33) one has:

$$\Delta\left(\frac{\phi_i + \pi}{2\pi}\right) = \Delta\left(\frac{\phi_i}{2\pi}\right) - \pi(n_f - n_i) \qquad (3)$$

where n is related to J by eq. (IV 73) and the subindices i and f refer to the value of the designated quantities at the starting and concluding points of the integration respectively.

From everything said so far one has that the integral equation for

the S-matrix is for the fission model of the form

$$I = \frac{1}{2\pi}\int_{-\pi}^{+\pi} g(x)\, e^{if(x)}\, dx \qquad (4)$$

where f(x) has two stationary points in the interval $[-\pi, 0]$, let's denote them by x_- and x_+, and the two stationary points in the interval $[0, \pi]$ being $x_- + \pi$ and $x_+ - \pi$.

In section II 4 a similar problem was considered; there the phase f(x) was mapped onto a cubic which lead to the Airy uniform approximation expression for the S-matrix. Here we will consider a different possibility and map the phase f into the following function (the following derivation is slightly modified and generalized from the one given by Stine and Marcus[57]):

$$f(x) = -\xi \cos(2y) - Ky + A \qquad (5)$$

According to eq. (3), K is to be associated with $n_f - n_i$. The other constants, A and ξ, have to be chosen so that the stationary phase points of f(x) in the interval $-\pi < x \leq \pi$ correspond to those of the new function in the new domain $-\pi < y \leq \pi$; the mapping is then one-to-one and uniformly analytic. The stationary phase points occur when

$$2\xi \sin(2y) = K \qquad (6)$$

The correspondence between the stationary points is therefore

$$X = X_+ \longleftrightarrow y = y_+ = \frac{1}{2}\,\mathrm{Arcsin}\left(\frac{K}{2\xi}\right) \equiv \Theta \tag{7a}$$

$$X = X_- \longleftrightarrow y = y_- = \frac{\pi}{2} - \Theta \tag{7b}$$

the other two saddle points being displaced by π. Using eq. (5) and (7) one finds

$$f_+ = f(X_+) = -\xi\sqrt{1-\left(\frac{K}{2\xi}\right)^2} + A + K\Theta \tag{8a}$$

$$f_- = f(X_-) = \xi\sqrt{1-\left(\frac{K}{2\xi}\right)^2} - \frac{K\pi}{2} + K\Theta + A \tag{8b}$$

from which one gets

$$\frac{1}{2}(f_- + f_+) = A + \frac{1}{4}K\pi \tag{9a}$$

$$\frac{1}{2}(f_- - f_+) = \sqrt{\xi^2 - \frac{K^2}{4}} - K\,\mathrm{Arccos}\left(\frac{K}{2\xi}\right) \tag{9b}$$

Expanding $\frac{dx}{dy}\,g(x)$ as:

$$\frac{dx}{dy}\,g(x) = p_0\cos(2y) + q_0\sin(2y) \tag{10}$$

one finds for the coefficient p_0 and q_0

$$P_0 = \frac{1}{2\sin(2\Theta)}\left[\left(\frac{dx}{dy}\right)_+ g_+ - \left(\frac{dx}{dy}\right)_- g_-\right] \tag{11a}$$

$$q_0 = \frac{1}{2\sin(2\Theta)}\left[\left(\frac{dx}{dy}\right)_+ g_+ + \left(\frac{dx}{dy}\right)_- g_-\right] \qquad (11b)$$

The value of the derivatives at the stationary points $(dx/dy)_\pm$ can be found by differentiating equation (5) twice and using the stationary phase condition eq. (6):

$$\left(\frac{dx}{dy}\right)_\pm = \left[\pm \frac{4\xi\cos(2\Theta)}{f''_\pm}\right]^{1/2} \qquad (12)$$

Substituting eqs. (10) and eq. (5) into eq. (4) one finds for the integral I:

$$I = \frac{1}{2\pi}\int_{-\pi}^{+\pi}\left(p_0\cos(2y) + q_0\sin(2y)\right)e^{i\left(-\xi\cos(2y) - Ky + A\right)}dy$$

$$= \frac{1}{4\pi}\int_{-2\pi}^{2\pi}\left(p_0\cos u + q_0\sin u\right)e^{-i\left(\xi\cos u + \frac{Ku}{2} - A\right)}du$$

$$= \frac{1}{4\pi}\left\{\int_{-2\pi}^{-\pi}\ldots + \int_{-\pi}^{+\pi}\ldots + \int_{\pi}^{2\pi}\ldots\right\} \qquad (13)$$

Let's make a change of variables in the first and third integral; one finds

$$\int_{-2\pi}^{-\pi}\left(p_0\cos u + q_0\sin u\right)e^{-i\left(\xi\cos u + \frac{Ku}{2} - A\right)}du =$$

$$= \int_0^{\pi} \left(P_0 \cos u + q_0 \sin u \right) e^{-i\left(\xi \cos u + \frac{Ku}{2} - A\right)} e^{iK\pi} du$$

$$\int_{\pi}^{2\pi} \left(P_0 \cos u + q_0 \sin u \right) e^{-i\left(\xi \cos u + \frac{Ku}{2} - A\right)} du =$$

$$= \int_{-\pi}^{0} \left(P_0 \cos u + q_0 \sin u \right) e^{-i\left(\xi \cos u + \frac{Ku}{2} - A\right)} e^{-iK\pi} dw$$

Since K is an integer one can write

$$I = \frac{1}{4\pi} \left(1 + (-1)^K\right) e^{iA} \int_{-\pi}^{+\pi} \left(P_0 \cos u + q_0 \sin u \right) e^{-i\left(\xi \cos u + \frac{Ku}{2}\right)} \tag{14}$$

Eq. (14) shows explicitly the "parity" selection rule: the S-matrix is non-vanishing only when $k = |n_f - n_i|$ is an even integer.

From the integral expression of the Bessel functions of integer order

$$J_n(z) = \frac{i^{-n}}{\pi} \int_0^{\pi} e^{iz\cos\theta} \cos(n\theta)\, d\theta \tag{15}$$

and the recursion relations one can find the following expressions:

$$\frac{K}{2\xi} J_{\frac{K}{2}}(\xi) = \frac{i^{\frac{K}{2}}}{2\pi} \int_{-\pi}^{+\pi} \sin u\, e^{-i\left(\xi \cos u + \frac{Ku}{2}\right)} du \tag{16a}$$

$$J'_{\frac{K}{2}}(\xi) = \frac{i^{\frac{K}{2}}}{2\pi i} \int_{-\pi}^{+\pi} \cos u\, e^{-i\left(\xi \cos u + \frac{Ku}{2}\right)} du \tag{16b}$$

Using eq. (16) one has for I

$$I = \frac{1+(-1)^K}{2} e^{i\left(A-\frac{\pi K}{4}\right)} \left\{ q_0 \frac{K}{2\xi} J_{\frac{K}{2}}(\xi) + i p_0 J'_{\frac{K}{2}}(\xi) \right\} \tag{17}$$

Substituting into (17) the expressions for q_0 and p_0 (eq. (11)) and using eq. (9a) one finally finds

$$I = \frac{1+(-1)^K}{2} \sqrt{\xi}\, e^{\frac{i}{2}(f_+ + f_-)} \left\{ \sqrt{\cos(2\Theta)} \left(\frac{g_+}{\sqrt{f_+''}} + \frac{g_-}{\sqrt{-f_-''}} \right) J_{\frac{K}{2}}(\xi) + \right.$$

$$\left. - \frac{i}{\sqrt{\cos(2\Theta)}} \left(\frac{g_+}{\sqrt{f_+''}} - \frac{g_-}{\sqrt{-f_-''}} \right) J'_{\frac{K}{2}}(\xi) \right. \tag{18}$$

For the S-matrix we have from eq. (1) and performing the change of variables $2\pi\hat{q} - \pi \equiv U_f$

$$S_{\nu \leftarrow \mu} = \frac{1}{2\pi} \int_{-\pi}^{+\pi} \frac{e^{i\Delta}\, dU_f}{\sqrt{\frac{dU_f(U_i)}{dU_i}}} \tag{19}$$

Eq. (19) is of the form of eq. (4) with the identifications

$$g(x) = \left(\frac{dU_f(U_i)}{dU_i} \right)^{-1/2} \tag{20a}$$

$$f(x) = \Delta \tag{20b}$$

The stationary phase points are found from

$$\frac{d\Delta}{dq_f} = 2\pi(n_f - n_\nu) = 0 \tag{21}$$

We have

$$(\Delta'')_\pm \equiv \left(\frac{d^2\Delta}{du_f^2}\right)_\pm = \left(\frac{d}{du_f}(n_f - n_\nu)\right)$$

$$= \frac{1}{2\pi}\left(\frac{dn_f}{dq_f}\right)_\pm \tag{22}$$

Using eq. (22) one finds that

$$\frac{g_\pm}{\sqrt{\pm f''_\pm}} = \left(\frac{1}{\pm\Delta''_\pm \frac{dq_f}{dq_i}}\right)^{1/2} = \left(\frac{2\pi}{\left(\frac{dn_f}{dq_i}\right)_\pm}\right)^{1/2} \tag{23}$$

For the S-matrix one has therefore

$$S_{\nu\leftarrow\mu} = \frac{1+(-1)^K}{2}\sqrt{\frac{2\pi\xi}{\cos(2\Theta)}}\, e^{\frac{i}{2}(\Phi_+ + \Phi_-)}\left\{\cos(2\Theta)\cdot\right.$$

$$\left(\frac{1}{\sqrt{\left(\frac{dn_f(q_i)}{dq_i}\right)_+}} + \frac{1}{\sqrt{-\left(\frac{dn_f(q_i)}{dq_i}\right)_-}}\right) J_{\frac{K}{2}}(\xi) +$$

$$\left. + i\left(\frac{1}{\sqrt{\left(\frac{dn_f(q_i)}{dq_i}\right)_+}} - \frac{1}{\sqrt{-\left(\frac{dn_f(q_i)}{dq_i}\right)_-}}\right) J'_{\frac{K}{2}}(\xi)\right\} \tag{24}$$

where

$$K = |\eta_\mu - \eta_\nu| \tag{25}$$

$$\cos(2\Theta) = \sqrt{1-\left(\frac{K}{2\xi}\right)^2} \tag{26}$$

and ξ is defined implicitly by eq. (9b), i.e.

$$\frac{1}{2}(\Phi_- - \Phi_+) = \xi\sqrt{1-\left(\frac{K}{2\xi}\right)^2} - \frac{K}{2}\,\mathrm{Arccos}\left(\frac{K}{2\xi}\right)$$

$$= \xi\sqrt{1-\left(\frac{K}{2\xi}\right)^2} - i\,\frac{K}{2}\,\mathrm{Log}\left(\frac{K}{2\xi} \pm \sqrt{\left(\frac{K}{2\xi}\right)^2 - 1}\right) \tag{27}$$

REFERENCES

1. W. H. Miller, J. Chem. Phys. 53, 1949 (1970)
W. H. Miller, J. Chem. Phys. 53, 3578 (1970)
2. W. H. Miller and T. F. George, J. Chem. Phys. 56, 5668 (1972)
T. F. George and W. H. Miller, J. Chem. Phys. 57, 2458 (1972)
J. D. Doll, T. F. George and W. H. Miller, J. Chem. Phys. 58, 1343 (1972)
3. W. H. Miller, Adv. Chem. Phys. 25, 69 (1974)
W. H. Miller, "The Classical S-Matrix in Molecular Collisions", in Milecular Beams, ed. K. P. Lawley, Wiley; to be published (1975)
4. R. A. Marcus, J. Chem. Phys. Lett., 7, 525 (1970)
R. A. Marcus, J. Chem. Phys. 54, 3965 (1971)
5. J. N. L. Connor and R. A. Marcus, J. Chem. Phys. 55, 5636 (1971)
6. F. Roesel, J. X. Saladin and K. Adler, "Quantum Mechanical Coupled Channel Code for Coulomb Excitation", University of Pittsburgh Progress Report (1972)
7. J. P. Bondorf, M. I. Sobel, D. Sperber Phys. Rep. 15C Nr. 2 83 (1974). J. P. Bondorf et al., Phys. Rev. C11, 1265 (1975)
8. R. Hasse, J. Math. Phys. (1975). C. F. Tsang, Talk presented at the Nobel Symposium on "Superheavy Elements, Theoretical Predictions and Experimental Generations", Ronneby Sweden (1974).
9. N. K. Glendenning, Proc. Intern. Conf. on Reactions Between Complex Nuclei, Nashville, Tennessee, June 10-14 (1974)

10. R. A. Broglia and Aa. Winther, Phys. Rep. C4, 153 (1972)
R. A. Broglia, S. Landowne, R. A. Malfliet, V. Rostokin and Aa. Winther, Phys. Rep. 11C, 1 (1974)

11. M. Rosen, Nucl. Phys. 31, 664 (1962)

12. R. A. Malfliet, Symp. on Classical and Quantum Mechanical Aspects of Heavy Ion Collisions, Heidelberg (1974)

13. T. Koeling and R. A. Malfliet, "Application of a New Semi-Classical Approach to Elastic and Inelastic Heavy Ion Scattering". Preprint Univ. of Groningen. (1975)

14. J. Knoll and R. Schaeffer, Phys. Lett. 52B, 131 (1974)
J. Knoll and R. Schaeffer, "Semiclassical Scattering Theory with Complex Trajectories, I-Elastic Waves". To be published in Annals of Physics (1975)

15. Aa. Winther and J. de Boer, in "Coulomb Excitation", K. Alder and Aa. Winther edts., Academic Press, New York, p. 303

16. J. N. L. Connor and R. A. Marcus, J. Chem. Phys. 55, 5636 (1971)

17. H. Goldstein, "Classical Mechanics", Addison-Wesley, Reading Mass., 1950

18. P. A. M. Dirac, "The Principles of Quantum Mechanics", Oxford U. P., New York, 1958, 4th ed.

19. J. B. Keller, Ann. Phys. 4, 180 (1958)

20. C. Chester, B. Friedman and F. Ursell, Proc. Cambridge Phyl. Soc. 53, 599 (1957)

21. J. N. L. Connor, Mol. Phys. 26, 1217 (1973)
J. N. L. Connor, Mol. Phys. 27, 853 (1974)

22. J. N. L. Connor, Mol. Phys. 25, 181 (1973)

J. N. L. Connor, Mol. Phys. 26, 1371 (1973)

23. M. Abramowitz and J. A. Stegun, "Handbook of Mathematical Functions", Dover Pub. Inc., New York (1968)

24. N. Bohr, Mat. Fys. Medd. Dan. Vid. Selsk. 18, Nr. 8 (1948)

25. S. Levit, U. Smilansky and D. Pelte, Phys. Lett. 53B, 155 (1975)

26. H. Massmann and J. O. Rasmussen, Nucl. Phys. A243, 155 (1975)

27. K. Alder and Aa. Winther, Kgl. Danske Videnskab. Selskab, Mat. Fys. Medd. 32, Nr. 8 (1960)

28. M. Guidry, H. Massmann and J. O. Rasmussen (to be published)

29. R. Vandenbosch, T. D. Thomas and M. Webb, Conf. on "Classical and Quantum Mechanical Aspects of Heavy Ion Collissions", Heidelberg, October 1974.

30. J. R. Birkelund, J. R. Huizenga, H. Freiesleben, K. L. Wolf and J. P. Unik (to be published)

31. V. M. Strutinsky, Ark. Fys. 36, 629 (1967); Nucl. Phys. A95, 420 (1967)

32. M. Brack, J. Damgaard, A. Jensen, H. C. Pauli, V. M. Strutinsky and C. Y. Wong, Rev. Mod. Phys. 44, 320 (1972)

33. S. G. Nilsson, C. F. Tsang, A. Sobiczewski, Z. Szymanski, S. Wyceck, C. Gustafsson, I. Lamm, P. Möller and B. Nilsson, Nucl. Phys. A131, 1 (1969)

34. V. M. Strutinsky and H. C. Pauli, Physics and Chemistry of Fission, (Proc. Symp. Vienna, 1969) IAEA, Vienna, p. 155 (1969)

35. M. Bolsteri, E. O. Fiset, J. R. Nix and J. L. Norton, Phys. Rev. C5, 1050 (1972)

36. H. C. Pauli and T. Ledergerber, Nucl. Phys. A175, 545 (1971)

37. P. Möller and J. R. Nix, Physics and Chemistry of Fission, (Proc. Symp. Rochester, 1973) IEAE, Vienna, p. 103 (1974)

38. M. G. Mustafa, U. Mosel and H. W. Schmitt, Phys. Rev. C7, 1519 (1973)

39. S. M. Polikanov, V. A. Druin, V. A. Karnaukhov, V. L. Mikheer, A. A. Plere, N. K. Shobelev, V. G. Subbotin, G. M. Ter-Akopyan, V. A. Fomicher, J. Exptl. Theoret. Phys. (USSR) 42, 1464 (1962), Soviet Physics JETP 15, 1016 (1962)

40. S. E. Larson, G. Leander, Physics and Chemistry of Fission, (Proc. Symp. Rochester, 1973) IAEA, Vienna, p. 177 (1974)

41. P. Möller and S. G. Nilsson, Phys. Lett. 31B, 283 (1970)
P. Möller, Nucl. Phys. A192, 529 (1972)

42. J. R. Nix, Nucl. Phys. A130, 241 (1969)

43. J. Damgaard, H. C. Pauli, V. M. Strutinsky, C. Y. Wong, M. Brack and A. Stenholm-Jensen, Physics and Chemistry of Fission (proc. Symp., Vienna, 1969), IAEA, Vienna, p. 213, (1969)

44. T. Ledergerber and H. C. Pauli, Nucl. Phys. A207, 1, (1973).

45. H. Hofman and K. Dietrich, Nucl. Phys. A165, 1, (1971).

46. H. Hofmann, Z. Phys., 250, 14, (1972)

47. L. G. Moretto and R. P. Babient, Phys. Lett. 49B, 147, (1974)

48. P. O. Fröman and N. Fröman, JWKB Approximation, Contribution to the Theory (North Holland Press, Amsterdam, 1965)

49. J. Randrup, C. F. Tsang, P. Möller, S. G. Nilsson and S. E. Larson, Nucl. Phys. A217, 221, (1973)

50. J. Griffin, Proc. of Heavy Ion summer study 1972, Oak Ridge p. 123, (1972)

51. L. D. Landau and E. M. Lifshitz, "Mechanics" (Pergamon, New York). (1960).

52. J. Maruhn and W. Greiner, Phys. Lett. 44B, 9, (1973)

53. W. D. Meyers and W. J. Swiatecki, Ark. Phys. 36, 343 (1967)

54. W. H. Miller, J. Chem. Phys. 62, 1899 (1975)

55. H. Hofmann, Nucl. Phys. A224, 116 (1974)

56. H. Massmann, P. Ring and J. O. Rasmussen, Phys. Lett. 57B, 417 (1975)

57. J. R. Stine and R. A. Marcus, J. Chem. Phys. 59, 5145 (1973)

58. M. W. Guidry, F. S. Stephens, R. M. Diamond, P. A. Butler T. Y. Lee and P. Colombani (private communication)

59. E. Grosse, J. de Boer, R. M. Diamond, F. S. Stevens and P. Tjøm. (submitted to Phys. Rev. Lett.)

60. P. Fröbrich, Q. K. K. Liu and K. Möhring (private communication)

61. W. Greiner (private communication)

62. K. A. Ter-Martirosyan, Zh. Eksperim. i Teor. Fiz. 22, 284 (1952)

63. J. de Boer, H. Massmann and Aa. Winther. Proc. of the International Workshop III on Gross Properties of Nuclei and Nuclear Excitations, pg. 89, Hirschegg, Austria (1975)

64. P. Ring, J. O. Rasmussen and H. Massmann (submitted to "Nuclei and Particles").

65. "Problems in Quantum Mechanics" Ed. D. ter Haar, Academic Press, New York (1964).

TECHNICAL INFORMATION DIVISION
LAWRENCE BERKELEY LABORATORY
UNIVERSITY OF CALIFORNIA
BERKELEY, CALIFORNIA 94720